

②

171300-1-F

AD-A171 484

Final Report

AN EVALUATION OF NONSINUSOIDAL RADAR TECHNIQUES

IVAN J. LaHAIE
ROBERT O. HARGER
STANLEY R. ROBINSON
JACK M. MILLER
Infrared and Optics Division

JUNE 1985

W.F.
Sponsored by:

Defense Advanced Research Projects Agency
Arlington, VA 22209
DARPA Order No. 4847

Monitored by:
Office of Naval Research
Arlington, VA 22217
Contract No. N00014-83-C-0754

DTIC
ELECTE
S **D**
SEP 02 1986
Al **E**

DTIC FILE COPY

ENVIRONMENTAL
RESEARCH INSTITUTE OF MICHIGAN
BOX 8618 • ANN ARBOR • MICHIGAN 48107

86 8 29 023

UNCLASSIFIED

SECURITY CLASSIFICATION OF THIS PAGE

ADA171484

REPORT DOCUMENTATION PAGE


| | | | | | |
|---|-------|--|---|---|--------------------------------|
| 1a. REPORT SECURITY CLASSIFICATION UNCLASSIFIED | | | 1b. RESTRICTIVE MARKINGS | | |
| 2a. SECURITY CLASSIFICATION AUTHORITY | | | 3. DISTRIBUTION/AVAILABILITY OF REPORT | | |
| 2b. DECLASSIFICATION/DOWNGRADING SCHEDULE | | | 107 | | |
| 4. PERFORMING ORGANIZATION REPORT NUMBER(S) 171300-1-F | | | 5. MONITORING ORGANIZATION REPORT NUMBER(S) | | |
| 6a. NAME OF PERFORMING ORGANIZATION Environmental Research Institute of Michigan | | 6b. OFFICE SYMBOL (If applicable) | | 7a. NAME OF MONITORING ORGANIZATION Office of Naval Research | |
| 6c. ADDRESS (City, State and ZIP Code) P.O. Box 8618 Ann Arbor, MI 48107 | | 7b. ADDRESS (City, State and ZIP Code) Office of Naval Research 800 North Quincy Street Arlington, Virginia 22217 | | | |
| 8a. NAME OF FUNDING/SPONSORING ORGANIZATION Defense Advanced Research Projects Agency | | 8b. OFFICE SYMBOL (If applicable) DARPA/TTO | | 9. PROCUREMENT INSTRUMENT IDENTIFICATION NUMBER N00014-83-C-0754 | |
| 8c. ADDRESS (City, State and ZIP Code) 1400 Wilson Blvd. Arlington, VA 22209 | | 10. SOURCE OF FUNDING NOS. | | | |
| | | PROGRAM ELEMENT NO. | | PROJECT NO. | TASK NO. |
| | | | | | WORK UN NO. |
| 11. TITLE (Include Security Classification) An Evaluation of Nonsinusoidal Radar Techniques (U) | | | | | |
| 12. PERSONAL AUTHOR(S) Ivan J. LaHaie, Robert O. Harger, Stanley R. Robinson, Jack M. Miller | | | | | |
| 13a. TYPE OF REPORT Final Report | | 13b. TIME COVERED FROM 10/83 TO 10/84 | | 14. DATE OF REPORT (Yr., Mo., Day) June 1985 | |
| 15. PAGE COUNT 184 | | | | | |
| 16. SUPPLEMENTARY NOTATION | | | | | |
| 17. COSATI CODES | | | 18. SUBJECT TERMS (Continue on reverse if necessary and identify by block number) | | |
| FIELD | GROUP | SUB. GR. | Nonsinusoidal Radar, Wideband Radar, Carrier-Free Radar, Radar Systems, Large Relative Bandwidth Signals | | |
| | | | | | |
| 19. ABSTRACT (Continue on reverse if necessary and identify by block number) A preliminary investigation into the feasibility of using large relative bandwidth signals and wideband radar systems in conventional narrowband radar system applications is presented. A generic set of radar applications is identified and the capabilities and limitations of current narrowband radars in these applications are discussed. An end-to-end formulation and analysis of a generic wideband radar system using signals of arbitrary spectral content is developed for the specific application of target detection in clutter plus noise. This analysis serves as the ground work for future analyses required to assess the performance of wideband systems of other radar applications. The results clearly show the tradeoff between the spectral content of the signal, the properties of the target, clutter, and propagation medium, and other system constraints. Current research at other organizations in large relative bandwidth radar applications and components is reviewed and evaluated. The results of the evaluation are used to identify those research efforts which merit further investigation particularly in the form of an end-to-end systems analysis similar to that. (OVER) | | | | | |
| 20. DISTRIBUTION/AVAILABILITY OF ABSTRACT UNCLASSIFIED/UNLIMITED <input type="checkbox"/> SAME AS RPT <input checked="" type="checkbox"/> DTIC USERS <input type="checkbox"/> | | | 21. ABSTRACT SECURITY CLASSIFICATION UNCLASSIFIED | | |
| 22a. NAME OF RESPONSIBLE INDIVIDUAL David C. Lewis | | | 22b. TELEPHONE NUMBER (Include Area Code) (202)696-4216 | | 22c. OFFICE SYMBOL Code 414 |

UNCLASSIFIED

SECURITY CLASSIFICATION OF THIS PAGE

19. ABSTRACT (Continued)

described above. Recommendations are made for future studies in both radar applications and system components.



UNCLASSIFIED

SECURITY CLASSIFICATION OF THIS PAGE

AN EVALUATION OF NONSINUSOIDAL RADAR TECHNIQUES

TABLE OF CONTENTS

| <u>SECTION</u> | <u>PAGE</u> |
|---|-------------|
| 1.0 INTRODUCTION..... | 1 |
| 1.1 REVIEW OF THE NONSINUSOIDAL RADAR CONTROVERSY..... | 2 |
| 1.1.1 THE CASE FOR NONSINUSOIDAL WAVES..... | 2 |
| 1.1.2 THE CASE AGAINST NONSINUSOIDAL WAVES..... | 5 |
| 1.2 PROGRAM OBJECTIVE AND APPROACH..... | 5 |
| 1.3 FINAL REPORT ORGANIZATION AND RESULTS..... | 7 |
| 2.0 GENERAL COMMENTS..... | 9 |
| 2.2 REVIEW OF NARROWBAND RADAR TECHNIQUES FOR CLUTTER- LIMITED APPLICATIONS..... | 10 |
| 2.2.1 STATIONARY TARGET DETECTION..... | 10 |
| 2.2.2 MOVING TARGET DETECTION: MTI..... | 17 |
| 2.2.3 MOVING TARGET DETECTION: PULSE DOPPLER..... | 28 |
| 2.2.4 LOW ANGLE TRACKING..... | 35 |
| 2.3 CONCLUSIONS..... | 38 |
| 3.0 THEORY OF WIDEBAND RADAR DETECTION..... | 39 |
| 3.1 SECTION SUMMARY..... | 39 |
| 3.2 RECEIVED SIGNAL MODEL..... | 40 |
| 3.2.1 NONSINUSOIDAL TRANSMITTED WAVEFORM..... | 45 |
| 3.2.2 SCATTERING REFLECTIVITY MODELS..... | 46 |
| 3.3 OPTIMUM PROCESSOR STRUCTURE AND RESULTING PERFORMANCE... | 58 |
| 3.4 OPTIMUM SIGNAL DESIGN..... | 62 |
| 3.4.1 NUMERICAL EVALUATION..... | 63 |
| 3.5 MULTIPLE PULSE (PERIODIC) SIGNAL DESIGN..... | 74 |
| 3.5.1 SOLUTION FOR OPTIMUM SIGNAL..... | 80 |
| 3.5.2 SPECIFIC NUMERICAL RESULTS..... | 82 |
| 3.6 OPTIMUM SIGNALS FOR DISPERSIVE PROPAGATION MEDIA..... | 85 |
| 3.6.1 INTRODUCTION..... | 85 |
| 3.6.2 A SIMPLE DISPERSION/ABSORPTION MODEL..... | 87 |
| 3.6.3 EXTENSION OF RADAR SYSTEM MODEL..... | 88 |
| 3.6.4 SPECIFIC NUMERICAL CALCULATIONS..... | 91 |

TABLE OF CONTENTS (Cont'd)

| <u>SECTION</u> | <u>PAGE</u> |
|--|-------------|
| 3.7 FURTHER DESIGN OBSERVATIONS..... | 92 |
| 3.8 CONCLUSIONS..... | 97 |
| 4.0 DISCUSSION OF SELECTED WIDEBAND RADAR (WBR) RESEARCH..... | 99 |
| 4.1 SEM-BASED METHODS..... | 100 |
| 4.1.1 RESONANCE REGION RADAR (R^3) - Research at General Research Corporation and The Naval Postgraduate School..... | 101 |
| 4.1.2 RADAR WAVEFORM SYNTHESIS - Research at Michigan State University..... | 106 |
| 4.1.3 THE K-PULSE CONCEPT - Research at the Ohio State University (OSU)..... | 109 |
| 4.2 "CARRIER-FREE" RADAR CONCEPTS..... | 111 |
| 4.2.1 CARRIER-FREE RADAR: APPLICATIONS STUDIES..... | 112 |
| 4.2.2 CARRIER-FREE RADAR: COMPONENTS STUDIES..... | 121 |
| 4.3 COMPARISON TO NARROWBAND RADAR SYSTEM..... | 127 |
| 5.0 CONCLUSIONS AND RECOMMENDATIONS..... | 133 |
| 5.1 SUMMARY..... | 133 |
| 5.2 RECOMMENDATIONS..... | 138 |
| APPENDIX A: REMARKS ON LINEAR MAPPINGS AND FREQUENCY DOMAIN ANALYSIS..... | 141 |
| APPENDIX B: THE GENERATION OF SPECIFIED SPECTRUM MODULUS WITH A SPECIFIED SIGNAL TIME ENVELOPE..... | 149 |
| APPENDIX C: GENERAL TRANSFER FUNCTION AND IMPULSE RESPONSE OF A WIDEBAND (NONSINUSOIDAL) MONOSTATIC RADAR..... | 155 |
| REFERENCES..... | 177 |

LIST OF ILLUSTRATIONS

| <u>FIGURE</u> | <u>PAGE</u> |
|--|-------------|
| 2-1 Sketch of Area CFAR Window (5 Cells by 5 Cells)..... | 12 |
| 2-2 Probability of Detection Versus Target-to-Clutter Ratio for a Rayleigh Target in Log-Normal Clutter..... | 16 |
| 2-3 Doppler Spectrum seen by MTI Receiver..... | 18 |
| 2-4 A Coherent MTI Implementation (with square-law detector)... | 10 |
| 2-5a The Effect of Doppler Offset Error E..... | 24 |
| 2-5b Offset Error with a Digital Filter Bank..... | 24 |
| 2-6 Probability of Detecting a Fluctuating Target..... | 27 |
| 2-7 Block Diagram of a Pulse Doppler Receiver..... | 29 |
| 3-1 Radar System Geometry..... | 41 |
| 3-2 Antenna Aperture Field Generation Model..... | 44 |
| 3-3 Scattering Object Geometry..... | 49 |
| 3-4 Linear Model for Clutter Reception..... | 53 |
| 3-5 Radar System Model for Target in Clutter..... | 59 |
| 3-6 Total Radar System Block Diagram..... | 61 |
| 3-7 Frequency Dependence for Assumed Target..... | 66 |
| 3-8 Assumed Antenna Frequency Response..... | 67 |
| 3-9 Effect of Energy Constraint on Particular Optimum Signal Design ($v_{\min} = 135$, $v_{\max} = 175$)..... | 69 |
| 3-10 Optimum Signal for Larger Bandwidth Interval ($v_{\min} = 35$, $v_{\max} = 200$)..... | 71 |
| 3-11 Optimum Signal for Wideband Reduced Energy Constraint ($v_{\min} = 35$, $v_{\max} = 175$)..... | 72 |
| 3-12 Optimum Signal with Reduced Energy Constraints..... | 73 |
| 3-13 Effects of Energy Constraint on a Broadband Optimum Periodic Signal Design ($v_{\min} = 25$, $v_{\max} = 200$)..... | 83 |
| 3-14 Effects of Lower Energy Constraints on Periodic Signal Design ($v_{\min} = 25$, $v_{\max} = 200$)..... | 84 |
| 3-15 Radar System Model for Weak Dispersive Media..... | 90 |
| 3-16 Effect of Energy Constraint on Optimum Signal for Dispersive Media ($v_{\min} = 25$, $v_{\max} = 200$)..... | 93 |

LIST OF ILLUSTRATIONS (Cont'd)

| <u>FIGURE</u> | <u>PAGE</u> |
|---|-------------|
| 4-1 Experimental Facilities for Time-Domain (TD) and Frequency Domain (FD) Target Backscatter Measurements..... | 103 |
| 4-2 Calibration Procedure for Scattering Data from the System in Figure 4-1..... | 104 |
| 4-3 Frequency and Time Domain Responses Compared to Theory for Generic Model, Nose Incidence..... | 105 |
| 4-4 Schematic Diagram of the Large Current Radiator..... | 122 |
| A-1 Defining Structure for Antenna (Radiating) Element..... | 144 |
| B-1 Constrained Signal Modulus with Allowable Instantaneous Phase Modulation..... | 150 |
| B-2 Typical Signal Modulus and Cumulative Distribution..... | 152 |
| C-1 Block Diagram of General Radar System..... | 156 |
| C-2 Scattering Geometry..... | 161 |
| C-3 Antenna Equivalent Circuits..... | 163 |

LIST OF TABLES

| <u>TABLE</u> | <u>PAGE</u> |
|---|-------------|
| 1-1 POTENTIAL MILITARY APPLICATIONS OF NONSINUSOIDAL RADAR..... | 4 |
| 1-2 DIFFICULTIES OF NONSINUSOIDAL-BASED RADAR..... | 6 |
| 3-1 ESTIMATES OF TERRAIN SPECTRAL DENSITIES..... | 57 |

AN EVALUATION OF NONSINUSOIDAL RADAR TECHNIQUES

1.0 INTRODUCTION

During the past decade, a seemingly insignificant, but highly emotional, controversy has existed on the use of nonsinusoidal "carrier-free" waveforms for applications in radar and communication. The debate apparently started on the utility of Walsh functions as compared to sinusoids [1,2]; it later evolved to the system implications of the utility of the large relative-bandwidth carrier-free waveforms as contrasted to the narrow relative-bandwidth of conventional carrier-based systems [33,53,54]. Indeed, the debate continued to such a point that proponents of the nonsinusoidal approach only published their work in the IEEE Transactions on Electromagnetic Compatibility; this action further fueled the skepticism of opponents since the objectivity of such a small peer group could be easily questioned. As a result, there had been no objective comparison made between carrier-free and conventional radar techniques for military applications. Such an assessment was needed by the Department of Defense (DoD) in order to understand the potential of nonsinusoidal radar to provide unique capabilities not achievable with conventional techniques. For example, it had been argued that nonsinusoidal radar could be used as an anti-stealth system; i.e., that it could be used to detect and track low-observable platforms [46]. A validation of that claim alone was of sufficient importance to merit an objective evaluation; however, there were undoubtedly other important applications for which nonsinusoidal radar may be well suited. The heated controversy which existed over a decade, combined with the need by the DoD to understand the military potential of such a radar, provided the motivation for the study whose results are presented herein.

1.1 REVIEW OF THE NONSINUSOIDAL RADAR CONTROVERSY

This section presents a brief overview of the "common" arguments for and against the use of nonsinusoidal waves in radar applications. It provides an important historical perspective of the controversy and thus also provides insight into why the issues were not easily resolved.

1.1.1 THE CASE FOR NONSINUSOIDAL WAVES

The beginning arguments for nonsinusoidal-based systems apparently goes back to the discovery of a set of orthogonal functions -- Walsh functions -- that could be used as a basis set for waveform analysis, coding, etc., in lieu of the traditional sinusoids. Since the functions were binary valued, it was felt that the computation of the required coefficients could be done much more efficiently than in the case of sinusoids. Even the pros and cons of Walsh function representation were presented in the midst of heated debate [1,2], and the IEEE Transactions of Electromagnetic Compatibility became the forum for such papers.

Soon after that, H.F. Harmuth developed the notion that all of electrical engineering was so biased by the use of sinusoids, starting with the practical hardware limitations faced by Marconi, that alternate system concepts, based upon nonsinusoidal waves, never received adequate treatment. This theme is repeated throughout his papers [32-51] and is adequately summarized in his recent book [52].

Current views in favor of nonsinusoidal-based systems are no longer exclusively tied to the merits of Walsh functions alone, but to the notion of the large relative bandwidths which can be achieved with "carrier-free" waveforms. Here, relative bandwidth n is defined by

$$n = \frac{f_H - f_L}{f_H + f_L}$$

where $f_H(f_L)$ is the highest (lowest) significant frequency component in the signal of interest.* Typical audio signals and pulse video waveforms have $\eta = 0.75$ to 1, while ≤ 0.1 is typical for radar. Thus, it is argued that to obtain the large bandwidths needed for high resolution, conventional radars must operate in the millimeter wave region (e.g., 35 or 95 GHz) with the attendant problems of high absorptive losses, high noise temperatures, and strong dependence on weather effects [33]. For example, a 1 nanosecond pulse system would have significant spectral content up to 1 GHz; a conventional system with the same bandwidth would require either a 35 or 95 GHz carrier.

With these concepts in mind, the proponents for nonsinusoidal radar present an impressive list of potential military applications; it is provided in Table 1-1. Note that all the justifications are based, in part, on the wide relative bandwidth of the technique and on the fact that many limiting propagation effects can be ameliorated by operating in a lower frequency band. A few quantitative analyses have been presented [32-51], but the results are technically incomplete as compared to similar system studies using conventional techniques.

It is interesting to note here that numerous nonsinusoidal radars have been built commercially for geophysical probing applications. In fact, one such radar was used to detect the tail section of the Air Florida Flight 90 which crashed into the Potomac several years ago. Positive results as these tend to make proponents all the more steadfast in their views. In fact, the public claims for utility are so often

*In the context of the present study, nonsinusoidal radar (NSR) and wideband radar (WBR) were used interchangeably for radar systems whose waveforms were of a large relative bandwidth. It was judged that the fundamental issue was that the waveform had a large relative bandwidth and not that it had to be considered carrier-free. In fact, Appendix A discusses that the concept of a carrier frequency is completely arbitrary when using complex notation to describe a waveform with large relative bandwidths.

TABLE 1-1. POTENTIAL MILITARY APPLICATIONS OF NONSINUSOIDAL RADAR

| <u>MILITARY APPLICATION</u> | <u>REASON</u> |
|---|--|
| Anti-stealth Radar | Wide bandwidth easily penetrate coating materials. Hard to defeat with active stealth techniques. Excites (unknown) body resonances. |
| All-weather, High-Resolution Line-of-Sight (LOS) Radar | Improved resolution with wide bandwidth. Better performance in rain, fog, snow, since spectrum below 5 GHz. |
| Anti-ballistic Missile (ABM) Defense Radar | Improved resolution to separate decoys from warheads. |
| Over-the-Horizon (OTH) Radar | Microsecond pulses provide better resolution with reduced dispersion. |
| Look-Down-Radar for detecting low-cross section platforms | Better range resolution to reduce clutter effects. High bandwidth enhances radar cross-section. |
| Synthetic Aperture Radar | Improved range resolution allows for enhanced image resolution. |

overstated that their credibility is in question. (It is important to observe that radar remote sensing is a "soft science" and, as such, is not conclusive support for complete success in military applications.) In short, nonsinusoidal techniques for radar have been advocated by a number of individuals. The advantages have probably been overstated based upon heuristic reasoning and have not been quantitatively proven.

1.1.2 THE CASE AGAINST NONSINUSOIDAL WAVES

The proponents of a conventional, sinusoidal-based radar have argued against the nonsinusoidal radar based primarily upon hardware and complexity issues. Stated simply, they say that since the implementation is so difficult and since there is no solid prediction of an attendant gain in performance, then there is no motivation to proceed further. For the record, Table 1-2 presents a partial list of the hardware and system related difficulties. In all fairness, the conclusions are also heuristically correct but quantitatively soft. Without specific system applications and performance parameters, it is difficult to predict which areas of difficulty are "fundamental" or which are just perceived based upon current design approaches. It is exactly that mismatch of glowing applications and sour implementation issues that motivated this study.

1.2 PROGRAM OBJECTIVE AND APPROACH

With the nonsinusoidal controversy as a background, the objective of the subject study was to provide an unbiased evaluation of nonsinusoidal radar (NSR) techniques for military applications and to identify future activities needed to realize the potential gain of NSR. The study objective was accomplished by a combination of (1) interviews with several of the key NSR proponents, including H.F. Harmuth, (2) original radar system modeling and performance prediction calculations,

TABLE 1-2. DIFFICULTIES OF NONSINUSOIDAL-BASED RADAR

| <u>RESTRICTIVE ELEMENT</u> | <u>COMMENTS</u> |
|--|---|
| Antenna | Poor radiative efficiency. Poor directivity. Phase center varies in time/space. Dispersive nature shapes pulse spectrum. |
| Waveform Generator/ Power Amplifier | Requires extreme power. Difficult switching requirements. |
| Propagation Media | Dispersive/absorptive media destroys specific pulse structure. |
| Timing/Synchronization | Extremely tight tolerances needed for resolution and reduction of "co-channel" interference. |
| Receiver Processing | Analog tapped delay line with very tight tolerances and thousands of taps. |
| Component (Front-end) Dynamic Range | Must be maintained without destroying temporal character. |
| Range Resolution | Too much. May unnecessarily resolve individual scattering centers of a target. |

and (3) critical review and critiques of numerous published literature on NSR and other related topics. Great care was taken to ensure that fundamental issues were not confused with current hardware limitations so that "pure" conclusions could be deduced from the analysis.

1.3 FINAL REPORT ORGANIZATION AND RESULTS

This report is organized as follows: Section 2.0 provides a summary of radar system requirements and conventional radar limitations for military applications. Emphasis is placed on target detection, and tracking in a heavy clutter environment. The study scope was limited to this application because, for certain military scenarios, it is still very stressing for conventional radars and there appeared to be few additional alternatives remaining. Moreover, it was judged that NSR techniques could be promising in that case.

Section 3.0 presents an end-to-end analysis and radar system model for detection of stationary targets in clutter. Using crude, but useful models for clutter and target frequency dependence, optimum radar waveforms are designed to maximize the target detectability. In some instances, the formalism dictates that optimum waveforms should have large relative bandwidths. The importance of the result is not the specific signal design, but rather the "existence proof" that signals with wide relative bandwidth may be optimum for detection of targets in clutter. This is particularly true when the target response and/or the intervening propagation media have significant frequency dependencies.

Section 4.0 presents critiques of many relevant papers published in the area of WBR techniques. Among many results, it demonstrates that the use of singularity-expansion methods (SEM) to describe target scattering provide a means to do target classification. (SEM techniques require WBR waveforms and are virtually unknown to the NSR proponents.)

Finally, Section 5.0 presents a summary of conclusions and recommendations for future activities. It is concluded that the formalism developed in Section 3.0 should be applied in detail to specific military problems to identify one or two most promising for which additional system/component hardware development work should be directed.

2.0 RADAR SYSTEM CONSIDERATIONS

2.1 GENERAL COMMENTS

The potential uses of radar for military applications are quite numerous so that to provide an extensive description is beyond the scope of the present study. However, it is useful to present some general considerations to focus the deliberation for NSR techniques. In the weapon system context, the required functions are (1) surveillance of an area of interest for potential military targets, (2) tracking of potential targets of interest, (3) classification/ identification of tracked target, (4) fire control for the weapon delivery, and (5) damage assessment after weapon delivery. Of course, these categories are "soft" depending upon the specific mission, e.g., the tactical problem of destroying armor on a road, or the strategic problem of destroying missile launch sites, or defending specific area against an air attack.

The type of radar required to do a specific function depends strongly on the location/platform constraints of the radar and expected targets/backgrounds. Radars are routinely considered for basing on satellites, aircraft (both large AWACS and fighter-type aircraft), ships and ground installations. The platforms typically dictate limitations on prime power and available antenna aperture sizes and the areas to be searched (relative to the platform motion/location). In addition, the radar basing will dictate the type of clutter background against which the target will be observed.

Depending on the mission, the target type will also dictate the available conventional (or narrowband) radar techniques which are applicable for a specific function. For example, an airborne radar searching for a moving tank column on a road can use MTI techniques, whereas detection of stationary tanks would require either CFAR or imaging (spatial) discrimination techniques.

It was decided that the ultimate end-to-end system analysis (presented in Section 3.0) would need to be limited to a specific scenario to yield quantitatively useful results. Thus, the detection of a target in clutter was selected to be the most interesting problem. It is representative for a number of scenarios, including an autonomous missile directed against tanks, an AWACS searching for penetrating enemy aircraft, as well as a surface-to-air missile (SAM) battery defending a specific area.

In the next section, we review the use of conventional (narrowband) radar techniques for such a problem. This review is necessary to underscore the fundamental limitations of conventional system and to illustrate the sophisticated signal processing used in such systems.

2.2 REVIEW OF NARROWBAND RADAR TECHNIQUES FOR CLUTTER-LIMITED APPLICATIONS

2.2.1 STATIONARY TARGET DETECTION

To motivate the stationary target detection problem, consider an anti-armor missile system. A key feature of such a system is the ability to reliably detect, discriminate and track both stationary and moving enemy vehicles such as tanks, self-propelled artillery, APC's, ammunition and fuel trucks, etc. These systems must operate in an autonomous mode once they are launched. There is no data link from missile-to-missile or from missile-to-launch aircraft, and the on-board missile processor performs all navigation, search, detection, classification and homing functions after launch.

A typical air-to-surface concept has a range of approximately 10 km and can be launched at a low altitude so that the target area does not need to be visible from the aircraft at the time of launch - thus increasing aircraft survivability. The launch aircraft is assumed to be vectored to the launch point by a surveillance system, such as J-STARs.

The mapped swath width and search length are chosen to permit reliable operation when both aircraft vectoring errors and missile guidance errors are present.

Since most of the primary and secondary roads in Europe and Asia are tree-lined, it is seen that a primary requirement of such a missile system is to detect targets against a harsh, non-homogeneous clutter background. This must be accomplished when armor is both moving and stationary, for example, at rest-stops and staging areas where tree cover will be used. Also, certain vehicles will usually be stationary, for example, parked anti-air units that protect advancing armor. The reliable detection of stationary and moving targets embedded in clutter is thus the primary problem that must be solved.

A constant false alarm rate (CFAR) is usually a requirement for any radar that is used to detect stationary or slowly moving ground targets embedded in a clutter background. This means that the false alarm rate should ideally be independent of the clutter distribution and clutter statistics. The usual way that this is accomplished is by comparing the power returned from a cell (or cells) being tested for the presence of a target with the power returned from a group of cells surrounding the test cell(s). If the ratio exceeds a threshold, then a potential target is declared. The cells surrounding the potential target are used to statistically characterize the local clutter background and the detection threshold is chosen (as a function of the local clutter background) to achieve a given probability of false alarm.

The CFAR property is achieved by adaptively changing the detection threshold as a function of the observed clutter statistics. An example of this type of CFAR "window" process is given in Figure 2-1 where the clutter returns from the 24 cells surrounding the test cell are used to control the detection threshold for the center target cell. As first

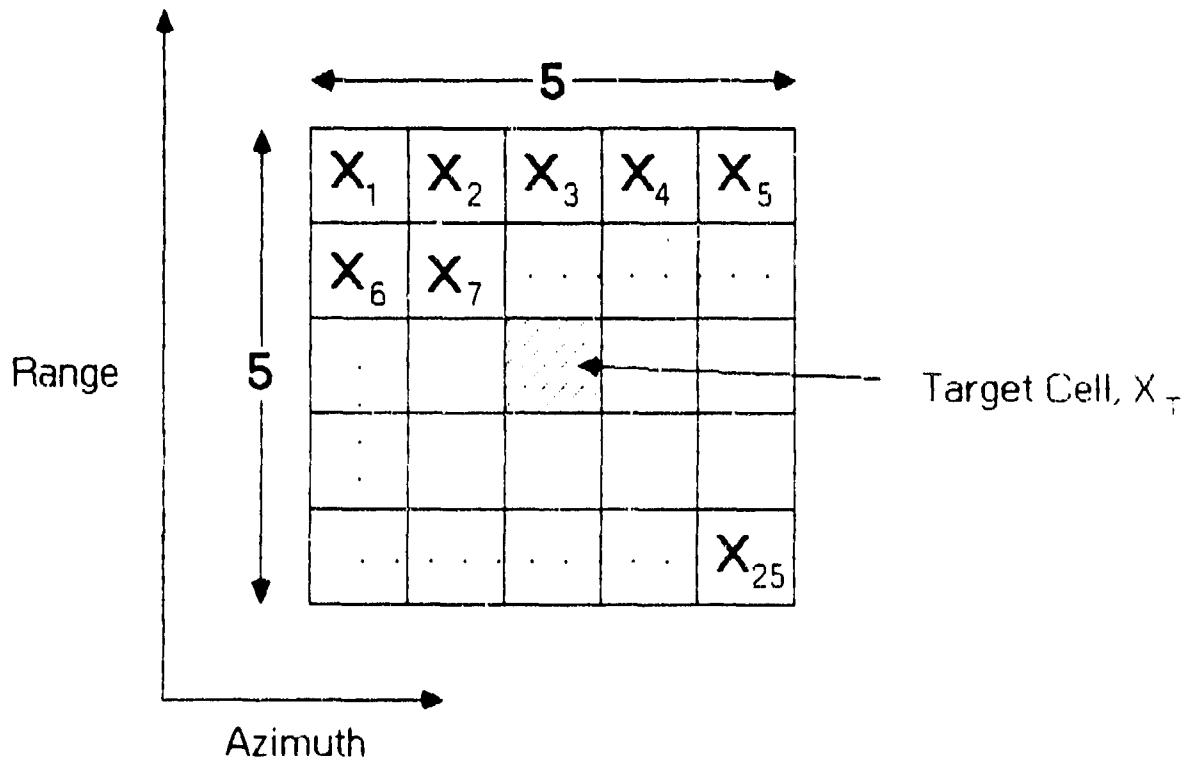


Figure 2-1. Sketch of Area CFAR Window (5 Cells by 5 Cells)

demonstrated by Finn [3] and Finn and Johnson [4], an adaptive threshold of this type is a key requirement, since it is possible to obtain false alarm rates that are orders of magnitude different if the form of the clutter distribution changes and the threshold is kept the same.

Usually the threshold adjustment is made on the basis of estimates of the first two moments of the local clutter distribution. In the detection literature these are usually called one or two parameter CFAR tests. A general two-parameter CFAR procedure was first given by Goldstein [5]. His processor will maintain a constant false alarm rate in either log-normal or Weibull clutter, however, a given threshold setting will give a larger P_{FA} in log-normal clutter as compared to Weibull clutter even though the clutter parameters are the same. Thus, his detection threshold must be changed as the clutter distribution changes. The Goldstein processor does not include a method for distinguishing clutter types and adjusting the detection threshold accordingly. More robust CFAR processors that are extensions of the Goldstein procedure have been analyzed.

The primary limitation on the detection performance of such a system is the effective signal-to-clutter that can be obtained. Present and planned tactical CFAR systems usually operate with a target-to-clutter ratio of 5 to 15 dB. As will be shown, even a small increase (3 to 5 dB) in signal-to-clutter ratio will have a large payoff in terms of detection performance.

It should finally be noted that any potential targets that pass the detection threshold of the above type of CFAR processor would be subjected to additional discrimination tests in order to further reduce the probability of false alarm and produce a final selected target. Such tests could include ranking by target-to-clutter ratio, target shape tests, length-to-width ratio tests, analysis of detection patterns

and edge detections, use of polarization discriminants, scene segmentation algorithms, taking another look at a finer resolution, and finally, scintillation vs. frequency tests.

All of these tests (except perhaps for the last one) will also be helped by any increase in effective target-to-clutter ratio that can be achieved. The majority of the research being conducted at the present time on signal processing for tactical missile seekers is in the area of target discrimination tests like those listed above. A large number of both analytically derived and heuristic algorithms are being tested using both simulated and live test data.

As shown in an article by Novak and Vote [6], many complex targets (assuming a narrowband waveform) may be characterized by a two-part statistical model. At any given aspect angle, the target radar cross section (RCS) exhibits a Rayleigh scintillation in amplitude while the average RCS over many aspect angles may be characterized by a log-normal density function. If a frequency diverse (and/or polarization diverse) pulse train is used to average out the Rayleigh scintillation component, then only the log-normal variation of average RCS with aspect angle remains. It is this component which dominates P_D - P_{FA} performance since the aspect angle at which the target will be viewed is almost always unknown. Thus P_D - P_{FA} performance predictions must be averaged over aspect angle. (This point will be discussed further in Section 3.7.)

Thus, the first way in which a large relative bandwidth waveform might assist the detection problem is in the elimination of the Rayleigh component of target fluctuation. Another way, which is probably of greater importance, is that such a waveform will result in an effective increase in target cross-section and an effective decrease in measured clutter cross-section (assuming the resolution cell size remains the same). The decrease in the reflection coefficient of clutter as

wavelength decreases is a well documented experimental fact as is the increase in target cross-section as the length of various structures on the target become comparable with the radiating wavelength. This effect will also be quantified in Section 3.0.

The overall effect of a wideband, non-sinusoidal waveform should therefore be an increase in the effective signal-to-clutter or target-to-clutter ratio. It is important to note that even a small increase (3 to 5 dB) in signal-to-clutter ratio will have a large payoff in terms of detection performance (i.e., present performance is below the "knee" of the detection curve). This can be seen on Figure 2-2 taken from the Goldstein paper which gives curves of P_D vs. target-to-clutter ratio, TCR, for three levels of P_{FA} . Log-normal clutter is assumed with a power (cross-section) mean-to-median ratio equal to $R=2.07$. A Rayleigh target is postulated in the cell under test. A very large number of auxiliary clutter cells are assumed so that there is no CFAR loss. The figure dramatically illustrates how difficult it is to detect a target in a severe clutter environment with small values of P_{FA} . This is a result which is well known to engineers who must design and develop CFAR processors to be used in a tactical environment. It is seen, for example, that for $P_{FA}=10^{-3}$, an increase of target-to-clutter ratio from 15 to 19.5 dB will increase P_D from 0.5 to 0.8. This increase in TCR will also improve the performance of non-parametric processors (i.e., those which utilize order statistics).

For the usual CFAR processor, a detection loss can be caused by non-homogeneous clutter in the auxiliary clutter cells used to determine the clutter statistics (and threshold). In general, the threshold does not raise fast enough in the vicinity of a clutter discontinuity so that false alarms are obtained along the clutter edge. In studies at MIT-Lincoln Laboratory [6,7], it has been found that the effects of clutter discontinuities can be decreased by the use of lead/lag CFAR

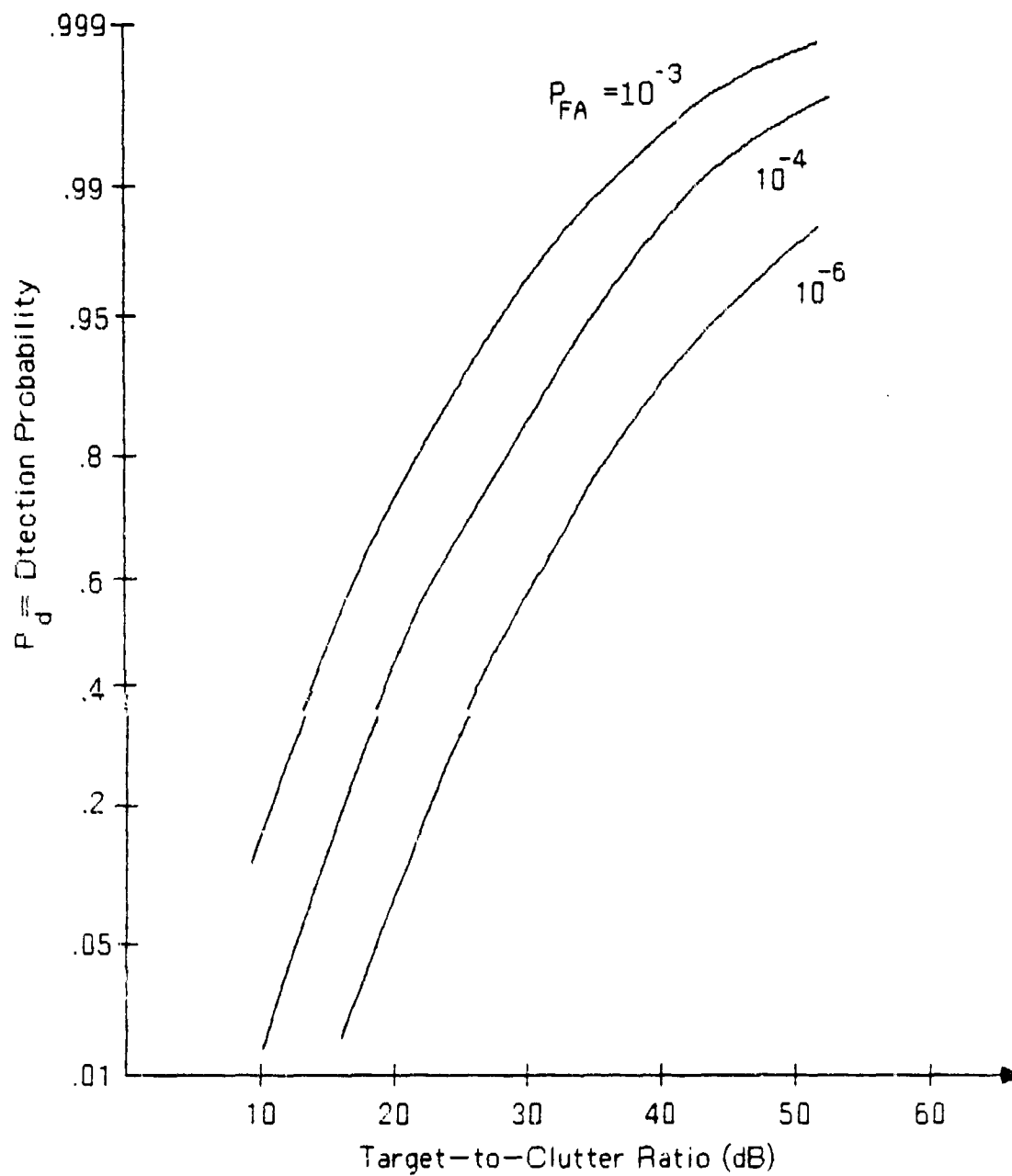


Figure 2-2. Probability of Detection Versus Target-to-Clutter Ratio for a Rayleigh Target in Log-normal Clutter

windows. These lead/lag techniques sense the presence of a clutter discontinuity and adapt the detection threshold accordingly. Such a technique should be even more effective when combined with the smoothing and reflectivity reduction that might be achieved by a wideband waveform.

2.2.2 MOVING TARGET DETECTION: MTI

Target motion information is obtained from two general classes of coherent radars - MTI and pulse Doppler. Although the distinction between these two types is somewhat hazy, the usual distinction is that an MTI radar normally operates with a pulse repetition frequency (PRF) that is low enough to avoid range ambiguities (accepting possible velocity ambiguities) while a pulse Doppler radar operates with a very high PRF that avoids all target velocity ambiguities (and nearly always has range ambiguities). The discussion of MTI systems will be in the general context of an airborne system. A hypothetical ground-based pulse Doppler system will then be discussed in slightly less detail in Section 2.2.3.

The Doppler spectrum seen by a moving airborne MTI radar is illustrated in Figure 2-3. The altitude line at the carrier frequency f_0 can be avoided by gating of the receiver. Assuming the antenna sidelobes are uniform, the sidelobe clutter will extend $\pm 2V/\lambda$ on either side of f_0 . The mainbeam clutter spike is the strong return from the mainbeam striking the ground. The width of the mainbeam clutter spectrum depends on a number of factors including antenna beamwidth, aircraft velocity, antenna look angle with respect to the velocity vector, type and rate of antenna scanning, rain clutter width and wind speed across the ground (causing an increase in the width of the internal clutter spectrum). Because the data is sampled at the PRF, there are replicas of the mainbeam region separated from f_0 by integer multiples of the PRF.

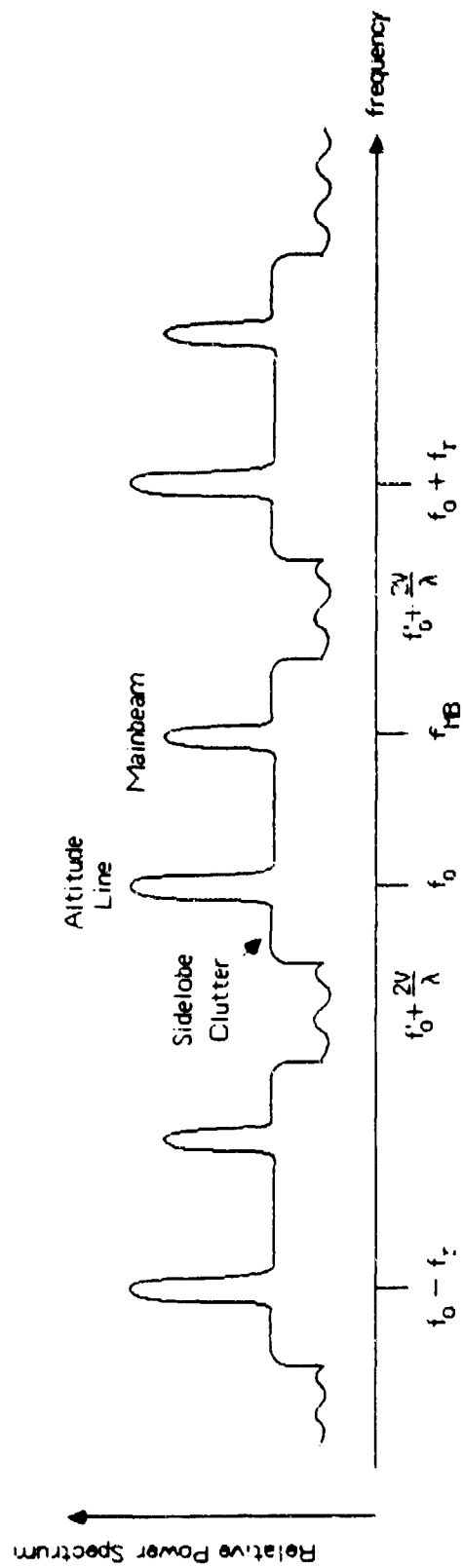


Figure 2-3. Doppler Spectrum Seen by MTI Receiver

bank of digital filters. The magnitude of the clutter return is usually much larger than the magnitude of the target return. Thus some type of filtering must be used to increase the effective processing gain. This is done by means of a clutter canceller after the signal is phase-detected. The theory behind such a canceller is that the successive returns from clutter will have the same phase while the successive returns from a target will have a phase shift caused by the component of target velocity in the direction of the radar. Thus, for example, a two-phase canceller which subtracts successive pulses will have only a very small (residual) output when clutter only is present and a much larger output when a moving target is present.

The canceller output is then passed through a Doppler filter bank. A system diagram is shown in Figure 2-4 where the MTI filter is a clutter canceller and Doppler filter. The returns from N pulse transmissions are processed by the FFT to provide N filter outputs covering the Doppler frequencies between zero and the PRF. The signal-to-noise ratio in each filter depends on the filter response and the clutter spectrum. Circuitry will offset the IF or RF frequency to center the clutter spectrum at zero frequency so that it can be removed by the pulse canceller.

The output of each of the Doppler filters is compared with a threshold. If the threshold is exceeded, it is assumed that a target is present, and a target will be indicated on the display for that range and azimuth position. If rain clutter is present in some of the filters, these filters can be desensitized.

Since the radar will detect only targets out of mainbeam clutter, the radar must have a long antenna and operate at a high frequency so that the Doppler shift of slowly moving targets will be outside mainbeam clutter. (Note however that the size of the aircraft carrying the radar

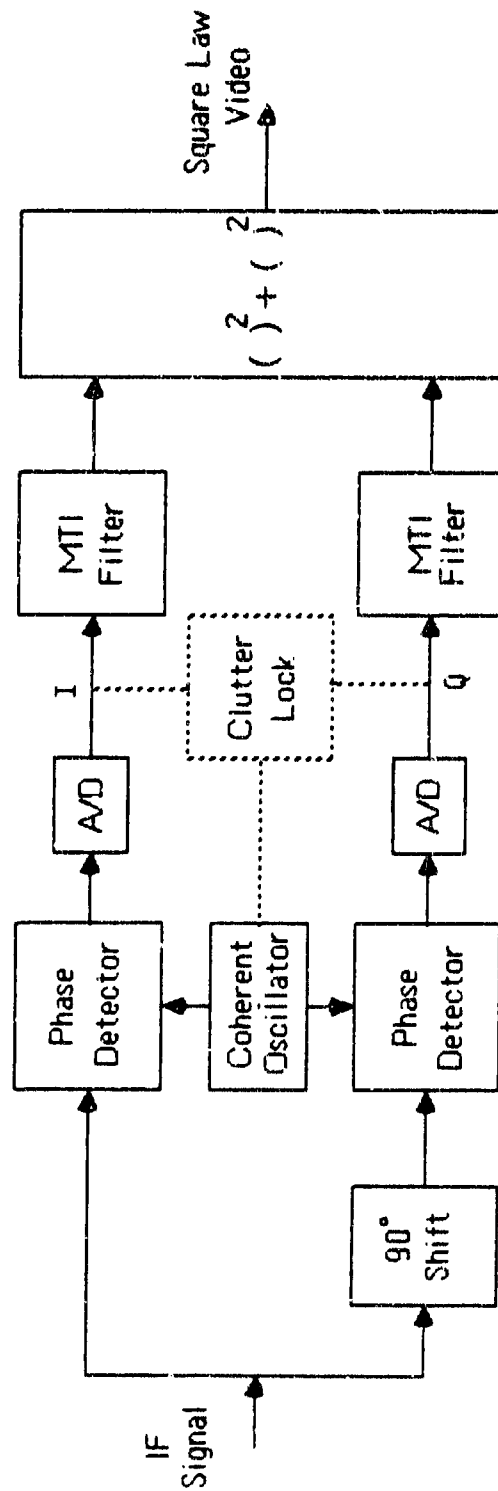


Figure 2-4. A Coherent MTI Implementation
(with square-law detector)

will impose important physical constraints on the antenna, prime power available, etc.) With a high operating frequency, rain clutter becomes significant.

The PRF is selected so that the unambiguous range will exceed the maximum surveillance range. At the high operating frequency of the radar, blind speeds will then occur within the ground target velocity spread expected. The PRF can be staggered to raise the lowest blind speed. The radar could transmit two bursts of pulses with different PRFs at one beam position or transmit pulse bursts with different PRFs on adjacent beam positions.

If we consider only mainbeam clutter, the signal-to-clutter ratio before MTI processing will be the ratio of the target cross section σ_t to the clutter cross section of a resolution cell given by

$$\frac{S}{C} = \frac{\sigma_t}{\phi \sigma_0 \rho \sec \delta R_0} \quad (2-2)$$

Typical values for these parameters are

$$\begin{aligned} \sigma_t &= 20\text{m}^2 \text{ (target cross section of a tank)} \\ \phi &= 0.01 \text{ rad (azimuth beamwidth} = 0.6^\circ) \\ \sigma_0 &= 0.03 \text{ (-15 dB, normalized clutter cross section)} \\ R_0 &= 10^5\text{m (range from aircraft to ground)} \\ \rho &= 10\text{m (range resolution)} \\ \sec \delta &\cong 1 \text{ (}\delta \text{ is depression angle)} \end{aligned}$$

for which $S/C = 0.07$ or -12 dB. Obviously, the S/C will be even smaller if targets with smaller σ_t are of interest.

Since a signal-to-clutter ratio of over 30/1 is typically needed for reliable detection, the MTI processing must improve the

With an airborne MTI radar, one attempts to center the mainbeam clutter spectrum in the notch at zero frequency in a Doppler filter bank by shifting an IF or RF frequency. Therefore, such a system attempts to filter out the mainbeam clutter by attenuating it in the stop band of a filter. If the mainbeam clutter spectrum is broad enough, it might also be necessary to ignore the output from the "lowest order" filters in the filter bank.

A major limitation of a conventional MTI radar is that the minimum detectable velocity is essentially governed by the antenna beamwidth. Only targets outside of the mainbeam clutter region will be detected. The equation for the ideal width of the clutter spectrum, Δf_d is

$$\Delta f_d = \frac{2V\phi \sin \theta \cos \delta}{\lambda} \quad (2-1)$$

where

- V = aircraft velocity,
- ϕ = antenna beamwidth,
- θ = squint angle from velocity vector,
- δ = depression angle,
- λ = wavelength.

A narrow azimuth beamwidth minimizes the clutter spread caused by platform motion. In elevation, the beam must be wide enough to cover the surveillance area, and the pattern is shaped to provide coverage over a range of depression angles.

Such a radar typically employs a linear FM waveform or some other form of pulse compression to obtain an adequate signal-to-noise ratio. At each beam position, the radar transmits a burst of pulses, and the returns are digitized and processed using digital techniques. The processor usually consists of a digital pulse canceller followed by a

signal-to-clutter ratio by about 27 dB to detect the target. A figure of merit, I , for an MTI system is the output target-to-clutter ratio divided by the target-to-clutter ratio at the input averaged over all target velocities.

Depending on the type of filter employed (two-pulse canceller, three-pulse canceller, digital canceller which employs feed-forward and feed-back), an overall improvement of 25 to 35 dB in the target-to-clutter-ratio can be achieved. Higher ratios are very difficult to achieve in a conventional operational system. Factors limiting improved performance include: Doppler filter straddling loss, increase in spectral width caused by platform motion and antenna scan motion, multipath loss, target fluctuation loss, timing jitter, pulse width variation, amplitude instability, second time around clutter, limiting in the receiver, and finally, noise quantization.

This means that such an MTI radar has another important limitation (in addition to a minimum target velocity) in that enough processing gain may not be available to see low cross-section targets embedded in harsh ground clutter. These limitations are discussed briefly in the following paragraphs.

The characteristics of the Doppler filter bank and the clutter spectrum affect the clutter improvement factor I . Figure 2-5a shows the frequency response of the Doppler filter bank as well as the clutter spectrum. Ideally, the control system would adjust the reference frequencies to center the clutter spectrum at zero frequency; however, there will normally be an error and the clutter spectrum will be offset from zero. A similar situation exists when a Doppler filter bank processes the data (see Figure 2-5b). As with the single filter, the clutter is moved into the notch at zero frequency. Although weighting will be applied to reduce filter sidelobes, the sidelobe level will limit the achievable value of I to something less than 40 dB.

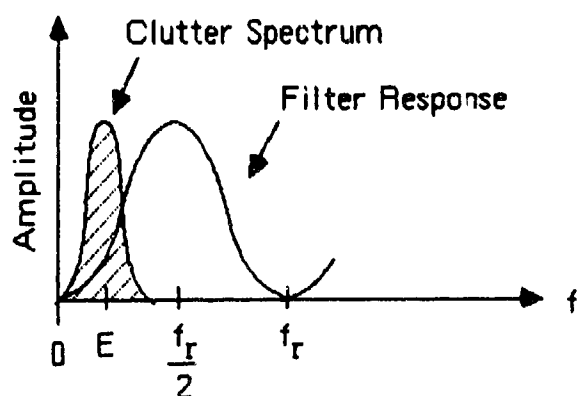


Figure 2-5a. The Effect of Doppler Offset Error E

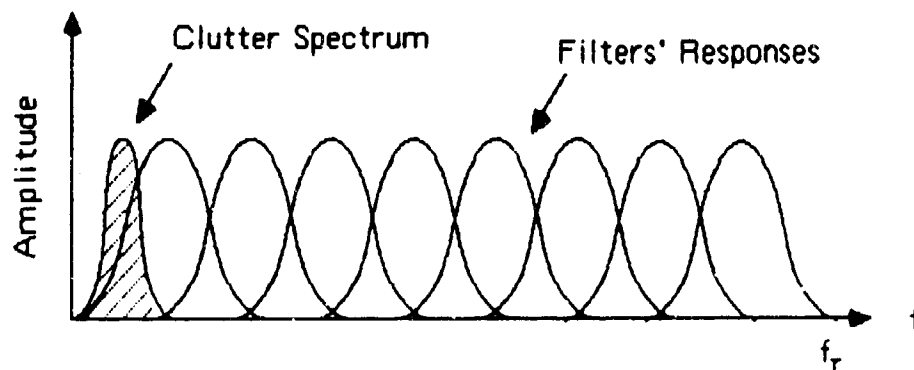


Figure 2-5b. Offset Error with a Digital Filter Bank

The clutter power in the antenna sidelobes also limits I because this power will be spread over Doppler frequencies between $\pm 2V/\lambda$. To achieve theoretical performance, there must be adequate short-term stability in the reference frequencies, the timing circuitry, and the signal processing circuitry; hence, system stability is another factor limiting I. The width of the clutter spectrum in the return depends on the antenna beamwidth and the aircraft velocity; the narrower the beamwidth and the slower the velocity, the narrower the spectrum. For the monostatic radar to do the job required, the moving targets of interest must lie outside the clutter in the mainbeam of the antenna.

When the targets of interest are inside the mainbeam clutter, displaced phase center antenna techniques (DPCA) are necessary [8]. These techniques require that the phase center of the antenna move toward the rear of the aircraft to compensate for the forward motion of the aircraft. Subtracting two successive pulses greatly reduces the clutter and permits the detection of targets with lower velocities. One DPCA technique uses an antenna with two different phase centers which can be switched in alternately from pulse to pulse. The conditions for cancellation are that the first pulse transmitted from the first phase center and the second pulse transmitted from the second phase center line up in the boresight direction and that the beams are matched. Another DPCA technique employs a two-lobe antenna pattern similar to a monopulse antenna with a sum pattern and a difference pattern, and the difference pattern is used to compensate for platform motions. Finally, it is possible to combine SAR and DPCA principles to achieve detection of even slower targets [9]. Significant clutter reduction (>80 dB) may be possible. It is also important to note that such systems are very complex, both in terms of hardware and signal processing.

Assuming the clutter is Gaussian, we can add the clutter power and noise power together to get the total background power which is Gaussian like noise. Standard curves for the detection of power targets in noise then apply. Let S/B be the signal-to-background power ratio. Then

$$\frac{1}{S/B} = \frac{1}{S/N} + \frac{1}{(S/C)I} \quad (2-3)$$

where S/N and S/C are the signal-to-noise and signal-to-clutter ratios respectively. (Usually the system is clutter limited and S/N can be neglected.) After S/B is calculated, the probability of detecting a target can be determined from standard detection curves or from equations.

A Swirling case I target model (scan-to-scan Rayleigh fluctuation in amplitude) is usually assumed. Figure 2-6 has plots of the probability of detection versus the signal-to-noise ratio (signal-to-background ratio for the case at hand). There are curves for several false alarm numbers. The false alarm number n' is the number of independent opportunities for a false alarm in the false alarm time. The false alarm time is the time during which the probability is 0.5 that there will be no false alarm. The false alarm probability P_{FA} is approximately

$$P_{FA} \approx \frac{0.693}{n'} \quad (2-4)$$

Examples of false alarm calculations are given in the section discussing pulse Doppler radars. After the signal-to-background ratio has been computed, the probability of detection can be read off of Figure 2-6 or calculated.

For each data cell, a threshold will be established and a detection will occur whenever the threshold is exceeded. The threshold settings will differ with the Doppler filter because there will be more clutter

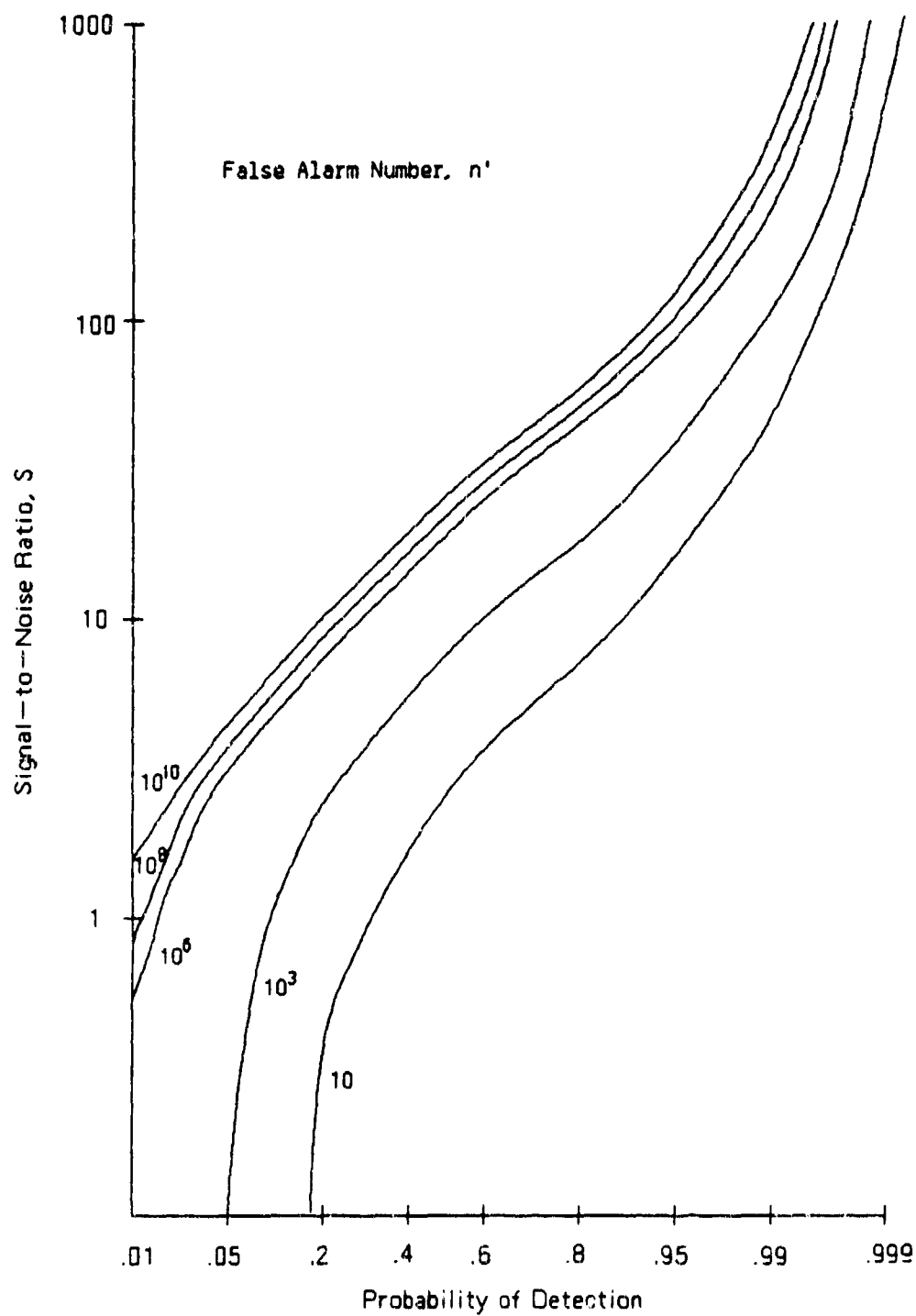


Figure 2-6. Probability of Detecting a Fluctuating Target
Cases 1 and 2
Pulses Integrated, $N = 1$

in the Doppler cells closest to the mainlobe clutter. The probability of detecting a Swerling case I target at a given slant range will depend on the radial velocity. The filter response varies with Doppler, and targets near zero velocity or the first blind speed will not be detectable. Since S/N and S/C are functions of the slant range, the probability of detection will vary with slant range for a constant radial velocity.

It is also possible to construct a non-coherent MTI system which essentially detects the beat frequency of the moving target and the clutter. Such a radar depends on a strong clutter return being present in the target cell and is not very effective in detecting moving targets against a low clutter background. The detection of moving vehicles on roads might be very difficult while the detection of airborne targets is generally impossible with a non-coherent MTI system. Another limitation of such non-coherent systems is that improvement factors are 3 to 5 dB lower than is the case with coherent MTI systems. This further reduces the possibility of seeing low cross-section moving targets.

2.2.3 MOVING TARGET DETECTION: PULSE DOPPLER

A pulse Doppler radar does not use a clutter canceller and, instead, uses the fact that a high PRF will separate the clutter and moving target frequency spectrums and prevent the target Doppler from being folded back into the clutter spectrum. A clutter rejection filter is used to separate the clutter and target returns. The output from each range gate is then passed through a bank of Doppler filters (which, for modern systems, is synthesized by an FFT operation). Each filter output is detected, non-coherently integrated, and finally thresholded to determine the presence of a target. A very understandable discussion of the performance of pulse Doppler radars is given by Meltzer and Thaler [10]. A schematic diagram of such a system is given in Figure 2-7.

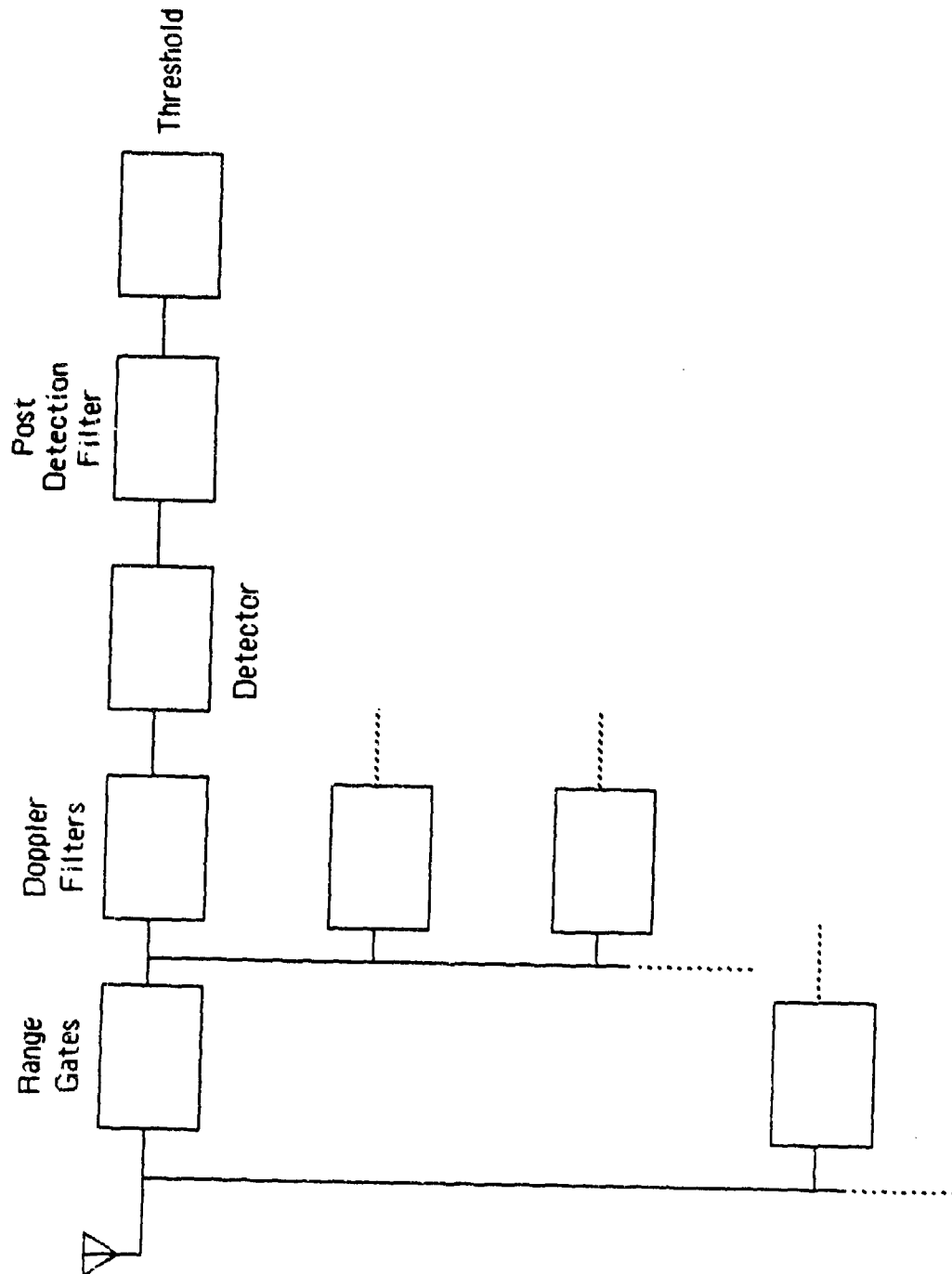


Figure 2-7. Block Diagram of a Pulse Doppler Receiver

To illustrate the uses and limitations of this concept, a ground-based radar will be hypothesized. A typical next generation ground-based SAM radar could have the following characteristics:

$$PRF = \begin{cases} 15,000 \text{ pps, search mode} \\ 100,000 \text{ pps, track mode} \end{cases}$$

center frequency, $f_0 = 3 \text{ GHz}$,
wavelength, $\lambda = 0.1\text{m}$,
azimuthal beamwidth, $BW = 10^\circ$
antenna scan rate, $SR = 180^\circ/\text{sec}$.

The radar is designed to detect aircraft and helicopters flying at tree-top altitude and against a foliage background. Another requirement is that such a system be capable of detecting sensors on helicopter hubs when the main body of the helicopter is beneath the tree tops. It is desired that the system have a range of about 35 km.

One minor limitation of this type of pulse Doppler system is that it is range-ambiguous. This can be corrected, however, by the use of multiple PRF's that are staggered from one burst of pulses to the next. For the hypothesized system, the unambiguous range, R_{amb} , has the values

$$R_{amb} = \frac{c}{2(PR F)} = \begin{cases} 10^4 \text{ m (Search Mode)} \\ 1500 \text{ m (Tracking Mode)} \end{cases}$$

The first blind speed, V_b , for this radar occurs at

$$V_b = \frac{\lambda(PR F)}{2} = 750 \text{ m/s}$$

and all radial velocities smaller than this are velocity unambiguous.

The number of pulses, N , which illuminate a target during an antenna scan is approximately given by

$$N = \frac{BW}{SR} \times PRF = 830.$$

It is postulated that a three PRF technique will be used to resolve range ambiguities where the PRF's are related by the ratios of closely spaced, relatively prime, integers. This means that approximately $N/3$ of the pulses per target scan will be at each PRF. For this reason, it will be assumed that the number of pulses at each PRF, denoted by N_p , which illuminate the target during a target scan, has the value

$$N_p = 256$$

This is the number of pulses that are coherently integrated by the Doppler filter.

The overall probability of detection, P_D , per scan depends on how the probabilities for each PRF are combined. For example, if the target must be detected by each of the three PRF groups, then the overall probability of detection per scan, $\overline{P_D}$, is given by

$$\overline{P_D} = (P_D)^3$$

Thus, if $P_D=0.99$, it follows that $\overline{P_D}=0.97$.

The probability of false alarm, P_{FA} , is the false alarm per threshold test. For purposes of illustration, a value of $P_{FA} = 5 \times 10^{-6}$ will be chosen. Thus, if there are M Doppler filters tested per range gate (resolution cell) and the filter outputs are independent, then it follows that the false alarm probability, $\overline{P_{FA}}$, per range gate tested (which is defined as the probability that at least one of the filter clutter noise outputs for one of the PRF groups exceeds a threshold) is

given by

$$\overline{P_{FA}} = 1 - (1 - P_{FA})^{3M} \approx 3MP_{FA}$$

The approximation holds since P_{FA} is usually a very small number.

For example, suppose the radar is scanning over a complete 360° circular sector which corresponds to approximately 36 independent range strobes since the azimuth beamwidth during search is 10° . A range resolution of about 1,500m in the search mode is assumed. If the range from 5 to 35 km is being searched for targets, then there are approximately 20 cells or range gates per strobe or about 720 independent cells per 360° sector. Finally, this corresponds to approximately

$$E_{FA} = 760 \overline{P_{FA}} \approx 760 (3M) P_{FA}$$

expected false alarms per rotation (i.e., every 2 sec).

As an example, assume that velocity will be coarsely quantized in the search mode of operation and a value of

$M = \text{number of Doppler filters per range gate} = 3,$

will be chosen for illustration. If a value of $P_{FA} = 5 \times 10^{-6}$ is chosen as the operating point, then the expected false alarm rate is

$$E_{FA} = 0.03 \text{ expected false alarms every two seconds.}$$

This corresponds to about 1 expected false alarm every minute. The verification of a detection before going into a tracking lock-on can be accomplished by requiring a detection at the "same" place on two

consecutive scans. This will lower the overall detection probability discussed above (0.97 per second) to a value of 0.94, which is the probability of getting a detection on two consecutive scans.

The false alarm number associated with P_{FA} is given by

$$n' \cong \frac{0.693}{P_{FA}} \cong 1.95 \times 10^5$$

As before, the signal-to-clutter ratio before MTI processing is given by

$$\frac{S}{C} = \frac{\sigma_t}{\phi \sigma_0 R \rho \sec \delta}$$

where

- $\sigma_t = 5m^2$ (helicopter hub cross section)
- $\phi = 0.17$ rad (azimuth beamwidth = 10°)
- $\sigma_0 = 0.03$ (-15 dB, normalized clutter cross section)
- $R = 10^4 m$ (range to target)
- $\rho = 1,500m$ (range resolution in search mode)
- $\delta = 0^\circ$ (depression angle)

This results in a signal-to-clutter ratio equal to

$$S/C = 6.5 \times 10^{-5} \text{ or } -42 \text{ dB.}$$

With a 50 dB improvement factor, this is equivalent to an 8 dB signal-to-clutter ratio after Doppler processing; while a 60 dB improvement factor results in an 18 dB signal-to-clutter ratio after processing.

Using the graph of P_D vs S/N given in Figure 2-6 with $P_{FA} = 5 \times 10^{-6}$, the result is

$$P_D = .25, \text{ for } I = 50 \text{ dB,}$$

and

$$P_D = .85, \text{ for } I = 60 \text{ dB.}$$

It would be noted that these are the probability of detection for a single scan (every 2 sec). Thus, for example, the probability of obtaining a detection within 5 scans (10 sec) is

$$P_D (5 \text{ scans}) = 0.76, I = 50 \text{ dB},$$

$$P_D (5 \text{ scans}) = 0.99, I = 60 \text{ dB}.$$

For future pulse Doppler radars, the improvement factor is in the range of 45 to 55 dB and 50 dB is a reasonable operational number. Experimental systems are under development to achieve an improvement factor as large as 60 dB. Thus, the hypothetical system is pushing the state-of-the-art. The limitations on the achievable value of I are: waveform stability and purity requirements, sidelobe clutter, various types of spurious modulation that can appear on the received signal, power supply and line ripple, pulse-to-pulse random modulation which causes clutter spreading, limiting in the receiver, and finally, noise quantization.

The biggest limitation is the stability requirement. The reference frequencies, timing signals and signal processing circuitry must have adequate short-term stability. The most severe stability requirement relates to the generation of spurious modulation sidebands on the mainbeam clutter which can appear as targets. Ways to reduce phase noise and increase component stability are the primary areas where pulse Doppler research is being conducted.

A number of loss factors are present that limit the improvement factors that can be obtained, such as eclipsing and range-gate straddling, multipath loss, target fluctuation loss, clutter power from range ambiguous areas, CFAR loss, and beam shape factor.

Because the receiver is gated off during the transmission time, targets received at this time are also blanked or "eclipsed". The multipath loss is caused by multipath cancellation effects that are present at small antenna elevation (or depression) angles when the antenna is pointed close to the horizon. The loss caused by clutter power obtained from range ambiguous areas must also be included. For example, suppose the target is located at a range of 20 km from the radar which is twice the ambiguous range for the search mode. This means that during the search mode, the target power must compete with the mainbeam clutter coming from both a range of 10 km and 20 km.

Another limitation of a pulse Doppler system is that monopulse is very difficult to mechanize. This is caused by the problem of matching multiple receiver channels. These receivers each must contain clutter rejection filters and must be phase-matched to permit proper tracking.

2.2.4. LOW ANGLE TRACKING

A number of techniques are available for the angle tracking of targets. The major categories are:

- 1) Amplitude comparison monopulse,
- 2) Simultaneous lobing,
- 3) Sequential lobing,
- 4) Conical scan.

Each method produces a target angle estimate relative to an antenna boresight position. This estimate is usually used to drive antenna gimbals (or phase shifters) so as to reduce the error between the target direction and boresight. The first two methods involve multiple squinted receive channels where the receive signal from multiple receive beams is simultaneously processed and an angle estimate formed. The second two methods are sequential in nature where returns separated in time are

processed from two or more squinted beam positions and the error angle obtained.

Thus, the second two methods are more sensitive to target cross-section fluctuations which might occur between pulses used to form the angle estimate. The radar has no way of knowing whether a reduction in received power between pulse positions is due to a cross-section fluctuation or is due to the target being further off boresight.

A monopulse system has both the theoretical and practical capability to make more accurate measurements than the other angle measurement schemes. The variance of the estimated angle is approximately 3 dB less under conditions of equal integrated signal-to-noise ratio and optimal beam cross-over points. The monopulse technique also has an inherent capability for high-precision angle measurement because its feed structure is rigidly mounted with no moving parts. Most other systems move the feed to produce the required squinted beams.

The theoretical standard deviation of all four estimates (for large signal-to-noise ratios) has the form

$$\sigma_{\theta}^2 = \frac{\tau \theta_B}{k_s \sqrt{S/N}}$$

where τ is a constant depending on the type of system (varying between 1 and 3); θ_B is the one-way half power beamwidth, k_s is a constant determined by the slope of the antenna gain pattern at the beam cross-over points, and S/N is the integrated signal-to-noise ratio over the number of pulses used to form the estimate.

All four types of angle trackers are almost equally susceptible to glint and multipath. Here, the term glint refers to the wander of the apparent center of reflection of the target due to relative phasing effects between the scattering centers making up the target. All four methods are vulnerable to angle capture which means that the boresight will tend to track the largest scatterer (if it is significantly larger). The effect of target glint is to add an additional variance factor to the angle estimate.

Finally, all four systems are vulnerable to multipath which is caused by the receive signal being received from two paths - one direct and one via a bounce from the surface of the earth. This also adds an additional variance and bias terms on the angle estimate which depends on (1) beamwidth, (2) ground reflectivity, and (3) relative sidelobe attenuation between the two paths.

A tremendous number of papers have been written on the effect of multipath and on various schemes for reducing multipath. For certain ground-based radars (such as FAA radars, for example), the best schemes appear to be a combination of very careful radar placement along with the use of clutter fences and ground planes.

Theoretically, one should be able to use multiple receive ports to sort out the direct and reflected paths. These methods are based on treating multipath as a second radar target and developing a two-target signal processor to analyze the combined waves and sort the direct from the reflected signal. The normal monopulse system, which is a one-target processor, cannot develop sufficient information to separate the two waves on a single pulse basis (monopulse). References 10-13 contain a description of the major concepts and simulation results.

The most modern method that is being tried to minimize multipaths is the use of very high frequencies (35 or 94 GHz) for relatively short range, ground based radars. The narrow beamwidths that result will very efficiently reduce multipath effects (unfortunately, such frequencies have a large attenuation factor in rain). Many organizations are working on millimeter wave monopulse feeds and receivers.

Multipath is by far the major item which limits monopulse performance. When it is not present, tracking accuracies of 1/15 to 1/20 of a beamwidth are routinely accomplished. The use of a wide bandwidth waveform that is linear or square-law detected, plus non-coherent integration, will reduce the effect of glint.

2.3 CONCLUSIONS

It was shown that the detection of targets in clutter is well studied and therefore understood for contentional radar designers. Both system level constraints and fundamental limitations were presented in the context of an airborne MTI and ground-based pulsed Doppler radar design. Performance improvements needed to detect next generation threats will require large processing gains (improvement factors) that range from 60 - 80 dB. These gains will not come about without significant hardware improvements. Thus, it seems that an investigation of alternate radar architectural paths, such as NSR, does seem warranted. The next section develops a generalized, wideband radar model to formally investigate the problem of target detection in clutter.

3.0 THEORY OF WIDEBAND RADAR DETECTION

3.1 SECTION SUMMARY

A radar detection system is modeled with attention paid to modeling all frequency-dependencies of devices, antennas, propagation, and scattering. The receiver and signal are selected optimally according to the Neyman-Pearson criterion. All operations are assumed linear and time-invariant (except, of course, the decision rule implementation in the receiver/processor).

The signal design problem, in this context, is to choose, as it turns out, the most favorable signal spectrum modulus; this was done under the assumption of constrained signal energy. The actual computation of the signal spectrum modulus in a particular instance requires numerical procedures; the method of bisection was implemented to do this.

Based on the one-shot (single pulse) results for a particular set of radar system parameters and models for the scattering by object and background, it appears that, at modest but acceptable (in performance) energy levels, the optimum signal spectrum modulus tends to have a narrow support, near a "resonance" of the scatterer. At rather high energy levels, apparently well beyond that required for satisfactory detection performance, the signal spectrum modulus can be of a broad support, possibly in separate "pieces" (sets) corresponding to "resonances" of the scatterer. However, this result is strongly dependent on the assumed antenna and target response characteristics. Additional energy/pulse duration constraints were included for optimum design of periodic waveforms, with the same general trends still remaining true. Finally, propagation media dispersion was shown to have a strong effect on the overall optimum signal spectrum.

A clutter/background model was incorporated as derived from a "two-scale" electromagnetic approximation. Assuming only a "five-scale" background, the clutter spectral density for this system follows a k^5 law; this has a dominant effect on the optimum signal spectrum modulus nature.

A singularity expansion method (SEM) based model was used for the scatterer wavenumber - dependent scattering. The information given by the SEM method does not, however, completely describe the scattering phenomenon.

In Appendices A and B, it is recalled that: (1) complex exponential (sinusoids) are the natural invariants of linear, time-invariant systems and hence the Fourier integral (transform) representation of a signal is a naturally powerful analysis tool; (2) the specific choice of a "carrier" frequency is completely arbitrary; however, once chosen, the resulting complex envelope representation is then unique, under a certain condition; (3) more generally, linear, time-variant systems ("operators") each have, generally, their own "generalized eigenvectors" and appropriate or natural "operational calculus", e.g., a certain time-variant, linear, ordinary "differential equation" operator is naturally associated with the Walsh functions.

3.2 RECEIVED SIGNAL MODEL

We consider a radar system geometry as sketched in Figure 3-1. It is a monostatic configuration, with the "radar set" and "object" in their mutual far-fields. We will review a model derivation for the received signal waveform at the antenna terminals, given a transmitted waveform of arbitrary shape. All transformations of fields and waveforms are assumed linear and time-invariant; therefore, sinusoids are invariant, being changed only in relative phase and magnitude, upon passage through the system (Appendix A).

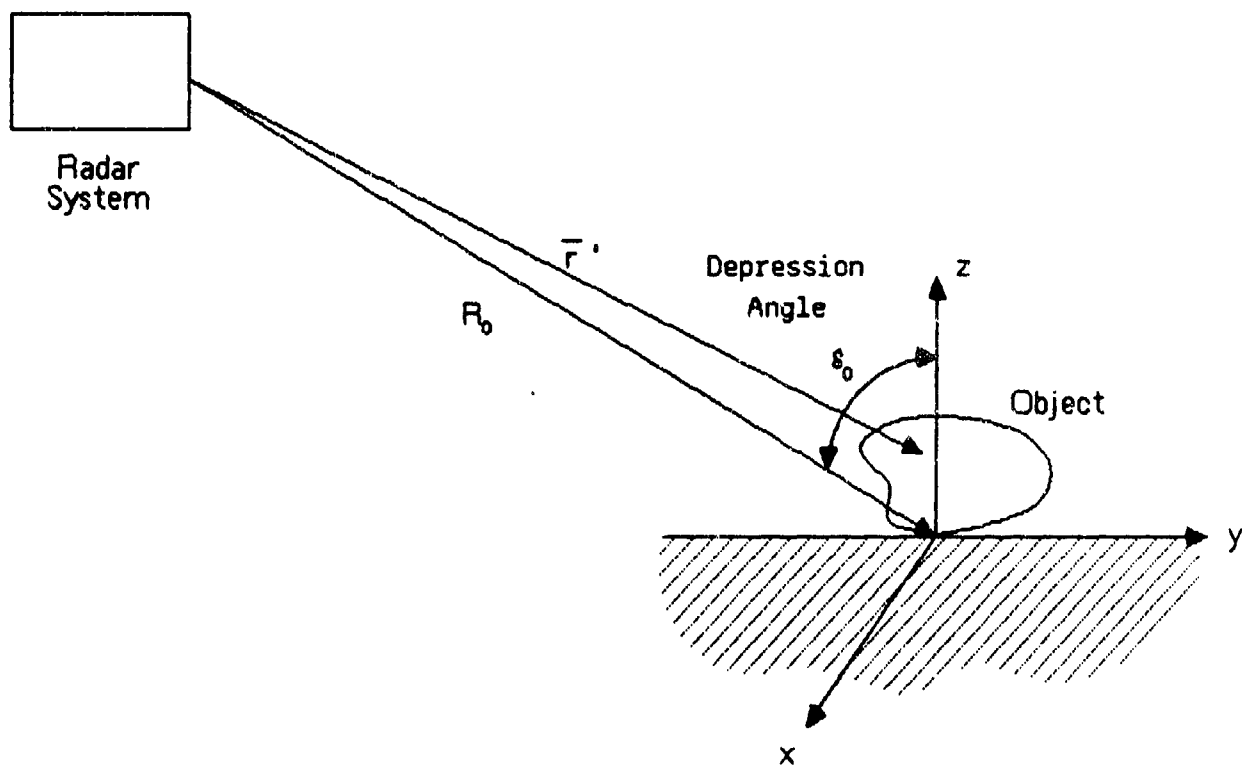


Figure 3-1. Radar System Geometry

This received waveform has in fact already been described in [14], ignoring some frequency dependent aspects that we do now wish to include. From page 63, Equation 3.6 of [14], the received waveform, for a transmitted waveform $\exp(-i\omega t)$, is (we consider at this point only scalar fields)

$$u(t; \omega) = \tilde{u}(0; \omega) e^{-i\omega t}$$

where

$$\tilde{u}(0; \omega) = \left(\frac{ik}{4\pi R_0} \right)^2 \iint dx dy \exp[i2ky \sin \delta_0] \mathcal{G}(x, y; k) g(x, y; k) \quad (3-1)$$

and

$$\mathcal{G}(x, y; k) = \exp[ik(x^2 + (y \cos \delta_0)^2)/2] \tilde{E}_0^2(kx/y', ky/y'; \omega)$$

and $y' = R_0 + y \sin \delta_0$, with $k = 2\pi/\lambda$.

Here \tilde{E}_0 is the (two-dimensional) Fourier transform of E_0 , an antenna aperture illumination and g is the "reflectivity density" characterizing the scene. For proper energy normalization, $\iint_A |E_0(x, y)|^2 dx dy = 1$. The reflectivity density g is defined simply as the multiplicative relation between the incident and scattered fields. This appears to be a sufficiently robust concept and is determined generally by the methods of electromagnetic scattering theory.

In the above development, the transmission medium is assumed to be free space and no transmitting and receiving antenna frequency dependencies are explicitly given, though they are implicit in E_0 's dependence on ω . The result will later be extended to include dispersive media in Section 3.6.

We may imagine the aperture field E_0 being created formally as in Figure 3-2. We assume that a plane PP' is definable, across which we denote the radiating field as $E_0(\bar{r}, t; \omega)$. When $v(t) = \exp(-i\omega t)$, then using the notation of Appendix A

$$E_0(\bar{r}, t; \omega) = E_0(\bar{r}, 0; \omega) e^{-i\omega t}, \quad \bar{r} \in PP'. \quad (3-2)$$

In order to proceed, we make the crude but useful approximation

$$E_0(\bar{r}, 0; \omega) = \tilde{a}_t(\omega) E_0(\bar{r}). \quad (3-3)$$

That is, we assume that factoring the frequency and spatial dependencies is possible. Conceptually, the analysis is easier but at very large relative bandwidths, this may be untenable. Similarly, upon reception, the received scattered field will produce a voltage at the antenna terminals, the mapping again depending on a frequency-dependent transfer function, which may be denoted $\tilde{a}_r(\omega)$. We incorporate these frequency dependencies by setting

$$u(t; \omega) = \tilde{a}(\omega) \tilde{u}(0; \omega) e^{-i\omega(t-2R_0/c)}, \quad (3-4)$$

where

$$\tilde{a}(\omega) = \tilde{a}_r(\omega) \tilde{a}_t(\omega).$$

With such a model, in any specific instance, the quantities E_0 , g , \tilde{a}_r , and \tilde{a}_t must be determined in some manner.

An alternative, more rigorous description has been derived and is presented in Appendix C. Instead of assuming an aperture is definable, the far field is described in terms of vector moments of electric and magnetic antenna currents distributed over a volume, which led to the notions of a "pattern factor" and a "vector effective height" for describing the transmitting and receiving transfer functions of an

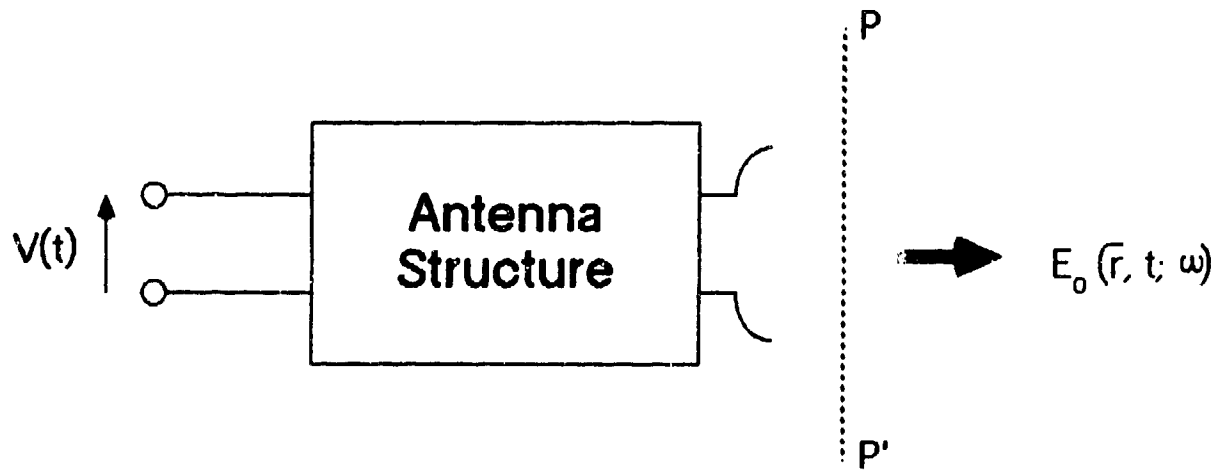


Figure 3-2. Antenna Aperture Field Generation Model

antenna. Furthermore, rather than employ a reflectivity density, a (dyadic) scattering matrix is used in the derivation. It, too, is a linear pointwise relation between incident and scattered fields. Finally, the formulation in Appendix C is in vector form, while the results of this section represent a single scalar component. This more detailed model of antenna reception and transmission transfer functions is developed by considering Thevenin equivalent circuits for the source generator and load impedance. Implicit in the model, nonetheless, are the same types of calculations required for specific antennas as used herein. It is probably fair to say that the "quasi-optical" aperture field approach will prove more directly applicable at higher frequencies for aperture antennas, while the "equivalent circuit/ antenna current" approach may be more amenable in describing low-frequency, wire-like structures. Further research is required to develop insight into the differences between the two modeling approaches.

3.2.1 NON-SINUSOIDAL TRANSMITTED WAVEFORM

If an arbitrary waveform $f(t)$, with Fourier integral/transform representation

$$f(t) = \frac{1}{2\pi} \int_{-\infty}^{+\infty} e^{i\omega t} \tilde{f}(\omega) d\omega \quad (3-5)$$

is actually transmitted instead of a complex exponential, then, by the linearity assumed everywhere, the corresponding received "non-sinusoidal" waveform is given simply by the superposition principle, namely

$$\begin{aligned} s(t) &= \frac{1}{2\pi} \int_{-\infty}^{+\infty} u(t; \omega) \tilde{f}(\omega) d\omega \\ &= \frac{1}{2\pi} \int_{-\infty}^{+\infty} e^{-i\omega(t-2R_0/c)} \{ \tilde{a}(\omega) \tilde{f}(\omega) \tilde{u}(0; \omega) \} d\omega. \end{aligned} \quad (3-6)$$

where c is the free space speed of light. (Note that this is not the conventional inverse Fourier transform used in communication theory, which employs the "kernel" $\exp(i\omega t)$, not $\exp(-i\omega t)$.) Similarly, if $F(t)$ is a "complex envelope representation", corresponding to a real waveform

$$f(t) = \text{Re} \left\{ F(t) e^{i\omega_c t} \right\},$$

where ω_c is a "carrier" frequency, the corresponding real received waveform is

$$s(t) = \text{Re} \left\{ u(t; \omega) e^{i\omega_c t} \right\}$$

with the complex envelope representation

$$s(t) = \frac{1}{2\pi} \int d\omega e^{i\omega(t-2R_o/c)} \left\{ \tilde{a}(\omega) \tilde{f}(\omega) \tilde{u}(o; \omega) \right\} \bigg|_{\omega \rightarrow -(\omega + \omega_c)} \quad (3-7)$$

3.2.2 SCATTERING REFLECTIVITY MODELS

We suppose that g is the superposition of two parts, a g_{ob} describing a scattering object whose presence (or not) is to be decided, and a background, or clutter, described by g_{cl} . Correspondingly,

$$\tilde{u}(o; \omega) = \tilde{u}_{ob}(o; \omega) + \tilde{u}_{cl}(o; \omega). \quad (3-8)$$

3.2.2.1 CHARACTERIZATION OF TARGET OBJECT

As is usually true, and assumed herein, the spatial extent of the object is sufficiently restricted so that

$$\tilde{u}_{ob}(0; \omega) = \left(\frac{ik}{4\pi R_0} \right)^2 \tilde{E}_0^2(0, 0) \iint_{S_{ob}} e^{i2kr'} g_{ob}(\bar{r}'; k) d\bar{r}' \quad (3-9)$$

where r' is the distance from the radar to the point \bar{r}' on the object's surface.

Recalling the normalization of E_c just mentioned,

$$\tilde{E}_0(0, 0) = \iint_{\substack{\text{antenna} \\ \text{aperture}}} E_0(x, y) dx dy = \int_{D_y} dy \int_{D_x} dx \frac{1}{\sqrt{D_y D_x}} = \sqrt{D_y D_x} = \sqrt{\mathcal{A}}$$

where \mathcal{A} is the effective aperture area.

Therefore

$$\tilde{u}_{ob}(0; \omega) = \left(\frac{ik}{4\pi R_0} \right)^2 \mathcal{A} \iint_{S_{ob}} e^{i2kr'} g_{ob}(\bar{r}'; k) d\bar{r}'. \quad (3-10)$$

It may be convenient at this point to mention the connection with the radar scattering cross-section (RCS), normally defined for historical reasons, for a scattering object. As in many other radar systems, the RCS alone does not sufficiently characterize a scatterer. Here, we shall find that more information is required to construct the optimal receiver, specifically, the matched filter. However, it does turn out that the optimal signal and the system detection performance depend only on the modulus-square of the (frequency-dependent) scattered field. In this case, a direct relation to the RCS is possible and useful because of the empirical data available concerning this parameter.

The RCS is defined to be

$$\sigma = 4\pi R_0 \frac{|E_s|^2}{|E_f|^2} \quad (3-11)$$

where E_f is the far-field incident on the object and E_s the received scattered field. It is easily seen from the calculations summarized above that

$$\frac{E_s}{E_f} = \frac{E_s}{\left(\frac{-ik}{4\pi R_0}\right) \tilde{E}_0(o,o)} = \left(\frac{-ik}{4\pi R_0}\right) \iint_{S_{ob}} e^{ikr'} g_{ob}(\bar{r}'; k) d\bar{r}' \quad (3-12)$$

and hence that the RCS

$$\sigma = k^2 \left| \iint_{S_{ob}} e^{i2kr'} g_{ob}(\bar{r}; k) d\bar{r}' \right|^2. \quad (3-13)$$

As inferred, we shall refer to this form later.

Now suppose that the object's surface, S_{ob} , is defined by the relation

$$F_S(x,y,z) = z - f_S(x,y) = 0, (x,y) \in P_{cb},$$

where P_{ob} is the projection of S_{ob} onto the (x,y) -plane (see Figure 3-3).

Then completing the x -integration in (3-10), we obtain

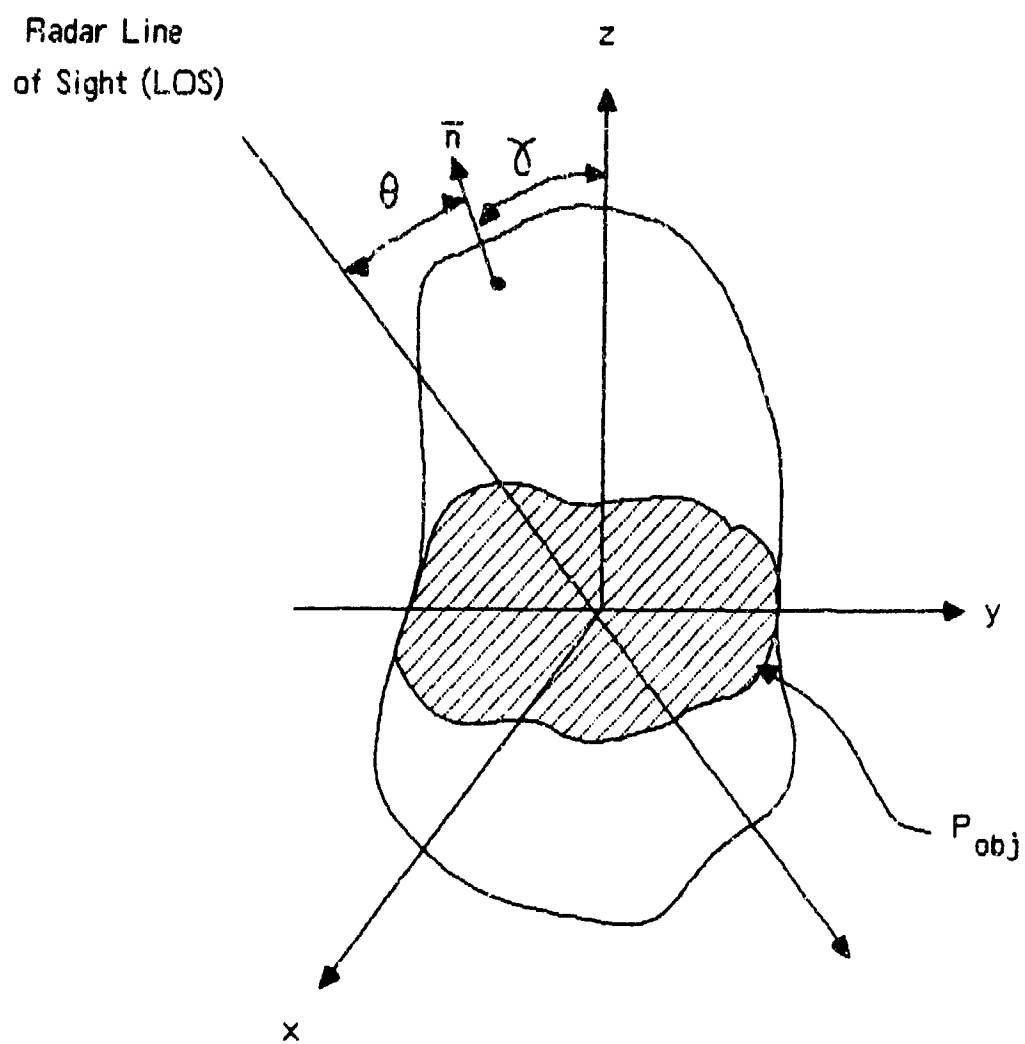


Figure 3-3. Scattering Object Geometry

$$\tilde{u}_{ob}(0; \omega) = \left(\frac{ik}{4\pi R_0} \right)^2 \mathcal{A} \int_{p_y} e^{i2ky \sin \delta_0} \Gamma(y; k) dy \quad (3-14)$$

where

$$\Gamma(y; k) = \int dx g_{eff}(x, y; k) \sec \gamma(x, y).$$

If, over a range of k of interest, $(ik/4\pi R_0)^2$ and Γ do not vary significantly from the value at, say, k_0 , then the relation for $\tilde{u}_{ob}(0; \omega)$ first above is a Fourier transform relation and we have

$$u_{ob}(0; \tau) = \left(\frac{ik}{4\pi R_0} \right)^2 \mathcal{A} \left(\frac{c}{2 \sin \delta_0} \right) \Gamma \left(\frac{ct}{2 \sin \delta_0}; -k_0 \right) \quad (3-15)$$

However, this form is not of immediate interest here, as we definitely want to observe the effect of the k -dependence of Γ and g .

The singularity expansion method (SEM) [15,16] can be of some assistance in characterizing the scattering from objects of interest here. It has been asserted, on the basis first of empirical evidence and later some theoretical support, that a class of scatterers can be characterized by their set of "poles" associated with their transient response. This is a useful categorization method because these poles appear to be rather independent of aspect angle.

Viewing the transient response's transform as a partial fraction expansion, the poles are explicit; however, the weights given to each such contribution (term) determine the zeros of this transform and these weights, hence zeros, apparently generally do depend upon aspect angle.

Since here we are interested in the wave-number, or frequency, response of a scatterer, we must know both pole and zero locations;

therefore, knowledge of the poles alone provides insufficient information for us here. However, for simplicity, we will later assume a specific pole/zero pattern in order to obtain a numerical frequency dependence for a target's cross section.

3.2.2.2 CHARACTERIZATION OF CLUTTER

In order to quantify the effect of clutter, we must examine the clutter contribution to $\tilde{u}(o; \omega)$, namely

$$\tilde{u}_{c1}(\sigma; \omega) = \left(\frac{ik}{4\pi R_0} \right)^2 \iint dx dy e^{ik2y \sin \delta_0} \mathcal{G}(x,y; k) g_{c1}(x,y; k). \quad (3-16)$$

There are two major problems involved. First, the clutter reflectivity, g_{c1} must be characterized using electromagnetic scattering theory, over a very broad range of k , for interesting background scenes. (This is viewed as fundamentally important.) Second, there is a requirement to clarify the effect of antenna pattern variation, via \mathcal{G} , over a very large range of k . (This is considered a tedious analysis problem.)

To see how the often-employed "convolution model" is obtained is initially helpful, though it is not sufficiently general for us here. If the spectrum of the transmitted waveform is sufficiently narrow, say about k_0 , then, in $\tilde{u}_{c1}(o; \omega)$ above, we may replace k by k_0 everywhere except in the phase $2ky \sin \delta_0$. We then get the Fourier transform relation

$$u_{c1}(o; \omega) = \left(\frac{ik_0}{4\pi R_0} \right)^2 \left(\frac{\pi c}{\sin \delta_0} \right) \left(\frac{1}{2\pi} \right) \int d\tau e^{i\omega\tau} G \left(\frac{c\tau}{2 \sin \delta_0}; k_0 \right) \quad (3-17)$$

where

$$G(y'; k_0) = \int_{-\infty}^{+\infty} dx' \mathcal{E}(x', y'; k_0) g_{c1} \left(\frac{ct}{2 \sin \delta_0}; k \right).$$

Therefore,

$$u_{c1}(0; t) = \left(\frac{ik_0}{4\pi R_0} \right)^2 \frac{\pi c}{\sin \delta_0} G \left(\frac{ct}{2 \sin \delta_0}; k_0 \right). \quad (3-18)$$

Using (3-18) and (3-7), we now have a simple linear system (convolutional) model as illustrated in Figure 3-4.

In order that G be a sample function from a wide-sense stationary random process, a very convenient property for subsequent analysis, we require the following correlation (covariance) to be a function of (t_1, t_2) only as $|t_1 - t_2|$:

$$\begin{aligned} E[G(y'; k_0) G^*(y''; k_0)] &= \iint dx' dx'' \mathcal{E}(x', y'; k_0) \\ &\quad \mathcal{E}^*(x'', y''; k_0) R_g(x' - x'', y' - y''; k_0) \end{aligned} \quad (3-19)$$

where we have made a simplification of variables $y = \frac{ct}{2 \sin \delta_0}$.

Here we assumed the clutter field $g_{c1}(x', y'; k_0)$ is homogeneous with covariance function R_g .

Suppose that $\{g_{c1}\}$ is, for wavenumbers of interest, "white", that is,

$$R_g(\cdot) = \frac{n_g}{c} \frac{2 \sin \delta_0}{c} \delta(x' - x'', t_1 - t_2) \quad (3-20)$$

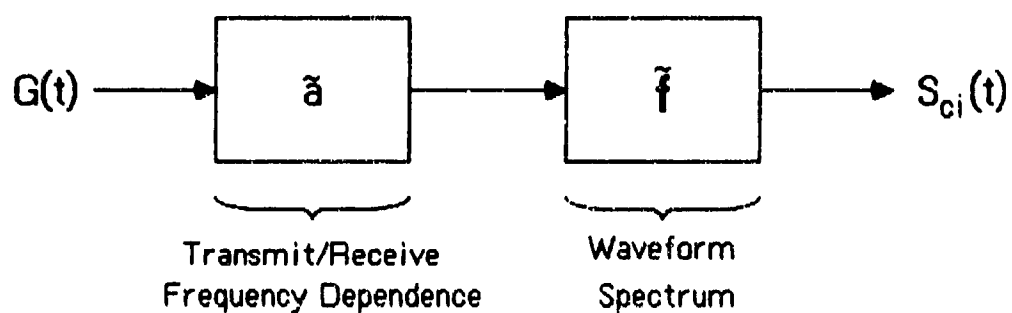


Figure 3-4. Linear Model for Clutter Reception

then

$$E[G(\cdot), G^*(\cdot)] = \frac{\eta_g}{c} \int dx' | \mathcal{E}(x', ct_1/2 \sin \delta_0; k_0) |^2 \delta(t_1 - t_2) \quad (3-21)$$

Recalling that

$$| \mathcal{E}(x, y; k_0) |^2 = | \tilde{E}_0\left(\frac{k}{R_0} x, \frac{k}{R_0} y; k_0\right) |^4 \quad (3-22)$$

there is, of course, now no phase of \mathcal{E} appearing and so this form essentially plays the role of a "window" (or truncation) on the sample function of the received clutter process. As usual, this window is broad relative to the time extent of the transmitted pulse and certainly the time-extent of the object, so we may ignore its windowing effect. (Of course, the associated gain is not neglected.) That is to say, ignoring the y and t dependence of $| \mathcal{E} |^2$, we have, as the spectral density of $u_{c1}(o; t)$,

$$\mathcal{P}_{u_{c1}}(\omega) = \left(\frac{k_0}{4\pi R_0}\right)^4 \left(\frac{\pi c}{\sin \delta_0}\right)^2 \int dx | \mathcal{E}(x, o; k_0) |^2 \eta_g(k_0) \quad (3-23)$$

where we have indicated that η_g could have wavenumber dependence.

Examining the integral in this last expression, and using (3-1) and (3-22), we obtain

$$\begin{aligned} \int dx | \mathcal{E}(x, o; k_0) |^2 &= \int dx \left| \tilde{E}_0\left(\frac{k_0 x}{R_0}, o; k_0\right) \right|^4 \\ &= \frac{R_0}{k} \int dp \left| \tilde{E}_0(p, o; k_0) \right|^4 \end{aligned} \quad (3-24)$$

If we assume, reasonably, a uniform aperture illumination, then doing the integrals, one finds

$$\int dx |\mathcal{E}(x, 0; k_0)|^2 = \frac{R_0}{k} \left(\frac{8\pi D_x}{6} \right) D_y^2 \quad (3-25)$$

where D_x and D_y are the antenna aperture's horizontal and vertical aperture dimensions.

Now we may write, on combining terms,

$$\mathcal{P}_{u_{c1}}^{(w)} = \left(\frac{k}{4\pi R_0} \right)^3 \left(\frac{4\pi^2}{3} \right) D_x D_y^2 \left(\frac{c}{2 \sin \delta_0} \right) \eta_g \quad (3-26)$$

Again, it is convenient to relate the spectral density level of the "white" clutter process' reflectivity density to the "historically defined" RCS density, σ_0 . The only time this is possible is when the clutter field (or process) is indeed white -- for only then, can a single parameter yield a useful characterization. It may be shown that

$$\eta_g(k_0) = \frac{4\pi}{k_0^2} \sigma_0(k_0).$$

There is available the "two-scale model" for rough surfaces composed of a slowly undulating "large-scale" fluctuations, treatable by physical optics, and a more rapidly fluctuating but small "fine-scale" variation, treatable by a "boundary perturbation." (All relative scales are with respect to the RF wavelength λ_0). Assuming that there is in fact no large scale present, one has

$$g_{c1}(x, y; k) = 2 \cos \delta_0 [1 - i2k \cos \delta_0 \xi(x, y)]. \quad (3-27)$$

where $\xi(x, y)$ is the scattering surface variation.

This model applies under reasonable conditions. In particular, at intermediate incident angles where there will be no "specular" (only "Bragg") scattering the "1" term may be neglected. So that

$$g_{c1}(x, y; k) \approx -i(2 \cos \delta_0)^2 k \xi(x, y) \quad (3-28)$$

and now

$$\eta_g(k) = (2 \cos \delta_0)^4 k^2 \eta_\xi. \quad (3-29)$$

Equivalently, the RCS density

$$\sigma_o(k) = \frac{k^2}{4\pi} \eta_g(k) = \frac{(2 \cos \delta_0)^4}{4\pi} k^4 \eta_\xi \quad (3-30)$$

where η_ξ is the spectral density of the scattering surface perturbation.

We may expect such a model to apply for rather flat terrain with small scale variations due to rocks/gravel or grass, e.g., to frequencies up to somewhere below X-band. In fact, it is observed empirically that over such types of terrain, $\sigma_o(k)$ does indeed have a k^4 -dependence on wavelength. This does allow a means of estimating the fundamental parameter η_ξ , by using the above relation and empirical measurements of σ_o of clutter at x-band. See Table 3-1 [26].

TABLE 3-1. ESTIMATES OF TERRAIN SPECTRAL DENSITIES

| <u>Terrain Type</u> | <u>"Typical"</u> <u>σ_0</u> | <u>Estimate of</u> <u>η_ξ</u> |
|----------------------|--|--|
| "dry, smooth desert" | 10^{-3} | 1.633×10^{-12} |
| "golf fairway" | 10^{-2} | 1.633×10^{-11} |

When the reflectivity density g_{c1} depends on k only as a factor, the above argument may be reviewed and it may be seen that the only assumption necessary to obtain the final result is a neglect of the windowing effect of the antenna pattern in y .

Combining the above discussions, the model for the spectral density of the clutter return yields

$$\mathcal{P}_{u_{c1}}(\omega) = \left\{ \frac{\cos^4 \delta_0}{6\pi \sin \delta_0} \cdot \frac{D_x D_y^2}{R_0^3} c \eta_\xi \right\} k^5 \quad (3-31)$$

It is interesting to recall how the k^5 dependence comes about in the clutter spectral density. First, there is a k^3 term because of the k^4 propagation factor $(k/4\pi R_0)^4$, decreased to k^3 by integration over the x -direction of the far-field antenna pattern. There is an additional k^2 because of the small-scale, rough surface scattering, consistently with a k^4 RCS density, σ_0 dependency.

As an example, suppose that $\sigma_0 = \pi/4$, $D_x = 1$ m, $D_y = 1/3$ m, $R_0 = 10$ Km, $\eta_\xi = 1.633 \times 10^{-12}$;

then

$$\mathcal{P}_{u_{c1}}(\omega) = 1.0210 \times 10^{-18} \star \left(\frac{\omega}{c} \right)^5$$

(It should be noted that this value of η_{ξ} was arrived at using a k^4 -dependent relation between η_{ξ} and empirically-derived σ_0 , thus, any error in σ_0 could be magnified at this point.)

We have therefore established the model as described in Eqs. 3-10 and 3-31 and illustrated in the block diagram shown in Figure 3-5.

The major limiting assumptions made in the course of the development are that: First, the "windowing", in the range dimension, of the antenna pattern is long relative to the pulse length and hence practically ignorable, and second, the "fine-scale" background is "white" over the bandwidth of interest. Although other assumptions could have been made, it is felt that the model presented by Figure 3-5, along with the supporting equations, is a reasonable first-cut for a broadband radar system model.

3.3 OPTIMUM PROCESSOR STRUCTURE AND RESULTING PERFORMANCE

In order to formulate a detection decision problem, we, first of all, acknowledge that $s(t)$ will always be received along with thermal noise so the data actually available for processing is

$$z(t) = s(t) + n(t), t \in T \quad (3-32)$$

where T is some reception interval, possibly delimited by the antenna pattern. The thermal noise $n(t)$, $t \in T$ is a Gaussian, zero mean, possibly white process. (However, the white assumption is not necessary

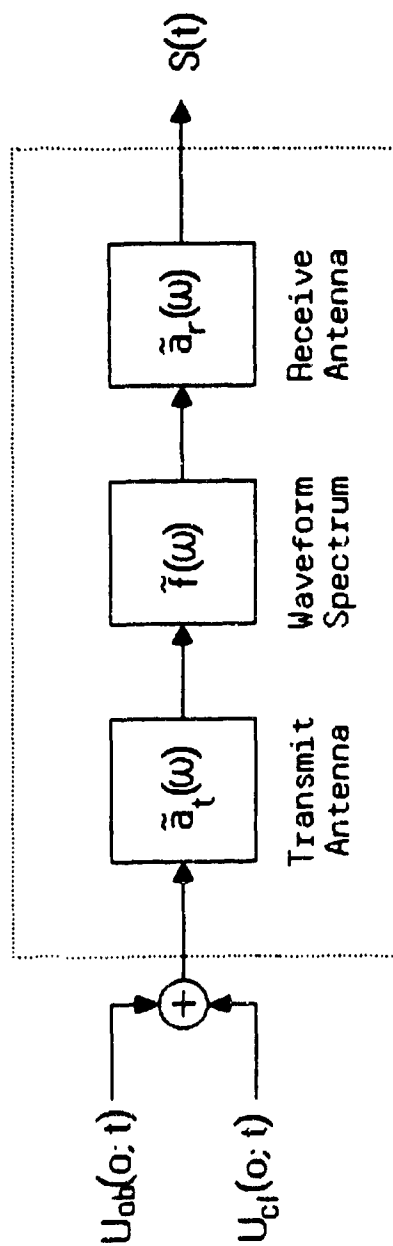


Figure 3-5. Radar System Model For Target In Clutter

for us to proceed here.) Also, it is assumed that the clutter-induced $u_{cl}(o, t)$ is, over T , a wide-sense stationary random process of zero mean, and that it is Gaussian.*

We have the following decision problem: given the data $z(t)$, $t \in T$, we must decide whether $z(t)$ is due to clutter-and-noise or due to signal (object) plus clutter-and-noise. Because of the assumption of normal distributions, it is well known that under, say, the Neyman-Pearson criterion, the optimum decision device is a "matched filter" followed by a "sampler", the sample being compared to a threshold [21,22]. The performance is uniquely determined by a signal-to-noise ratio (SNR) parameter, denoted as " d^2 " in the following. Here d^2 is the normalized "distance" between the two hypothesized signals.

Without loss of generality, we may allow a "pre-receiver" with transfer function $\tilde{H}(\omega)$. Also, we should note that the predominant thermal noise at these frequencies is likely due to that radiated by the viewed terrain. Thus, one arrives at the sketched system model shown in Figure 3-6.

To abbreviate notation at this point, set

$$B(t) = u_{ob}(o; t), \quad C(t) = u_{cl}(o; t).$$

Also, denote as $s(t)$ and $n(t)$ the resultant signal, due to B , and thermal (effective) noise, due to C , n_{ter} , and n_{rcv} , respectively.

*If we do not assume Gaussian distributions and then adopt the softer maximum signal-to-noise ratio (SNR) criterion, we are led to precisely the same results.

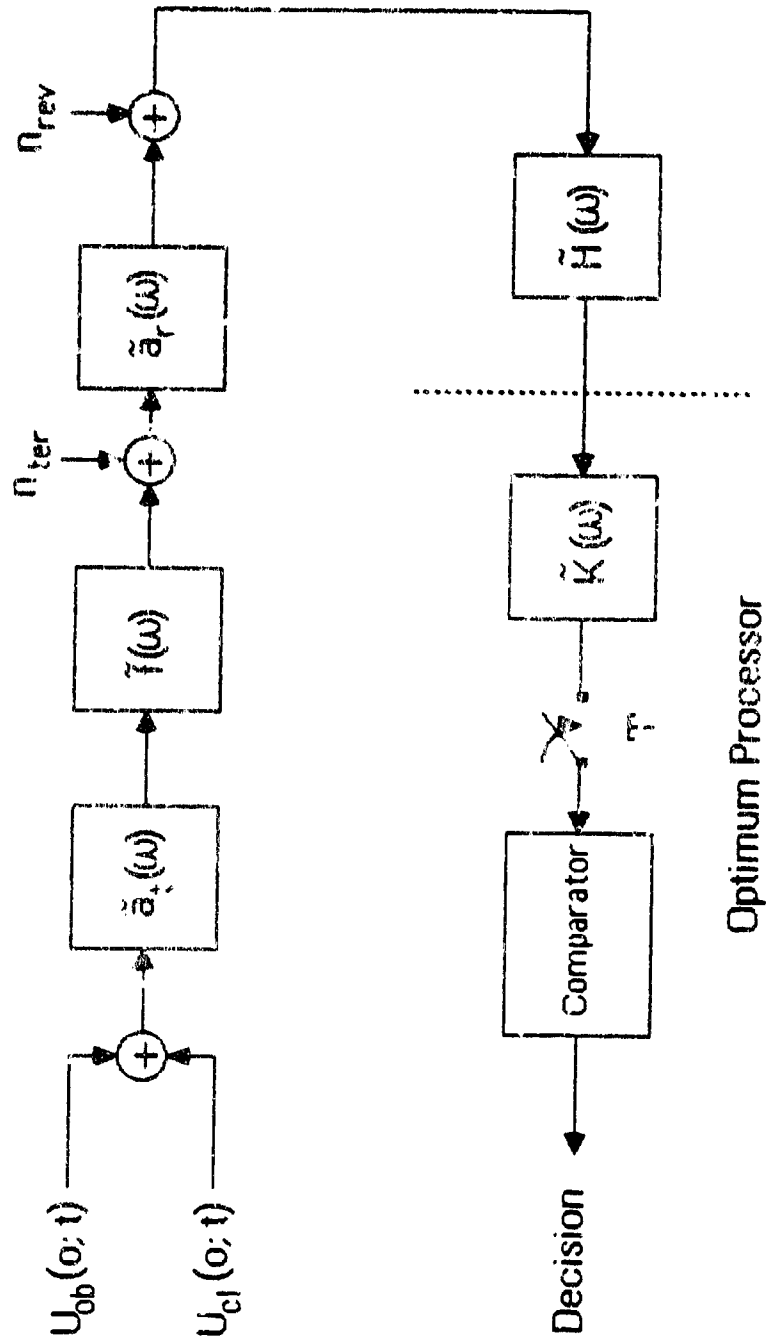


Figure 3-6. Total Radar System Block Diagram

It is well known [21] that the optimum ("matched") filter is given by

$$\tilde{K}(\omega) = \frac{\tilde{S}(\omega)^*}{\mathcal{P}_n(\omega)} = \frac{(\tilde{B}\tilde{f}\tilde{a}\tilde{H})^*}{\left(\mathcal{P}_{n_{ter}}(\omega)|\tilde{a}_r|^2 + \mathcal{P}_{n_{rcv}}\right)|\tilde{H}|^2 + \mathcal{P}_c|\tilde{f}\tilde{a}\tilde{H}|^2} \quad (3-33)$$

where $\mathcal{P}_n(\omega)$ is the power spectrum to the total received noise.

The detection performance is completely characterized by the parameter

$$\begin{aligned} d^2 &= \frac{1}{2\pi} \int \frac{|\tilde{S}(\omega)|^2}{\mathcal{P}_n(\omega)} d\omega \\ &= \frac{1}{2\pi} \int \frac{|\tilde{B}\tilde{f}\tilde{a}\tilde{H}|^2 d\omega}{\left[\mathcal{P}_{n_{ter}}|\tilde{a}_r|^2 + \mathcal{P}_{n_{rcv}} + \mathcal{P}_c|\tilde{f}\tilde{a}|^2\right]|\tilde{H}|^2} \cdot \quad (3-34) \end{aligned}$$

We notice $|\tilde{H}|^2$ multiplies all and hence cancels out of the d^2 expression where it is not zero. Thus, we ignore it in what follows, except we may wish to restrict $|\tilde{f}(\omega)|^2$ to some ω -set, e.g., for practical reasons.

3.4 OPTIMUM SIGNAL DESIGN

We now have arrived at a position where one can address the problem of special interest here: "How should the signal spectrum $\tilde{f}(\omega)$ be chosen?"

We observe immediately that the only dependence of d^2 on \tilde{f} is through $|\tilde{f}(\omega)|^2$, that is, in choosing \tilde{f} to maximize performance that is done by maximizing d^2 , we are only concerned with the choice of $|\tilde{f}(\omega)|^2$. As is well known in radar work, this may leave freedom to choose f to meet other design restraints, e.g., Doppler "resolution."

We will choose \tilde{f} under an energy constraint, as will be true in practice and as a constraint is necessary to avoid impractical solutions. We, therefore, have the following problem:

$$\max_{|\tilde{f}|^2} \{d^2\}, \text{ subject to the constraint: } \frac{1}{2\pi} \int |\tilde{f}(\omega)|^2 d\omega = E_f$$

The solution to this problem is given on page 95 of [14]: for all permitted ω ,

$$|\tilde{f}(\omega)|^2 = \max \left\{ 0, \frac{1}{|\tilde{a}|^2 \mathcal{S}_c} \left[\sqrt{\frac{|\tilde{a}|^2 |\tilde{B}|^2 \mathcal{S}_n}{\lambda_1}} - \mathcal{S}_n \right] \right\} \quad (3-35)$$

The Lagrange multiplier parameter λ_1 is to be chosen so as to meet the energy restraint. This apparently must be done by an approximation technique. Here, we use an algorithm method based on the technique of "bisection." Given appropriate choices of lower and upper bounds on the frequency range of interest, the algorithm always converges because, as may be observed, the energy increases monotonically (but not strictly so) with increasing frequency interval length.

This solution has a nature especially interesting here: As the energy constraint is varied, the ω -support of $|\tilde{f}(\omega)|^2$ can dramatically change, e.g., from "narrow-band" to "broad-band". The variation is much more complex than a simple scale change. This is demonstrated in Section 3.4.1.

3.4.1 NUMERICAL EVALUATION

For the calculations to follow, we suppose that $\tilde{a}_t(\omega) = \tilde{a}_r(\omega)$ and that the terrain thermal noise, with spectral density η_0 , dominates the

receiver thermal noise. Using such assumptions, (3-35) can be written as

$$|\tilde{f}(\omega)|^2 = \max \left\{ 0, \frac{1}{|\tilde{a}|^2 \mathcal{P}_c} \left[\sqrt{\frac{|\hat{a}|^2 |\hat{g}|^2 |\hat{a}| \eta_0}{\lambda_1}} - |\hat{a}| \eta_0 \right] \right\}. \quad (3-36)$$

In addition, it will be numerically convenient to consider all terms as a function of the frequency ν , expressed in Megahertz. That is, we use

$$k = \frac{\omega}{c} = 2.0944 \times 10^{-2} \nu \quad (\nu \text{ in MHz}) \quad (3-37)$$

On substituting (3-37), and changing variables in (3-36), we obtain

$$|\tilde{f}(\nu)|^2 = \max \left\{ 0, \frac{A_1}{|\tilde{a}(\nu)| \nu^5} \left[c_0 \nu \sqrt{|\tilde{a}(\nu)| \sigma(\nu)} - 1 \right] \right\} \quad (3-38)$$

where c_0 is chosen to meet the energy constraint and

$$A_1 = \frac{\sin \delta_0}{\cos^4 \delta_0} \frac{R_0^3 D_x}{\mathcal{A}^2} \frac{\eta_0}{\eta_\xi} \times 1.559 \times 10^3. \quad (3-39)$$

For completeness, the same assumptions yield an energy expression

$$E_f = 10^6 \int |\tilde{f}(\nu)|^2 d\nu \quad (3-40)$$

and

$$d^2 = A_2 \int \frac{|\tilde{f}(\nu)|^2 |\tilde{a}(\nu)|^2 \nu^2 \eta(\nu) d\nu}{1 + |\tilde{f}(\nu)|^2 |\tilde{a}(\nu)|^2 \nu^5 / A_1} \quad (3-41)$$

where

$$A_2 = \frac{c}{2\pi} \frac{\mathcal{A}^2}{(4\pi R_0)^4 \eta_0} (2.0944 \times 10^{-2})^3 = 1.759 \times 10^{-2} \frac{\mathcal{A}^2}{R_0^4 \eta_0}.$$

3.4.1.1 TARGET CROSS SECTION MODEL

Of course, the specific frequency dependence of the target cross section will have a strong effect on the optimum signal spectrum. We model the cross section dependence by

$$\sigma(v) = \sigma_m W(v) \quad (3-42)$$

where $\max_v \{W(v)\} = 1$.

Moreover, we assume a specific $W(v)$ dependence as sketched in Figure 3-7. It is motivated by the pole pattern for a MIG 19 obtained by the SEM method [15,16]. (In later computations, we will approximate the response by a suitably chosen "Butterworth" filter characteristic.)

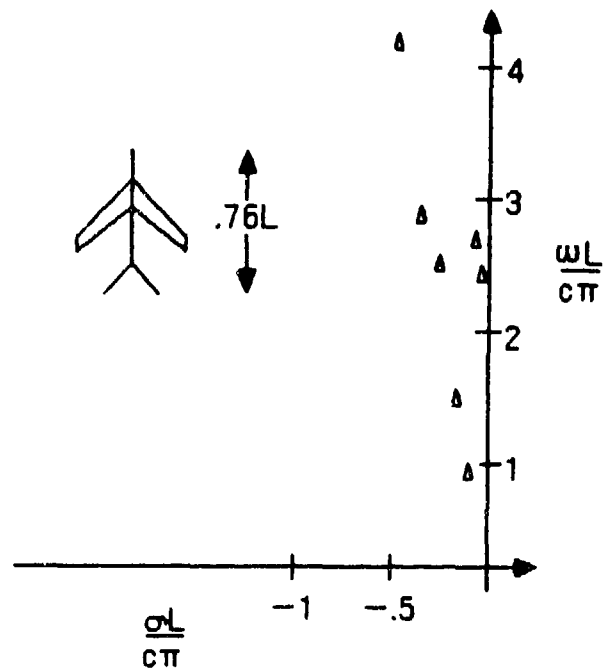
3.4.1.2 ANTENNA FREQUENCY DEPENDENCE

It is also obvious that the antenna response will strongly drive the signal design. For the numerical examples to follow, we use the transfer function for a resistively loaded horn, as reported by Kanda [17] and sketched in Figure 3-8. It, too, was modelled by a suitable Butterworth response in the analysis to follow.

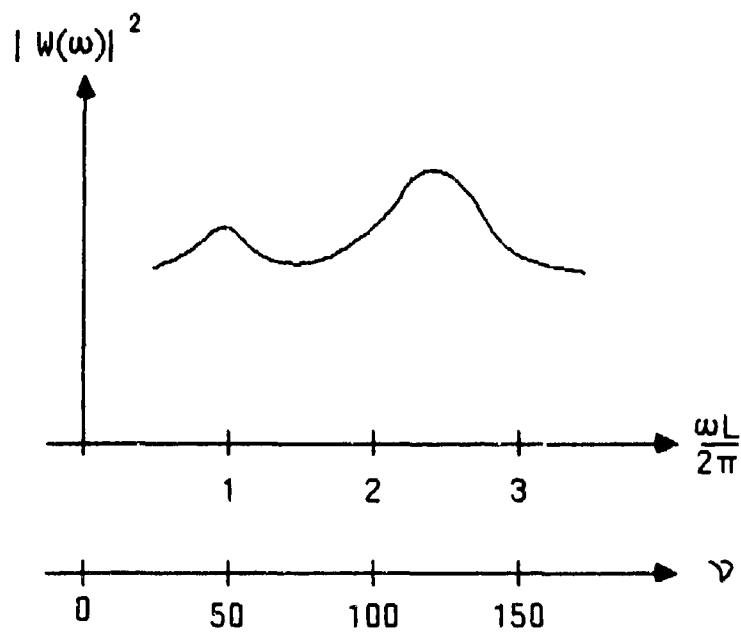
3.4.1.3 SPECIFIC NUMERICAL CALCULATIONS

We begin by taking $A_1 = 10^6$ and $A_2' = \sigma_m A_2 = 5 \times 10^6$ and suppose that, for whatever practical reasons, the signals spectral support is restricted to

$$v_{\min} = 135 \quad \text{and} \quad v_{\max} = 175 \text{ (MHz)}.$$



a) Target Pole Plot



b) Target Frequency Response

Figure 3-7. Frequency Dependence for Assumed Target

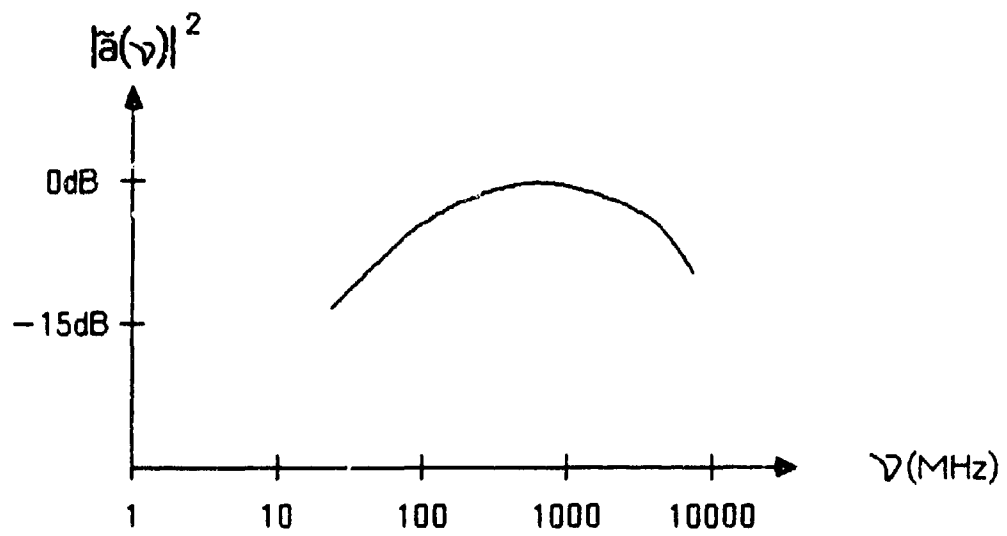


Figure 3-8. Assumed Antenna Frequency Response

Recall that from Figure 3-7, this frequency interval contains the higher frequency resonance of the subject target.

The resulting normalized optimum signal spectrum* is presented in Figure 3-9 for energy constraints of 1, 10^2 and 10^4 Joules, respectively. In addition, the figure presents the resulting SNR parameter, d^2 . It may be observed that for $E_f = 1$, the resultant $|\tilde{f}(\omega)|^2$ is quite narrow relative to the permitted bandwidth and that the system performance would be quite good, since d^2 is roughly 60 dB. Increasing the allowable energy does result in a signal which fills the available bandwidth and produces an even larger d^2 .

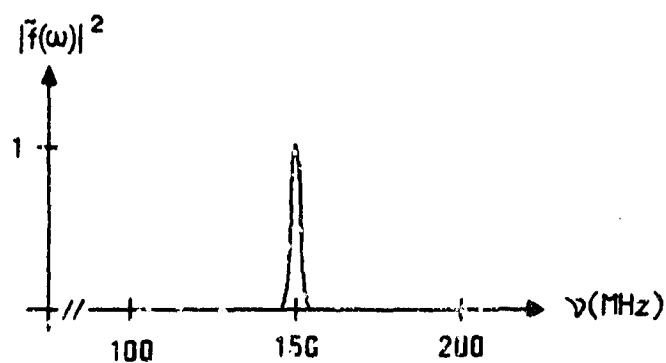
Additional computations were made to examine the effects of the frequency dependence of the clutter spectrum $S_c(k)$. (Recall that the original dependence was shown to be a k^5 dependence.) A clutter spectrum dependence of k^3 and k^0 was used with a wide variety of signal energy constraints. In all cases, the signal spectrum was quite narrow and centered at 150 MHz. Moreover, for fixed energy, the system performance measure d^2 increased as the clutter "power law" decreased, as would be expected. For example, with $E_f = 10^4$, d^2 went from 90 dB to 90.3 dB as the clutter spectrum went from a cubic to a zero exponential dependence.

It seemed that little additional frequency dependence would exist without including a broader allowable interval to include the additional target resonance. Thus, we started with

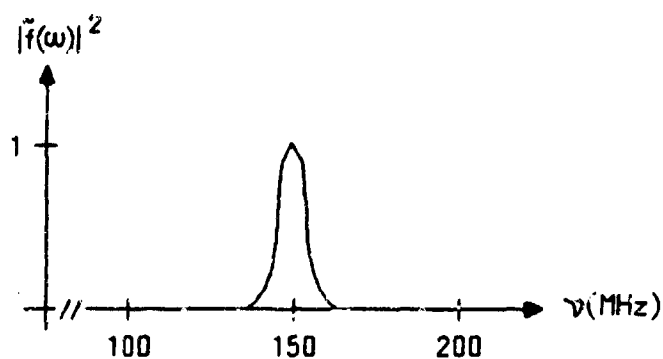
$$v_{\min} = 35 \quad \text{and} \quad v_{\max} = 200$$

and again assumed a fifth law clutter spectrum.

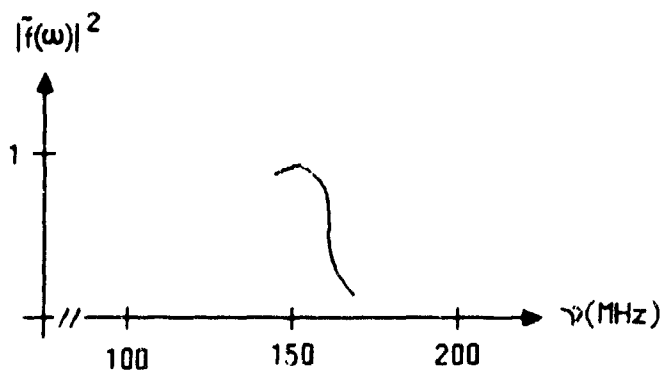
*The optimum spectrum is plotted in a normalized way such that $|\tilde{f}_0(\omega)|^2 / \max |\tilde{f}_0|^2$ is unity.



a) Energy Constraint = 1 Joule; Resulting $d^2 = 60\text{dB}$



b) Energy Constraint = 100 Joules; Resulting $d^2 = 74\text{dB}$



c) Energy Constraint = 10^4 Joules; Resulting $d^2 = 78\text{dB}$

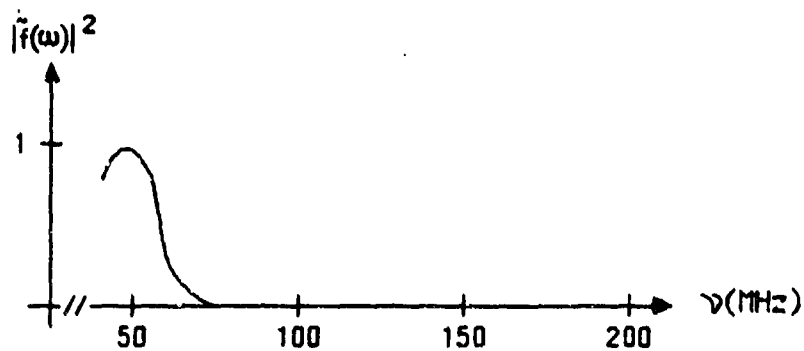
Figure 3-9. Effect of Energy Constraint on Particular Optimum
Signal Design ($\nu_{\min}=135, \nu_{\max}=175$)

Allowing for a large signal energy, $E_f = 10^6$ Joules, we obtained the signal spectrum presented in Figure 3-10a. Note the signal is now matched to the target's lower resonance (compare to Figure 3-9c).

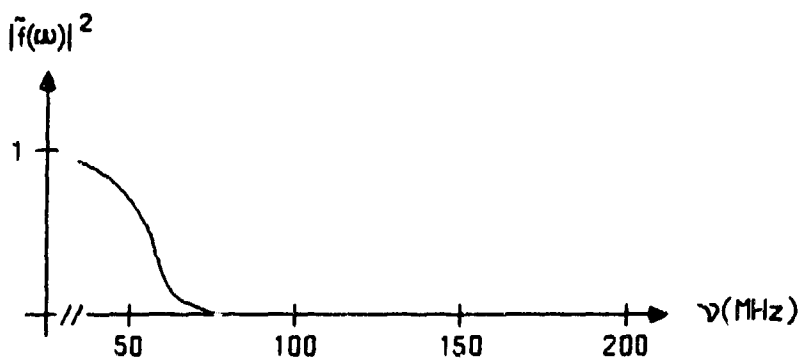
We would guess that $|\tilde{f}(\omega)|^2$ should generally broaden as A_1 is decreased because λ_1 must be larger to meet the energy constraint. This can be easily accomplished by increasing the clutter reflectivity by a factor of ten (see Eq. 3-39). The resultant signal spectra is shown in Figure 3-10b; indeed it has broadened as expected.

The constant A_1 may be decreased further, and A_2' increased by decreasing the range R_0 to 1 Km (see Eqs. 3-39 and 3-41). In that instance A_1 becomes 10^2 and A_2' is increased to 5×10^{10} . For the constraint of $E_f = 10^6$, the resultant signal is the same as that plotted in Figure 3-10b. If, however, we use $E_f = 100$, the $|\tilde{f}(\omega)|^2$ has perhaps narrowed some, as shown in Figure 3-10c. The narrowing is even more pronounced for $E_f = 10$, as shown in Figure 3-11a. Note also there is a slight signal component centered at the other object resonance. If the energy is further decreased to $E_f = 0.01$, then rather surprisingly, the support of $|\tilde{f}(\omega)|^2$ jumps to a location around the larger resonance of the object, as shown in Figure 3-11b. As E_f is further decreased to 10^{-2} , a relative narrowing of the $|\tilde{f}(\omega)|^2$ again occurs.

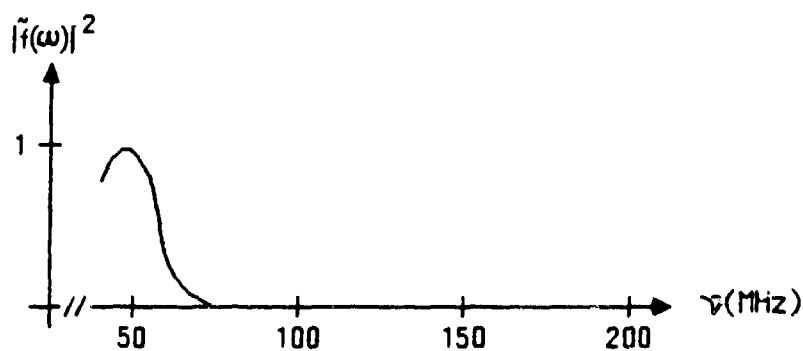
The above results were obtained with $A_1 = 10^2$ and $A_2' = 5 \times 10^{10}$. If we again return to a longer range of $R_0 = 10$ Km and a smoother terrain background so that $A_1 = 10^6$ and $A_2' = 5 \times 10^6$ and use $E_f = 10^{-2}$, the resulting sharply narrowed spectrum is obtained, as shown in Figure 3-12.



a) Energy Constraint = 10^6 Joules, $d^2 = -82.3\text{dB}$



b) Energy Constraint = 10^6 Joules, $A = 10^5$, $d^2 = -72.3\text{dB}$

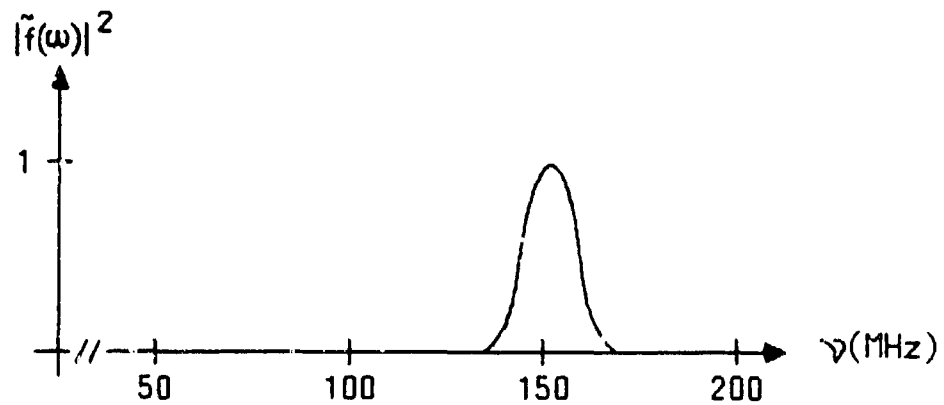


c) Energy Constraint = 100 Joules, $A_1 = 10^2$, $A' = 5 \times 10^{10}$, $d^2 = -82.3\text{dB}$

Figure 3-10. Optimum Signal for Larger Bandwidth Interval
($\nu_{\min} = 35$, $\nu_{\max} = 200$)

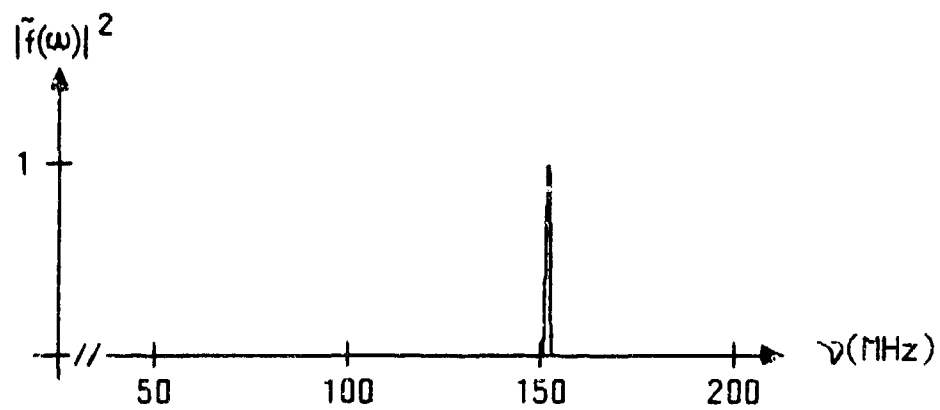


a) Energy Constraint = 10 Joules, $A_f = 10^2$, $A'_f = 5 \times 10^{10}$, $d^2 = 75.3 \text{ dB}$



b) Energy Constraint = .01 Joules, A_f reduced by 10, $d^2 = 68 \text{ dB}$

Figure 3-11. Optimum Signal For Wideband, Reduced Energy Constraint
($\nu_{\min} = 35$, $\nu_{\max} = 175$)



a) Energy Constraint = 10^{-2} Joules, $A = 10^6$, $A'_2 = 5 \times 10^6$, $d^2 = 30.3\text{dB}$

Figure 3-12. Optimum Signal With Reduced Energy Constraints

3.5 MULTIPLE PULSE (PERIODIC) SIGNAL DESIGN

It is frequently true in radar systems that the waveform modulation transmitted should be pulsed. This may be because an area is to be scanned or that peak power and resolution requirements are such that adequate detection and parameter measurement performance can only be met by utilizing a number of pulse returns.

Thus we assume now

$$f(t) = \sum_{n=0}^{N-1} f_0(t - nT_s), \quad (3-43)$$

a repetition, with period T_s , of a transmitted waveform f_0 . We see that the waveform spectrum (Fourier transform)

$$\tilde{f}(\omega) = \tilde{Q}(\omega) \tilde{f}_0(\omega)$$

where

$$\tilde{Q}(\omega) = \sum_{n=0}^{N-1} e^{-inT_s\omega} = e^{-i(N-1)T_s\omega/2} \left\{ \frac{\sin(NT_s\omega/2)}{\sin(T_s\omega/2)} \right\} \quad (3-44)$$

In principle, it is straightforward to employ the signal optimization already discussed in Section 3.4. It is readily seen that, again assuming thermal noise from the terrain dominates that from the receiver, the optimum pulse modulation f_0 is specified insofar as $|\tilde{f}_0|^2$, which is given by

$$|\tilde{f}_0(\omega)|^2 = \max \left\{ 0, \frac{1}{|\tilde{a}_t \tilde{Q}|^2 \mathcal{G}_c} \left[\sqrt{\frac{|\tilde{B} \tilde{a}_t \tilde{Q}|^2 \mathcal{G}_n}{\wedge_1}} - \mathcal{G}_n \right] \right\} \quad (3-45)$$

Additionally, ω is restricted to be in the set $\omega \in \Omega_*$, where $|\tilde{a}_r(\omega)|^2 \neq 0$.

Implied in the above discussion is that the optimum filter \tilde{K} will also contain this "comb structure" $\tilde{Q}(\omega)$, see Equation 3-34 with $\tilde{f} = \tilde{Q} \tilde{f}_0$. This "comb structure" \tilde{Q} fluctuates very rapidly, of the order of ω_s/N , and hence so would the optimum $|\tilde{f}_0(\omega)|^2$. For example, if $T_s = 1$ ms, then $f_s = 1/T_s = 1$ KHz and this is quite small relative to the allowed bandwidth interval Ω_* .

Conversely $|\tilde{f}_0(\omega)|^2$ will fluctuate very rapidly generally with respect to its permitted bandwidth Ω_* . This results in a tendency for $f_0(t)$ to have a long time extent.

For example, if the required energy E is relatively quite small, and \mathcal{P}_c , \mathcal{P}_n , $|B|$, and $|\tilde{a}_t|$ are uniform over Ω_* , then $|\tilde{f}_0(\omega)|^2$ tends to have its support on narrow intervals, say of width Δ , centered on $k\omega_s$, where k is such that $k\omega_s \in \Omega_*$ and also $\Delta \ll \omega_s/N$. That is, roughly,

$$|\tilde{f}_0(\omega)|^2 \approx \sum_{k: k\omega_s \in \Omega_*} \text{rect}\left(\frac{\omega - \omega_s k}{\Delta}\right) \quad (3-46)$$

Suppose $\Omega_* = \{\omega: -\Omega/2 + \omega_0 < \omega < \omega_0 + \Omega/2\}$. Then, if we assume \tilde{f}_0 is real (this results in minimal time extent for f), we find

$$f_0(t) \approx \frac{\sin(2\pi t/\Delta)}{\pi t} \frac{\sin[(K+1)\omega_s t/2]}{\sin(\omega_s t/2)} \quad (3-47)$$

If $\Delta \ll \omega_s/N$, then $2\pi/\Delta \gg NT_s$ and there is an inconsistency with the desire to have a periodic, pulse-like modulation.

In order to find a desirable $f_o(t)$, it is necessary that, e.g., its time-extent be constrained, in order that it represent a possible pulse to be periodically repeated. This problem is discussed in the next section.

(It may be seen that, as $\mathcal{P}_n \rightarrow 0$, f tends toward $|\tilde{Q}|^{-1}$ (in its dependence of \tilde{Q}). That is, \tilde{k}_{opt} and f_{opt} bear an inverse relationship with respect to $|\tilde{Q}|$. The "overall" dependence of the system on $|\tilde{Q}|$ tends to disappear. This is actually reasonable. It is only the total energy of f that is constrained and SNR becomes independent of f_r .)

3.5.1 FORMATION WITH ENERGY AND TIME-EXTENT CONSTRAINTS

When a periodic pulse modulation is imposed for reasons such as discussed above, we also often want to constrain the time extent of the periodically repeated pulse, typically to a small fraction of the period. Thus, analytically, we would straightforwardly impose another constraint. We will discuss two ways this can be done in a reasonably tractable manner, though only one is considered at length here.

The most straightforward method, perhaps, is to use a "radius of gyration" measure, τ , of the time extent of the pulse modulation, defined by

$$\tau_1^2 = \int_{-\infty}^{+\infty} t^2 |f(t)|^2 dt \left(\frac{1}{E_f} \right) \quad (3-48)$$

assuming that

$$\int_{-\infty}^{+\infty} t |f(t)|^2 dt = 0$$

i.e., the centroid of $|f(t)|^2$ is at zero. The denominator is the energy, E_f , of f which is also to be constrained. Also by Parseval's relation,

$$E_f \tau_1^2 = \frac{1}{2\pi} \int |\tilde{f}'(\omega)|^2 d\omega \quad (3-49)$$

which is therefore a reasonable form to constrain.

Forming the Lagrangian

$$\begin{aligned} \mathcal{L}(\tilde{f}) = & \frac{1}{2\pi} \int \frac{|\tilde{B}_1| |\tilde{f}|^2 d\omega}{P_n + P_c |\tilde{f}|^2} \\ & - \lambda_1 \frac{1}{2\pi} \int |\tilde{f}(\omega)|^2 d\omega - \lambda_2 \frac{1}{2\pi} \int |\tilde{f}'(\omega)|^2 d\omega \end{aligned} \quad (3-50)$$

where we have used $|\tilde{B}_1|^2 \equiv |\tilde{B}|^2 |\tilde{a}_t|^2$, $P_n \equiv \mathcal{P}_{n_{\text{ter}}}$, and $P_c \equiv \mathcal{P}_c |\tilde{a}_t|^2$. Furthermore, λ_1 and λ_2 are Lagrange multipliers and \tilde{f} is to be chosen to maximize $\mathcal{L}(f)$ while satisfying the two constraints on energy and time extent.

In a classical way, we are led to the Euler-Lagrange necessary condition for \tilde{f} to be a stationary point of $\mathcal{L}(\tilde{f})$. If \tilde{f}_R is the real part of \tilde{f} , then \tilde{f}_R must satisfy

$$\lambda_2 f_R'' + \lambda_1 f_R - \frac{|\tilde{B}_1| P_n f_R}{P_n + P_c |\tilde{f}|^2} = 0 \quad (3-51)$$

The same relation holds for f_I . This is a nonlinear, ordinary differential equation for which suitable boundary conditions are to be imposed, e.g., f having support confined to Ω may be desirable. The solution of this problem, which can only be done numerically, guided by fairly sophisticated analysis, is beyond the scope of this study.

To impose a constraint on the modulation time-extent that is more tractable while still reasonably meeting the constraint requirement, we note that, if f has support $|t| < T$, then ϕ , where $\tilde{\phi} = |\tilde{f}|^2$, has support confined to $|t| < 2T$. So we impose the constraint directly on ϕ . To avoid a nonlinear differential equation, we use the "equivalent rectangle" definition of time extent:

$$\tau_2 = \frac{\int |\phi(t)|^2 dt}{|\phi(0)|^2} = \frac{\frac{1}{2\pi} \int_{\Omega} |\tilde{\phi}(\omega)|^2 d\omega}{\left| \frac{1}{2\pi} \int_{\Omega} \tilde{\phi}(\omega) d\omega \right|^2} \quad (3-52)$$

The denominator is again recognized as the energy, E_f , of f , which will also be constrained. We are therefore led to the two constraints:

$$\frac{1}{2\pi} \int_{\Omega} \tilde{\phi}(\omega) d\omega = E_f \quad (3-53a)$$

$$\frac{1}{2\pi} \int_{\Omega} \tilde{\phi}(\omega)^2 d\omega = \tau E_f^2 \quad (3-53b)$$

and also, of course,

$$\tilde{\phi}(\omega) \geq 0, \quad \omega \in \Omega. \quad (3-53c)$$

We are now formally led to the problem: maximize $\mathcal{L}\{\tilde{\Phi}\}$ by the choice of $\tilde{\Phi}$, where

$$\mathcal{L}\{\tilde{\Phi}\} = \frac{1}{2\pi} \int_{\Omega} \frac{|\tilde{B}|^2 \tilde{\Phi} d\omega}{p_n + p_c \tilde{\Phi}} - \lambda_1 \frac{1}{2\pi} \int_{\Omega} \tilde{\Phi} d\omega - \lambda_2 \frac{1}{2\pi} \int_{\Omega} \tilde{\Phi}^2 d\omega. \quad (3-54)$$

We must first be concerned by the possible conflict of (3-53a) and (3-53b). $\tilde{\Phi}$ which satisfy 3-53a and 3-53b will be called "admissible". Intuitively, from the usual theory of the Fourier transform, we know that any function and its transform cannot be simultaneously "too constrained" in time extent and bandwidth. Here, the consequences are readily seen. Dividing (3-53b) into the square of (3-53a), we have

$$\rho = \frac{\left(\frac{1}{2\pi} \int_{\Omega} \tilde{\Phi} d\omega \right)^2}{\frac{1}{2\pi} \int_{\Omega} \tilde{\Phi} d\omega} = \frac{1}{\tau} \quad (3-55)$$

by the Schwarz inequality,

$$\rho \leq \frac{1}{2\pi} \frac{\int_{\Omega} (1)^2 d\omega \cdot \int_{\Omega} \tilde{\Phi}(\omega)^2 d\omega}{\int_{\Omega} \tilde{\Phi}(\omega)^2 d\omega} = \frac{\mu(\Omega)}{2\pi} \quad (3-56)$$

where $\mu(\cdot)$ is the measure (interval length) of the set Ω and equality holds if and only if $\tilde{\Phi}(\omega) = \text{constant}$ for $\omega \in \Omega$. If the support of $\tilde{\Phi}(\omega)$ is confined to $\Omega_{\star} \subset \Omega$, the same bound occurs, with Ω_{\star} replacing Ω . Thus, if the "bandwidth" $\mu(\Omega_{\star})$, the (Lebesgue) measure of the set Ω_{\star} , $\Omega_{\star} \subset \Omega$, is too small, i.e., if

$$\mu(\Omega_*) < 2\pi/\tau, \quad \Omega_* \subset \Omega \quad (3-57)$$

then there are no admissible functions $\tilde{\Phi}$. Further, often we are interested in meeting another constraint not explicitly mentioned: $f(t) \leq f_{\max}$, corresponding to a peak power restraint. This constraint is conventionally met by use of "large-time bandwidth product" signals, i.e., here we may well want

$$\frac{\mu(\Omega_*)}{2\pi} \tau \gg 1, \quad \Omega_* \subset \Omega. \quad (3-58)$$

Note also that if $\tilde{\Phi}$ is a constant over a set $\Omega_* \subset \Omega$, then necessarily

$$\rho = \frac{\mu(\Omega_*)}{2\pi} = 1/\tau \quad (3-59)$$

therefore, such $\tilde{\Phi}$ do not seem to be all that interesting, as again, they will be of "unity time-bandwidth product."

3.5.1 SOLUTION FOR OPTIMUM SIGNAL

Considering the maximization of (3-54), we see that the Lagrangian is the form

$$\mathcal{L}\{\tilde{\Phi}\} = \frac{1}{2\pi} \int_{\Omega_*} F(\tilde{\Phi}, \omega) d\omega \quad (3-60)$$

where suppressing its ω -dependence, F functionally depends on Φ as

$$F(x) = \frac{c_1 x}{1 + c_2 x} - c_3 x - c_4 x^2 \quad (3-61)$$

where $c_1 = |\tilde{B}_1|^2/P_n$, $c_2 = P_c/P_n$, $c_3 = \lambda_1/P_n$ and $c_4 = \lambda_2/P_n$; we assume P_n

is independent of ω . It is clear that \mathcal{L} is maximized over $\tilde{\phi}$ by choosing each $\tilde{\phi}$ value to maximize $F(\tilde{\phi}(\omega), \omega)$ for each $\omega \in \Omega_* \subset \Omega$. That is, we wish to find $x \geq 0$ maximizing $F(x)$ for a set (c_1, c_2, c_3, c_4) .

We compute

$$F'(x) = \frac{c_1 - (1 + c_2 x)^2 (c_3 + 2c_4 x)}{(1 + c_2 x)^2} \quad (3-62)$$

the equation for stationary points,

$$F'(x) = 0,$$

has the same solution ($x \neq -1/c$) as the equation

$$(c_3 + 2c_4 x)(1 + c_2 x)^2 - c_1 = 0. \quad (3-63)$$

This is a cubic equation whose roots may be found by a well known formula.

We can demonstrate that the solution to Equation (3-63) may have one positive solution and two negative solutions (possibly the same). We also see that it has one (at most) positive solution, and then only if $c_3 < c_1$. Therefore, if $c_3 > c_1$, we take $x_{\text{opt}} = 0$. Otherwise, we solve the cubic equation for its single positive root. We notice also that, keeping in mind c_1 represent $|\tilde{B}_1|^2/P_n$, which depends on ω , the smaller we make c_3 ($c_3 \geq 0$), the more ω for which a nonzero x_{opt} is found. Further, making c_4 very large tends to make x_{opt} very small. These two observations elucidate how a broad bandwidth, hence small time-extent, solution can occur.

3.5.2 SPECIFIC NUMERICAL RESULTS

It is now straightforward to numerically find $\tilde{\Phi} = |\tilde{f}_0|^2$ for a given set (c_1, c_2, c_3, c_4) . We will employ numerical values already given in Section 3. 4.

The energy constraint is

$$E_f = \frac{10^6}{2\pi} \int_{\Omega_*(v)} \tilde{\Phi}(v) dv \quad (3-64)$$

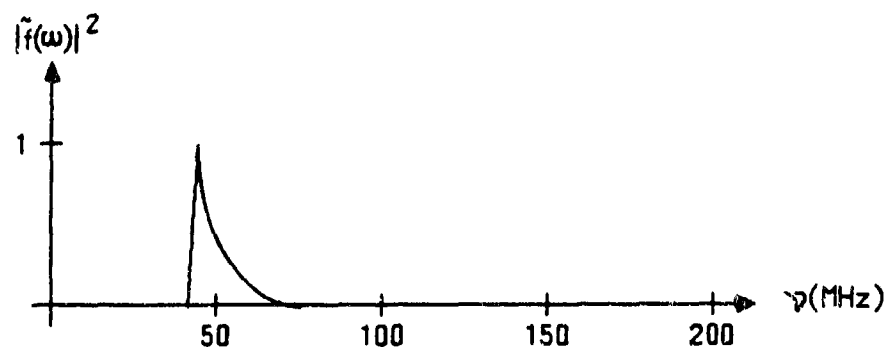
the time-extent-related constraint is

$$\tau E_f^2 = \frac{10^6}{2\pi} \int_{\Omega_*(v)} \tilde{\Phi}(v)^2 dv \quad (3-65)$$

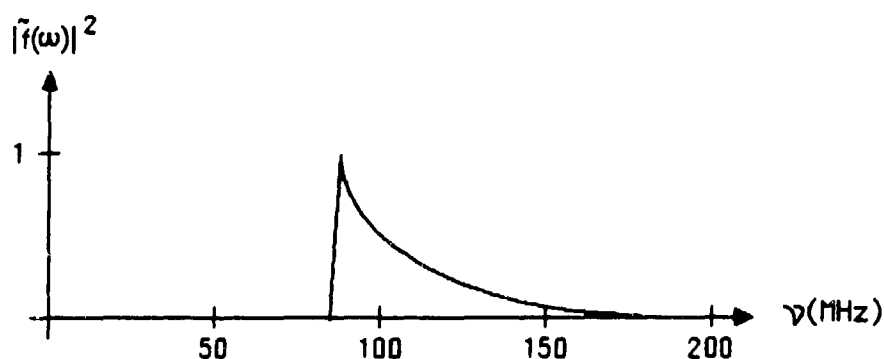
and the SNR is

$$d^2 = \frac{10^6}{2\pi} \int_{\Omega_*(v)} \left\{ \frac{c_1(v)\tilde{\Phi}(v)}{1 + c_2(v)\tilde{\Phi}(v)} - c_3\tilde{\Phi}(v) - c_4\tilde{\Phi}(v)^2 \right\} dv.$$

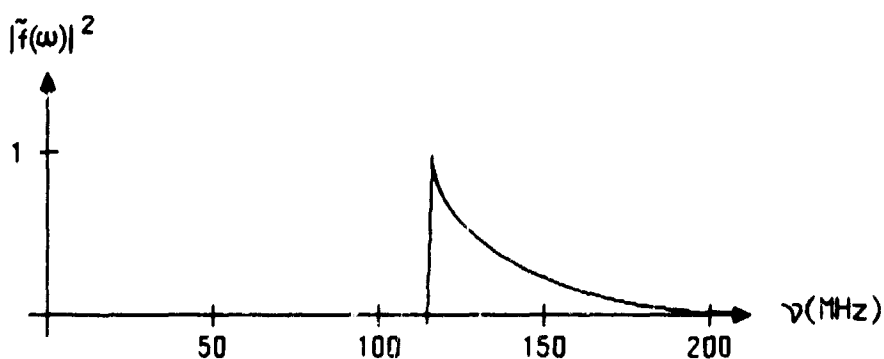
A series of optimal signal spectra were computed for numerous energy/signal duration extents, E_f/τ . Selected examples are presented in Figures 3-13 and 3-14. It was determined that, generally speaking, the time extents were of a "practical" nature, ranging from about 5×10^{-7} sec to 314×10^{-6} sec. The narrower signal extents are associated with rather large energies, providing SNRs much larger than would be required for adequate detection probability. Moreover, as the signal energy constraint decreases, the optimum signal spectra "gravitates" from the lower end of Ω_* , (near the maximum (resonant) response of the



a) Energy Constraint $\approx 10^4$ Joules, Pulse Extent $= 3.0 \times 10^{-7}$ sec, $d^2 = 67.7$ dB

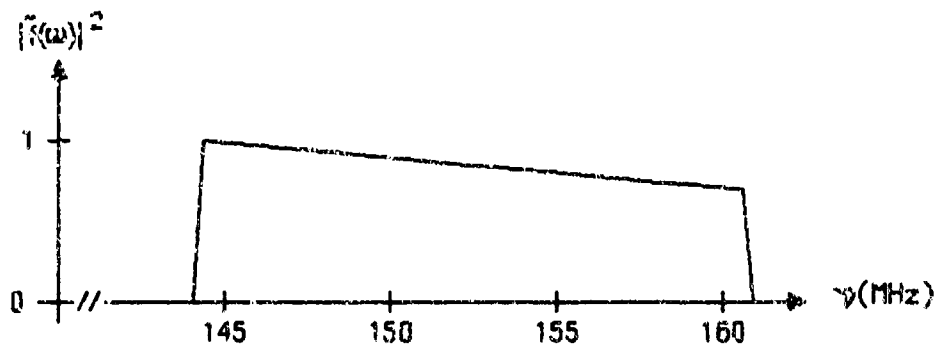


b) Energy Constraint ≈ 380 Joules, Pulse Extent $= 1.42 \times 10^{-7}$ sec, $d^2 = 64.5$ dB

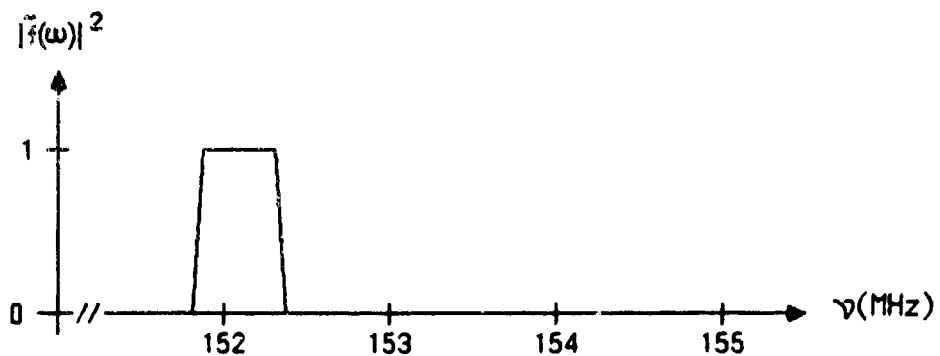


c) Energy Constraint ≈ 78.5 Joules, Pulse Extent $= 1.2 \times 10^{-7}$ sec, $d^2 = 63.6$ dB

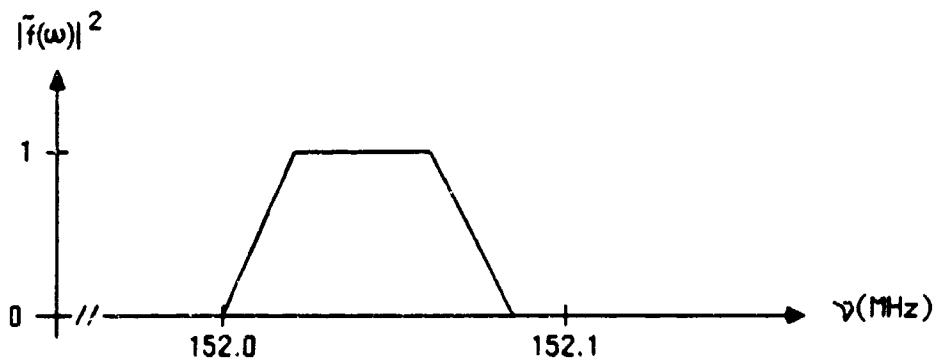
Figure 3-13. Effects of Energy Constraint on a Broadband Optimum Periodic Signal Design ($\nu_{min} = 25$, $\nu_{max} = 200$)



a) Energy Constraint = 15.5 Joules, Pulse Extent = 3.9×10^{-7} sec, $d^2 = 59.7$ dB



b) Energy Constraint = 0.4 Joules, Pulse Extent = 1.57×10^{-7} sec, $d^2 = 43.9$ dB



c) Energy Constraint = 0.028 Joules, Pulse Extent = 2.1×10^{-4} sec, $d^2 = 32.7$ dB

Figure 3-14. Effects of Lower Energy Constraints on Periodic
Signal Design ($\nu_{\min} = 25$, $\nu_{\max} = 200$)

reflecting object), to an increasingly narrow support near the higher frequency (resonant) response of the object.

The results of this computation illustrate that there is a strong spectral dependence of the optimal signal in the assumed energy/pulse duration constraint. Undoubtedly other target cross section and antenna response functions would have yielded different signal spectra, although the trend would undoubtedly be to follow the resonance of the target response, if it were within the overall system passband. (It is surprising, however, that the spectra gravitates towards the higher resonance, despite of the v^5 clutter law dependence.) Further results should be computed for specific targets that are of interest for military applications.

3.6 OPTIMUM SIGNALS FOR DISPERSIVE PROPAGATION MEDIA

3.6.1 INTRODUCTION

In some situations, the propagation path may contain, perhaps in part of its extent, a material consistency that is described by a complex dielectric constant that depends significantly upon wavenumber, or frequency. Such constituents may be due to suspended molecules (such as oxygen and water vapor normally present in the atmosphere), suspended particulates (water droplets and aerosols, e.g., in the atmosphere), and also peculiar propagation media such as plasmas (e.g., the ionosphere) and soils (e.g., when objects of interest may be buried).

Because of the causality property of Maxwell's equation for the electromagnetic field, the real and imaginary parts of a complex dielectric constant are necessarily related. That is, dispersion and absorption (attenuation) are encountered together. Of course, the dispersion effect is to degrade the pulse shape and hence detection and

resolution capabilities of a radar. The effects of attenuation are to, in effect, negate radiated power and hence degrade the detection performance. When present with sufficient influence, these effects can dramatically effect the optimal signal design.

To exemplify the impact on the signal design, we will consider dispersion due to a molecular constituency present in the propagation path. Further, we shall consider the effect of a single "resonance" or "absorption line." (The extension of these results to multiple resonances is, in principle, straightforward.) For simplicity, we shall assume either that the entire propagation path is homogeneous or that a "slab" of dispersive media is present in such a way that diffraction (at the boundaries) need not be considered. Also, it would often be the case that the density (in gm/cm^3) of the molecular constituents would be low, so that the resultant wavenumbers (for plane waves) do not differ greatly from those for an in-vacuo path.

A review of the previous development shows that, generally speaking, all results carry forward with the wavenumber k replaced by $k(\omega)$, as determined by the dispersion relation. The end effect is that the "block diagram" for the overall system model will have an additional "box", a linear, coordinate invariant transformation characterizing the dispersion and attenuation effects. Further, then, as we have shown that only the modulus-squared of the transfer function of these "boxes" enters into the signal-to-noise ratio formula, given that the processor is the optimal matched-filter, as discussed previously. Thus, it will be only the attenuation that will enter into the optimum signal design problem. We re-emphasize that, among the a priori data that is assumed known, will now be $k(\omega)$, the dispersion and attenuation relations. This, in a particular situation may, or may not be, a reasonable assumption.

It might be that only an a priori knowledge of certain statistical distributions about $k(\omega)$ are reasonably assumed. In such an instance, the "signal" and "terrain-emitted noise" will be correlated as both traverse the same dispersive medium. Then, the likely difficult optimal approach must follow the path generally discussed above, or more simply and sub-optimally, we may simply use an averaged $k(\omega)$ in place of the unknown random $k(\omega)$.

We begin by briefly reviewing a standard molecular absorption model that will serve us "canonically" here [24,25].

3.6.2 A SIMPLE DISPERSION/ABSORPTION MODEL

One considers the propagation of plane waves in an isotropic medium containing a dielectric constant and it is found that the phase velocity of a plane-wave can depend upon an index of refraction dependence upon frequency. The fundamental model for this phenomenon depends upon a dynamical model for the molecular constituents in the medium. The simplest such dynamical model is a simply resonant oscillator possessing a free period which is excited by the traversing/incident electromagnetic field. The resulting complex wavenumber that is associated with a permissible solution of the wave equation may have a form such as

$$\frac{c}{\omega} k(\omega) = 1 + \frac{1}{2} \left(\frac{b_1^2}{\omega_0^2 - \omega^2 - i\omega b_2} \right) \quad (3-66)$$

where ω_0 is the resonant frequency, b_1^2 is proportional to the number of such resonant molecules/oscillators per unit volume, and b_2 accounts for the dissipative effect of molecular collisions. (The in-vacuo wavenumbers permitted are $k = \omega/c$ as noted and used above.) The determination of these constants in any specific instance, is an object

of theory and experiment. Resolving such a $k(\omega)$ into its real and imaginary parts results in, respectively, the "dispersive part"

$$\frac{c}{\omega} \operatorname{Re}\{k(\omega)\} \equiv n = 1 + \frac{b_1^2}{2} \frac{\omega_0^2 - \omega^2}{(\omega_0^2 - \omega^2)^2 + \omega^2 b_2^2} = \frac{c}{\omega} \alpha \quad (3-67)$$

and the "attenuation part"

$$I_m\{k(\omega)\} = \frac{b_1^2}{2c} \frac{b_2}{(\omega_0^2 - \omega^2)^2 + \omega^2 b_2^2} = \beta \quad (3-68)$$

3.6.3 EXTENSION OF RADAR SYSTEM MODEL

If we review the derivation of the basic system model employed here, under the assumption that $k(\omega)$ does not depart greatly from $k = \omega/c$, we see that we need only replace k by $k(\omega)$ in all forms. Thus, the form (Equation 3-8) for the received signal waveform is now

$$s(t) = \frac{1}{2\pi} \int_{\Omega} d\omega \hat{f}(\omega) e^{-i\omega t + 2iR_0 k(\omega)} \tilde{Q}(\omega) \tilde{u}(0; \omega) \quad (3-69)$$

where, as stated, in the representation of $u(0; \omega)$ in Equation 3-1, k is everywhere replaced by $k(\omega)$.

Generally, if the dispersive effects are "weak", we can write

$$k(\omega) = 1 + k_D(\omega) \quad (3-70)$$

In the specific instance of molecular absorption mentioned above this is the case, with the obvious definition of $k_D(\omega)$. Thus, we may write

$$s(t + \tau_0) = \frac{1}{2\pi} \int_{\Omega} d\omega \tilde{f}(\omega) e^{i\omega t} e^{i2R_0 k_D(\omega)} \tilde{a}(\omega) \tilde{u}(0; \omega)$$

provided $\tau_0 = 2R_0/c$. The "new" system block diagram is as shown in Figure 3-15.

It is clear that, under the assumptions stated above, that any region traversed by the ray path does not cause diffraction effects, if a subpart of the ray path is the only part in the dispersive region, and is of "thickness" r_0 . Then we can replace $(2R_0)$ by $(2r_0)$ in the above.

We see that all of the earlier development now carries over if we simply replace $\tilde{a}_t(\omega)$ everywhere by $\tilde{a}_t(\omega) \tilde{h}_D(\omega)$, where $\tilde{h}_D(\omega) = \exp[i2r_0 k_D(\omega)]^*$

We thereby can readily include the dispersion and attenuation due to a frequency-dependent dielectric constant characterizing (part of) the propagation path.

The optimal receiver contains a filter matched to the received waveform, $s(t)$. Assuming that $\tilde{h}_D(\omega)$, that is, $k_D(\omega)$, is known, then the overall system transfer function and the SNR maximized over receiver choice depends functionally only upon

$$|\tilde{h}_D(\omega)|^2 = \exp[-4r_0 k_{DI}(\omega)] \quad (3-71)$$

where $k_{DI}(\omega) = \text{Im} \{k_D(\omega)\} = \beta(\omega)$

*To correctly model the thermal noise, that component due to terrain-emitted thermal radiation should also be modified by its propagation through the dispersive medium. Thus we should replace $\mathcal{P}_{n_{\text{ter}}}$ by $\mathcal{P}_{n_{\text{ter}}} |\exp[iR_0 k_D(\omega)]|^2$ where R_0 is the length of the one-way propagation path.

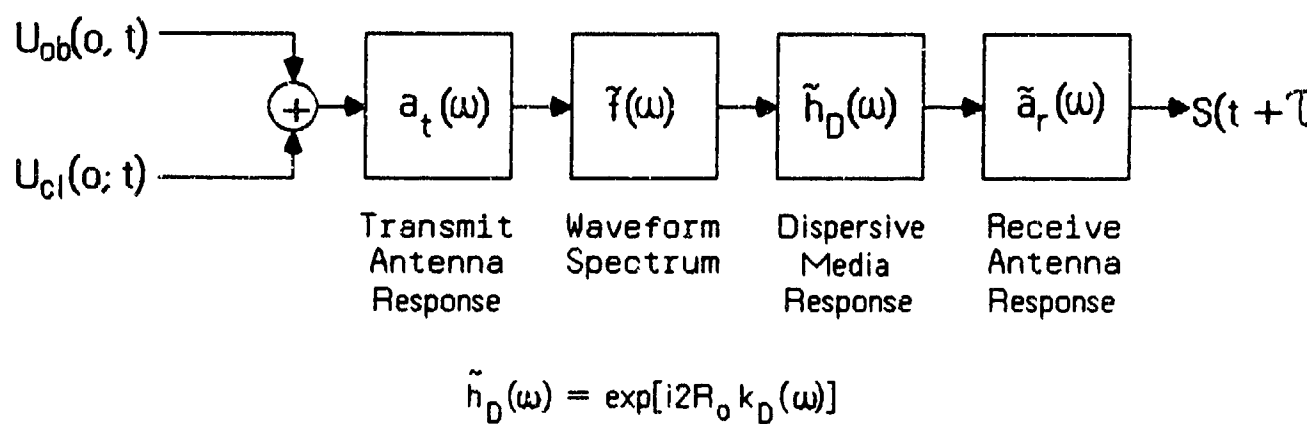


Figure 3-15. Radar System Model For Weak Dispersive Media

Of course, it also remains true that the SNR, maximized over receiver choice, depends only upon $|\tilde{f}(\omega)|^2$, the magnitude-square of the signal spectrum. Thus, we may utilize the same algorithms for this optimization problem solution by just replacing $|\tilde{a}_t(\omega)|^2$ by $|\tilde{a}_t(\omega)|^2 |\tilde{h}_D(\omega)|^2$.

In particular, we shall now carry over the choice of an optimum signal under energy and time extent restraints.

3.6.4 SPECIFIC NUMERICAL CALCULATIONS

To exemplify these matters, we shall employ a single, simple resonance with parameters, attenuation and bandwidth, chosen in a reasonable way, namely to be comparable to those of the oxygen absorption "line" for a "normal" atmosphere. However, we shall choose a resonant frequency considerably lower, in the general band of frequencies we have considered in the principal example studied in Section 3-5. We model $\beta(\omega)$ as

$$\beta(\omega) = \frac{\beta_0}{(\omega - \omega_0)^2 + (\Delta\omega)^2} \quad (3-72)$$

with $\beta(\omega_0) = \max_{\omega} [\beta(\omega)] = 10^{-2}$, corresponding to a 10 dB/Km attenuation. The width $\Delta f = \Delta\omega/2\pi$ of the oxygen line is about 6×10^4 Hz. We shall take Δf here a few MHz for a "cleaner" effect.

In view of the specific object (scatterer) "resonance" curve chosen in Section 3-4, we here will find it especially interesting to choose $f_0 = \omega_0/2\pi$ equal to one of those resonance lines, namely, 150 MHz. In terms of the normalized frequency $v = f/10^6$, Equation 3-72 becomes

$$\beta(v) = \frac{10^{-2}}{[(v - v_0)/\Delta v]^2 + 1} ; \quad v, \Delta v \text{ in MHz} \quad (3-73)$$

For the 10 Km path length R_0 used in above examples, we find

$$\exp[-4R_0\beta(v)] = \exp\left\{\frac{-40}{1 + \left(\frac{v-v_0}{\Delta v}\right)^2}\right\} \quad (3-74)$$

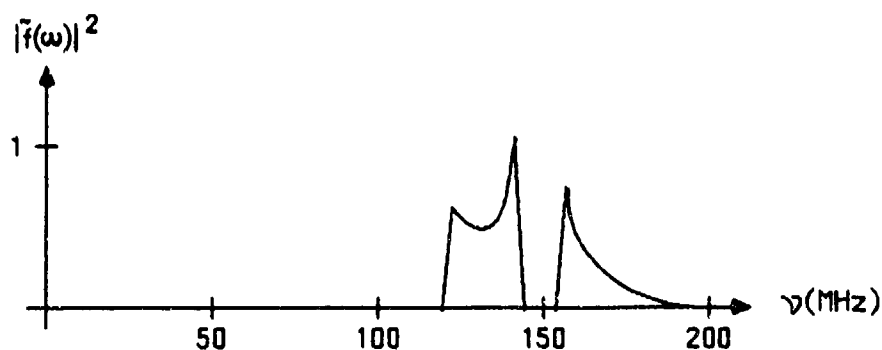
This is a rather severe attenuation and we may find it convenient to replace (-40) by, e.g., -4, corresponding to a less dense dispersive constituency or, e.g., a 1 Km thick medium.

Typical results of the signal optimization are shown in Figure 3-16. As expected, the signal modulation is chosen as in the non-dispersive case, except that no signal spectrum is "wasted" where the attenuation is too great. Also, there seems to be a tendency toward a curious increased weighting near the edge of the heavily attenuated region.

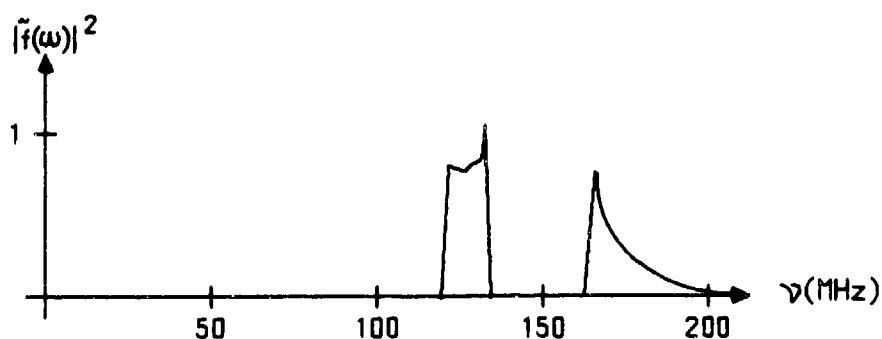
3.7 FURTHER DESIGN OBSERVATIONS

The preceding developments, in particular the design examples, show that the optimum signal's spectrum modulus can assume a rich variety of forms, depending upon the signal energy and pulse duration constraint, the maximum permitted bandwidth, the nature of the path dispersion, and the remaining free system parameters. Additionally, the spectral modulus is strongly influenced, as was seen, by the form of the frequency response of the object to be detected, denoted $|W(v)|^2$.

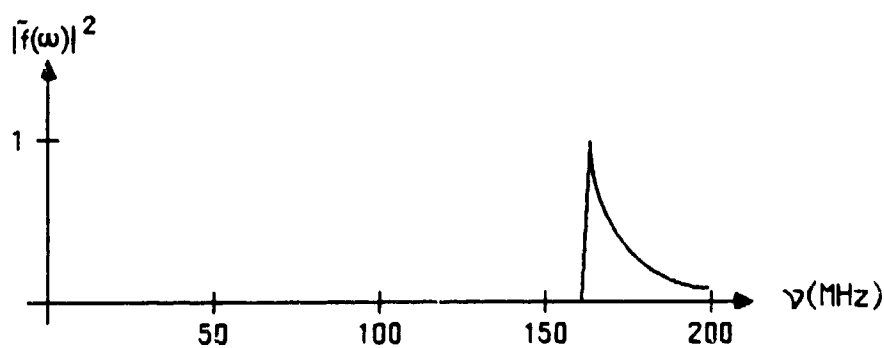
This being the case, the question naturally arising next concerns how one might design such a detection system for a realistic practical application. While the designer desires an optimal, or near optimal, design, the latter should also possess a certain robustness with respect to some degree of departure of parameters from their a priori assumed



a) Energy Constraint = 136 Joules, Pulse Extent = 1.8×10^{-7} sec



b) Energy Constraint = 106 Joules, Pulse Extent = 2.6×10^{-7} sec



c) Energy Constraint = 30.2 Joules, Pulse Extent = 3.0×10^{-7} sec

Note: Maximum attenuation of media is at 150 MHz.

Figure 3-16. Effect of Energy Constraint on Optimum Signal
For Dispersive Media ($\nu_{\min} = 25$, $\nu_{\max} = 200$)

values. The most straightforward procedure is to assume an a priori distribution is known, or can be estimated, for such parameters. Then, "standard" statistical procedures can be employed. We will sketch this out in the case of variable object (target) frequency responses. Clearly, there, if we design a system for certain resonances of one object, the detection performance may be very poor relative to other objects with differing resonances.*

For example, it is conceivable that a particular radar system might be dedicated to detecting an object which is a member of a small number of possible classes. It may also be reasonable to assume estimates of the a prior probability of a given class can be made available. Roughly speaking, we might expect that an appropriate system design would then be concerned with an "average object response", in place of a single object class response. This will be the case under the "soft" maximum signal-to-noise ratio (suitably defined) criterion as we shall see. However, this is likely not an optimal procedure when the optimality criterion is, e.g., maximizing the decision error probability.

We now revisit the basic hypothesis testing problem. We fix α , the class, and actually repeat the considerations implicit in the prior discussion, finally averaging over α . That is, the likelihood ratio, for fixed α and random phase θ , is well known [22,23] to be

$$L(z|\theta, \alpha) = \exp \left\{ \operatorname{Re} \left[\frac{e^{i\theta}}{\eta_0} \int_T z(t) S_\alpha^*(t) dt - \frac{1}{2\eta_0} \int_T |S_\alpha(t)|^2 dt \right] \right\} \quad (3-75)$$

where z denotes the data

$$z(t) = e^{i\theta} S_\alpha(t) + n(t), \quad t \in T, \quad (3-76)$$

*Happily, however, resonances are strongly related to an object's size, so that certain classes (sizes) of military objects (e.g., manned bombers) are likely to have similar responses.

where $n(t)$ is a sample function of white Gaussian noise, and α signifies class membership. Carrying out the average over θ , one obtains the well known form [22,23]

$$\ell(z|\alpha) = I_0\left(\left|\frac{1}{\eta_0} \int_T z(t) S_\alpha^*(t) dt\right|\right) e^{-E_\alpha/\eta_0} \quad (3-77)$$

where I_0 is the modified Bessel function of the first kind, order zero, and the real signal $s_\alpha(t)$, corresponding to the complex signal $S_\alpha(t)$, has energy

$$E_\alpha = \frac{1}{2} \int_T |S_\alpha(t)|^2 dt. \quad (3-78)$$

Suppose that the number of classes is countable, with a priori probabilities P_α , then the desired likelihood ratio, which specifies the optimal processor, is

$$\ell(z) = \sum_\alpha P_\alpha I_0\left(\left|\frac{1}{\eta} \int_T z(t) S_\alpha^*(t) dt\right|\right) \exp [E_\alpha/\eta_0]. \quad (3-79)$$

Thus, this optimum processor, for the detection purpose, is in fact the approximately weighted sum of all the subprocessors required in order to perform object classification. Generally, because of the nonlinear forms, a simpler form is not assumed. In principle, the error performance can now be determined. The signal is then chosen to minimize the error.

For example, suppose that the probability of error, given α , has a bound and approximation of the form

$$P(E|\alpha) \leq 1/2 \exp[-d_\alpha^2/4] \quad (3-80)$$

as is precisely the case when "signal plus noise" and "noise alone" are equally likely [22,23]. Averaging over the a prior probability of the classes, the desired error bound is of the form

$$P(E) \leq \frac{1}{2} \sum_{\alpha} p_{\alpha} \exp [-d_{\alpha}^2/4]. \quad (3-81)$$

Here d_{α}^2 is given by (3-34), with $|\tilde{B}|^2$ replaced by $|\tilde{B}_{\alpha}|^2$. The optimal signal spectrum modulus is now reasonably chosen to minimize the bound/approximation, e.g., with an energy restraint. This appears to be a more difficult optimization problem than that already considered above and we do not pursue it further here.

A simple approach to which it may be necessary to resort anyway when the distribution laws of the "noises" are non-Gaussian or even unknown, is to choose the signal in order to maximize a signal-to-noise ratio (SNR). We carry over the definition already made above, except additionally we average over the a prior distribution of α . As we have seen, for fixed α , we have the SNR

$$d_{\alpha}^2 = \frac{1}{2\pi} \int \frac{|\tilde{B}_{\alpha}|^2 |\tilde{f}aH|^2 dw}{\left\{ \mathcal{P}_{n_{ter}} |\tilde{a}_r|^2 + \mathcal{P}_{n_{rcv}} + \mathcal{P}_c |\tilde{f}a|^2 \right\} |\tilde{H}|^2}. \quad (3-82)$$

It is therefore clear that the SNR

$$d_{\alpha}^2 = E_{\alpha} \{d^2\}$$

has the same form as d^2 employed earlier, except that $|B_\alpha|^2$ is replaced by the average

$$E_\alpha\{|\tilde{B}_\alpha|^2\} = \sum_\alpha p_\alpha |\tilde{B}_\alpha|^2. \quad (3-83)$$

Therefore, the signal spectrum modulus, optimum according to this SNR criterion, is first the solution we found before, except $|B|^2$ is now replaced by $E_\alpha\{|\tilde{B}_\alpha|^2\}$, the expected, or averaged object frequency response (modulus-squared). Of course, this is an intuitively agreeable result.

3.8 CONCLUSIONS

The foregoing development is typical of the analysis that can and should be made for any radar system. The basic procedure is to, first, establish as comprehensive an analytic model as possible for the radar system in its entirety and then, second, establish a design criterion by which the processor and waveform modulations, and perhaps other system parameters, are chosen. Naturally, the success of this approach will depend upon the adequacy of the model, the appropriateness of the criterion, and the ability to perform the requisite analysis including optimization.

Here a "monostatic" radar detection system was modeled rather completely with respect to a matter of principal concern: the system's overall wavenumber, or frequency, dependence. The employed receiver and decision structure is optimal, according to the Neyman-Pearson criterion, under normal distributions and, additionally, in the absence of normal distributions, is optimal under the softer maximum signal-to-noise ratio criterion. The optimality criterion dictated how the signal, or modulation, should be designed. Under a constraint on

allowable signal energy, this optimization problem has a known solution which can be found numerically by a "bisection type" algorithm. It turned out that solely the modulation's spectral magnitude is thereby specified, leaving other attributes free to perhaps meet other desirable properties of the modulation, e.g., Doppler resolution. An approximate "synthesis" procedure was given to realize such waveforms in the large time-bandwidth product case (Appendix B).

The foremost importance of the work given here in the present context is, then, the optimal signal/modulation spectrum modulus. Its "support", i.e., frequencies where its non-zero values reside, is thereby given indirectly, without any a priori explicit restrictions. The radar system parameters entered the signal optimization problem as two parameters plus the energy constraint parameter. As these were varied, it was observed that the signal spectral modulus exhibited a wide range of interesting behavior, occupying location at or near "resonances" of the object to be detected and which lay within the system passband, and varying from narrow to broad with even disjoint supports. Not all of these variations could be predictable a priori, apparently, demonstrating the value of this development.

Additional results were obtained for periodic (pulse) modulation formats as well as including the effects of weak dispersion in the propagation path. It is concluded that solutions to the rich signal design problem for detection of targets in clutter does indeed yield, in some cases, signals that are of wide relative bandwidths. Thus, future applications analyses for specific targets of interest should be conducted to quantify the expected utility of such an approach.

The next section critically reviews the available literature on NSR techniques and on related topics which strongly depend on relative wideband waveforms.

4.0

DISCUSSION OF SELECTED WIDEBAND RADAR (WBR) RESEARCH

Section 2 outlined the principal radar applications for which WBR systems offer potential for improved performance and summarized the capabilities and limitations of current narrowband radars in these areas. In Section 3, a general theory for detection of targets in clutter was presented for systems of arbitrary bandwidth. This theory is relevant to several of the radar applications identified in Section 2, and serves as a means for evaluating present research efforts into WBR methods.

This section reviews selected areas of current WBR research and compares the potential of the techniques with the capabilities of present narrowband radar systems. Although the review is by no means exhaustive, the areas considered herein are representative of research which most significantly deviate from the standard, narrowband systems approaches. Specifically, they were chosen for having satisfied one or more of the following criteria: (1) a novel approach which cannot be realized with conventional, narrowband systems, (2) a controversial method for which a unified, end-to-end model is required for evaluation, (3) a technique which was specifically identified for consideration as part of the objectives of the NSR Techniques research program.

To this end, a pair of topical areas in WBR research are discussed in the sections that follow. The first encompasses work in techniques based on the singularity expansion method (SEM), which relates the transient response (radar return) of a target to a set of poles in the complex frequency domain [27-31]. These poles depend solely upon the shape and material parameters of the target, and are independent of the aspect or form of the incident radiation. This representation of a target's radar signature suggests several potential approaches toward improved performance in the applications outlined in Section 2.1; these are described in Section 4.1.

A second research area has been expounded almost exclusively by H. Harmuth and involves the use of what have been called "carrier-free" or large relative bandwidth signals for improving performance in virtually all radar applications [32-52]. This work has been the subject of extensive controversy [53,54], and a need to resolve these issues and identify the merit of Harmuth's claims have been explicitly included as part of the objectives of the program. A discussion of Harmuth's work is presented in Section 4.2.

Section 4.3 compares the approaches discussed in Sections 4.1 and 4.2 with the capabilities of present narrowband radar systems on the basis of technical merit, potential performance improvement, and practical implementation limitations.

4.1 SEM-BASED METHODS

The singularity expansion method was first applied to transient electromagnetic problems by C. Baum and his colleagues [27,28] in an effort to characterize the currents induced on targets by a nuclear electromagnetic pulse (NEMP). More recently, the SEM has been identified as a useful method in radar applications, particularly for target discrimination and/or classification [55-67]. The essence of the SEM and its utility in target ID can be summarized briefly as follows.

Let $f(t)$ represent the temporal impulse response of a target, i.e., $f(t)$ is an arbitrary component of the vector field scattered by a target under illumination by an impulsive plane wave incident field of arbitrary polarization and direction of incidence. For $t > \tau$, where τ is a sufficiently large delay (late-time response), $f(t)$ can be expanded as a sum of complex exponentials [55,56], namely

$$f(t) = \sum_{n=1}^{\infty} a_n e^{-s_n t} \quad (4-1)$$

where the a_n are independent of time. The natural frequencies s_n correspond to poles in the complex frequency response $F(s)$ of the target, which is obtained via a two-sided La Place transform on $f(t)$. The s_n have been shown to be independent of the form, direction of incidence, or polarization of the incident field. Conversely, they depend quite strongly on the shape and material composition of the scattering body. As such, they are characteristic of a particular target and are invariant to the geometry in which $f(t)$ is measured. All effects of the geometry and incident field are contained in the coefficients a_n [27-31].

This invariant property of the natural frequencies is the principle upon which all SEM-based radar applications are founded. Through either direct or indirect measurement of a subset of the s_n from the received signal of an impulse-like radar, discrimination and perhaps even classification of the target which produced the return can potentially be achieved. In the subsections that follow, a review of the research programs in SEM-based radar at specific institutions is presented.

4.1.1 RESONANCE REGION RADAR (R^3) - Research at General Research Corporation and The Naval Postgraduate School

Perhaps the most advanced application of the SEM to radar is the work of M. L. VanBlaricum and his associates at General Research Corporation (GRC) and M. A. Morgan and his co-workers at the Naval Postgraduate School (NPS) [29,55-57,65]. Beginning with VanBlaricum's thesis work at the University of Illinois [29], a systematic theoretical, numerical, and experimental research program has evolved for performing target identification by extraction of the natural resonances from the target's time domain response to broadband excitation. A brief outline of the methodology follows.

The transient response of a target is obtained by measuring the scattered field produced by an incident, pulse-like waveform from an impulse generator exciting a broadband horn antenna. A similar antenna is used to receive the scattered field. Alternatively, a transfer function, which is the Fourier transform of the transient response, can be measured by replacing the impulsive incident field with a series of CW fields produced by a swept frequency transmitter. In either case, calibration data from a known scatterer (sphere) and from the environment (chamber) are used to remove the effects of the clutter, transmitter, and receiver responses from the measured target response. The measurement system is illustrated in Figure 4-1 and the calibration procedure in Figure 4-2. The calibration is performed in the frequency domain.

The calibrated data represent the target impulse response (or transfer function) to an excitation with a uniform spectrum over all frequencies transmitted. Typical frequency and time domain responses for a generic, simplified target model are shown in Figure 4-3. This sampled response is input to an algorithm which estimates the natural resonance frequencies representing the poles in the complex spectrum. A modified version of Prony's method is used in performing the required computations [29,57].

The target discrimination function as demonstrated in the most recent GRC/NPS results [55-57] is achieved using a two step process. First theoretical and/or experimental impulse response data from a variety of aspects are processed using Prony's method to build up a histogram of pole occurrences in the complex frequency plane for each target of interest. Based on the pole clustering that occurs in the histograms, a set of circular regions are identified about each pole cluster. In the second step, the poles of the response from an unknown

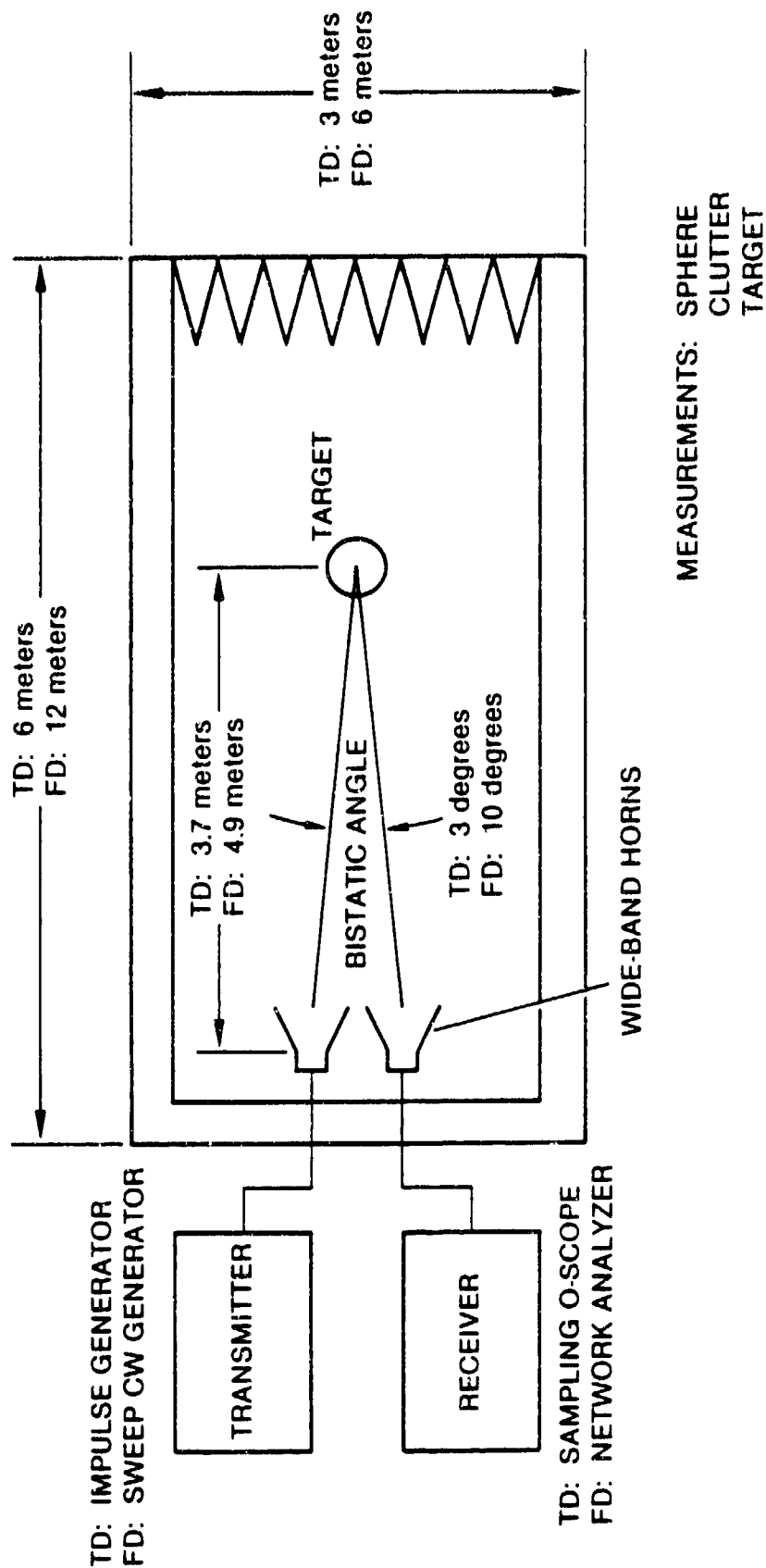


Figure 4-1. Experimental facilities for time-domain (TD) and frequency-domain (FD) target backscatter measurements (after [57]).

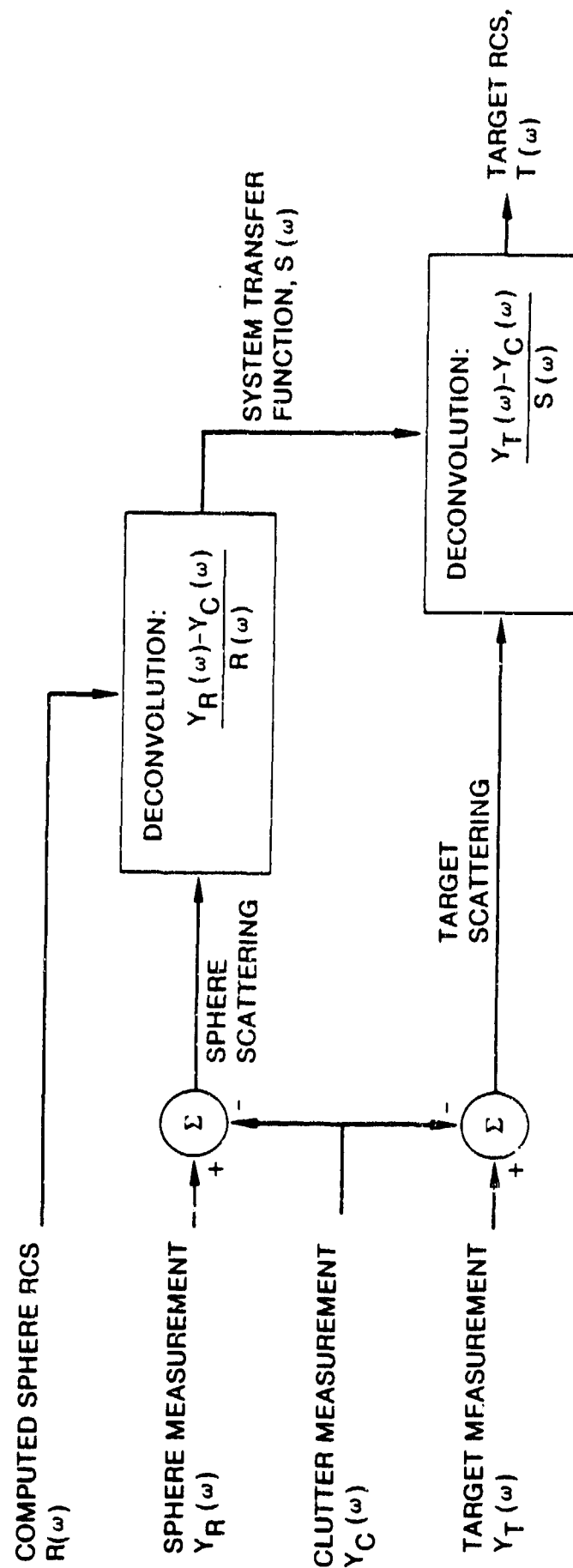
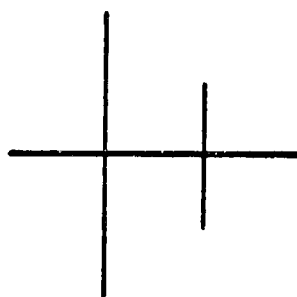


Figure 4-2. Calibration procedure for scattering data from the system in Figure 4-1 (after [57]).

SNR = 30 DECIBELS



○ MEASURED RCS
△ THEORETICAL RCS

— MEASURED RESPONSE
--- THEORETICAL RESPONSE

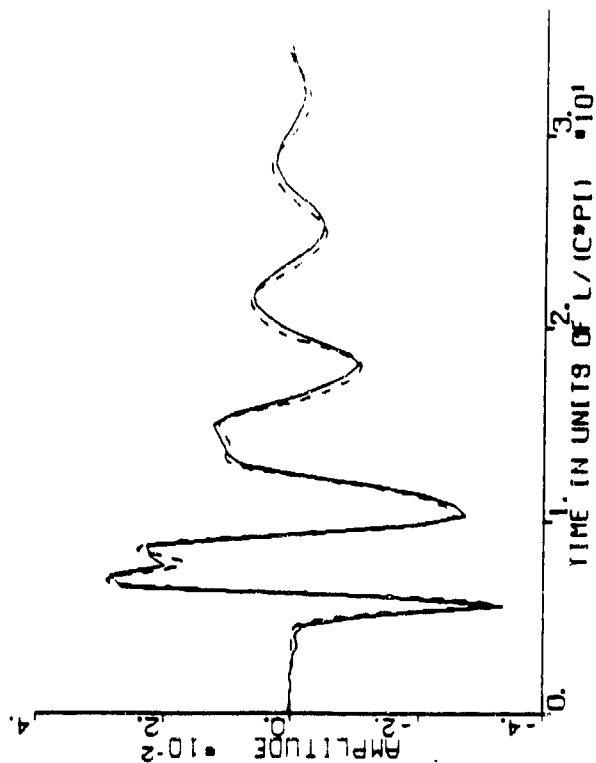
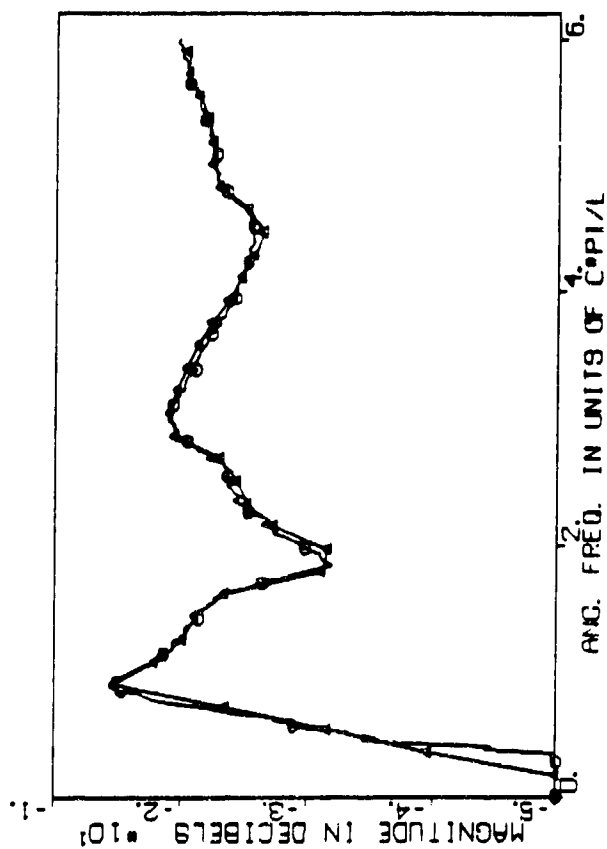


Figure 4-3. Frequency and time domain responses compared to theory for generic model, nose incidence (after [57]).

target are obtained and characterized as falling either inside or outside the regions for each of the targets "cataloged" in the first step. A positive identification is assumed when the number of poles falling in the cluster regions of a particular target exceeds the number for any other target. Preliminary results from the laboratory indicate reasonable success at discrimination between two classes of targets [65]. Failures occurred primarily with data collected at nulls in the radiation pattern of the natural resonances (aspects for which $a_n = 0$, Eq. (4-1)), or for data within insufficient signal-to-noise ratio (< 20 dB).

While the GRC/NPS research has successfully demonstrated the applicability of the SEM to aspect-independent target identification in the laboratory, there are several important considerations which must be addressed before a practical version of a resonance region radar can become operational. These are discussed in Section 4.3.

4.1.2 RADAR WAVEFORM SYNTHESIS - Research at Michigan State University

The use of the SEM in radar applications is not restricted to the explicit calculation of natural resonance poles from radar backscattered signals. Indeed, VanBlaricum has suggested that the eventual operational radar system for target identification based on the research described in Section 4.1 would not rely directly on pole extraction from each transmitted pulse [57]. Instead, a data base of known pole distributions would be used to perform a "correlation- prediction" with the return from an unknown target to arrive at a "most likely" target identification. In this approach, the incident waveform would not be tailored to a specific target or class of targets, except perhaps to the extent of selecting the appropriate spectral content of the transmitting signal so as to maximize the signal-to-noise ratio in the backscattered return (see Section 3).

An alternative approach can be taken when it is necessary to discriminate a single target or set of targets from a larger class. In this case, the transmitted and/or received signal can be tailored to result in a return which is characteristic of the target of interest and at the same time significantly different from the returns due to other scatterers. This concept of "Radar Waveform Synthesis" has been the subject of significant research activity at Michigan State University under K. M. Chen and his colleagues [58-60]. The foundation of their approach is again based on the SEM. In this case, a transmitted waveform is designed such that a single natural resonance frequency is excited on the target of interest. The late-time scattered waveform then appears as a single damped sinusoid. For targets significantly different from that for which the transmitted waveform was designed, the return signal is distorted due to the presence of more than one natural resonance. In this manner, the desired target can conceptually be discriminated from the others. Of course, the technique implicitly requires a knowledge of the natural resonant frequencies, i.e., the SEM poles, in order to synthesize the proper transmitted waveform, but this is probably not a restrictive assumption.

Numerical results for the radar waveform synthesis method have been reported for the case of a high-Q target (a thin wire at both normal [58] and oblique [60] incidence), as well as for a low-Q target (a sphere) [59]. The results include examples of the synthesized waveforms required to excite either the first or third natural resonance with either a zero or maximum initial value for the late time return, as well as illustrations of the scattered waveforms for both the desired target and targets whose characteristic dimensions differed by 5 to 20 percent from those for which the incident waveform was designed [58-60]. While the latter do contain some deviation from a single damped sinusoid, there is an issue as to whether the observed differences are sufficient

to provide robust discrimination in the presence of noise. This concern is further complicated by the lack of similar data for more complex targets such as the scale model aircraft used by VanBlaricum. For these classes of targets, the differences in target geometry are more pronounced than the simple scaling considered by Chen, et al., in his calculations, and hence the variations in the return waveform may be more significant. This advantage may be offset, however, by the lack of a precise knowledge of the location of the SEM poles for noncanonical scatterers. The poles must instead be obtained through experimental and/or numerical techniques such as Prony's method as described in the previous section. The generation and radiation of the required radar waveform is also a potential limiting factor in implementing this technique.

This latter concern has been addressed recently by Rothwell, et al., [66] and Webb and Chen [67]. They suggest a method wherein a somewhat arbitrary waveform is transmitted and the scattered return is processed by convolution with stored versions of the synthesized waveforms for single mode target excitation. This process effectively achieves the same result as transmission of the synthesized waveforms themselves; the convolved signal's late-time response will consist of a single damped sinusoid provided the return originated from the desired target. The original transmitted waveform need only contain the appropriate frequency content so as to insure excitation of all relevant natural resonances with sufficient signal power in the presence of noise. It is important to note that this frequency content could be determined by a process similar to that discussed in Section 3. Additional considerations in the practical implementation of the radar waveform synthesis method are presented in Section 4.3.

4.1.3 The K-PULSE CONCEPT - Research at the Ohio State University (OSU)

One of the earliest and most significant contributors to radar target characterization using time-domain scattering data was E. M. Kennaugh and others at Ohio State University [61-64]. He and his colleagues were instrumental in laying the groundwork for utilizing both the early-time forced response and late-time natural resonance response of the total time domain scattered field for target identification and discrimination.

Research regarding the former centered around the concept of the ramp response waveform technique for target shape reconstruction [66,67]. Under the physical optics approximation, it was shown that the field scattered by a target as a function of time when illuminated by a ramp waveform is directly proportional to the cross-sectional area of the target as a function of range over the illuminated portion of the target surface. This result can be shown to be a time domain representation of the Bojarski-Lewis physical optics inverse scattering theory [68,69]. Hence, a reconstruction of the target profile can be obtained by collecting ramp response waveforms over several aspect angles (provided the requirements of the physical optics approximation are satisfied). Because the physical optics response is zero when the incident field is zero, it follows that the ramp response consists only of that portion of the signal corresponding to the time during which the incident ramp waveform passes over the target (early-time response). This is not particularly a disadvantage, however, because a large portion of the total energy in the scattered field is contained in the early-time [65]. Experimental demonstration of reconstructions of the basic shapes of military aircraft and missiles has been reported [63].

As Kennaugh, Moffatt, and others at OSU continued their work in transient scattering, it became apparent that the approximations

inherent in the physical optics theory limited the overall applicability of the ramp response technique when used strictly as described above. In order to extend the potential of their methods for target discrimination into the low-frequency and resonance scattering regimes so as to include the late-time response, the concept of natural resonances (i.e., the SEM) and the geometrical theory of diffraction (GTD) were brought to bear on the problem. By integrating the ramp response concept with the waveform predicted from a knowledge of the natural resonances for a variety of targets, a predictor-correlator technique was formulated from which target discrimination capability was successfully demonstrated experimentally [62,63]. The method, like VanBlaricum's proposed classification scheme, requires a catalog of the complex SEM poles in order to predict the response from a "candidate" target. The classification is achieved by comparing the measured ramp response with the predicted waveforms and determining the normalized mean-square error. The effects of noise are a major concern [62] and are a topic of further research, particularly in the prediction portion of the algorithm. Similarly, by combining the ramp response with GTD contributions such as creeping waves and/or edge diffracted fields, the total target transient response can more accurately be approximated. Examples for spheres, cones, and cones spheres have been reported which validate this approach [61].

More recently, Kennaugh has proposed an approach to target discrimination, based almost exclusively on the SEM, known as the kill-pulse or K-pulse concept [64]. This technique can be viewed as a special case of the radar waveform synthesis method, although it predates Chen's work by several years. Like the radar waveform synthesis method, the K-pulse concept requires illumination (effectively) of the target with a specific incident field whose complex frequency spectrum is chosen to null out all the complex poles of the target's response. Thus, the radar return consists only of the early-time forced response, which is

by nature of finite duration. Because several such incident waveforms exist, the K-pulse is defined as the incident waveform of minimum duration having the above properties.

The principal advantage of K-pulse excitation is that it produces a time-limited response from the desired target regardless of both the aspect and range (i.e., near-field or far-field) of the target. It may therefore prove useful in situations where insufficient data is available for imaging or other more data intensive identification schemes. Like many of the other techniques described in the previous section, a catalogue of the complex natural resonances of targets of interest is required for the K-pulse concept. The number of data entries required for each target is small, however, because of the aspect-independence of the complex natural resonances. This compares favorably with imaging methods, where keys must be developed for a wide range of aspect direction.

4.2 "CARRIER-FREE" RADAR CONCEPTS

A second area of research in wideband radar theory and applications has been conducted almost exclusively by H. Harmuth and his students at Catholic University [32-52]. The work centers around the use of carrier-free or large relative bandwidth signals as opposed to the conventional radar waveforms which impress the "useful" signal information on a sinusoidal carrier, the bandwidth of the former being only a few percent of the frequency of the latter.

Although Harmuth's research has continued for over a decade, it has been the subject of intense controversy [53,54] and has to some extent motivated the research reported herein. A survey of the published work in carrier-free radar suggests a division into two principle areas: (1) utilization of carrier-free radar concepts in present-day narrowband

radar applications [33-46,52], and (2) analysis and design of broadband components for the generation, transmission, radiation, reception, and processing of carrier-free radar signals [32,47-52]. A review and assessment of each of these areas are presented in the subsections that follow.

4.2.1 CARRIER-FREE RADAR: APPLICATIONS STUDIES

Harmuth's earliest papers addressed the application of carrier-free radar principles to a series of generic radar and/or radio communication problems [33-46].

The subject of spread-spectrum communications was addressed in an article [33] which suggested the use of periodic nonsinusoidal waveforms as carriers for modulation by the baseband spread-spectrum signals. It was shown that the choice of broadband carriers leads to spectrum spreading over several times the bandwidth achievable when the signal is modulated on a sinusoidal carrier. This result should not be at all surprising. In addition, the bandwidth of the signal is on the order of its center frequency, i.e., the transmitted signal is of large relative bandwidth, measured in terms of [33]

$$\eta = \frac{f_H - f_L}{f_H + f_L} \quad (4-2)$$

where $f_{L,H}$ are the upper and lower frequency limits of the signal spectrum.

Sinusoidal carrier systems for spread-spectrum communications are limited by hardware considerations (transmitters, antennas, and receivers) to values in the range of $\eta \leq 0.1$. Thus, large spectrum spreadings requires a correspondingly high carrier frequency for transmission. Attenuation due to atmospheric losses can limit the

operating distance over which acceptable communications can take place. Harmuth addresses these issues in a cursory manner by describing conceptual hardware implementations of receivers which selectively respond to nonsinusoidal waves of a particular period [32,33]. He argues that these equipment would permit the use of large relative bandwidth signals (having η approaching unity) which would not suffer from the atmospheric attenuation present at higher frequencies [33]. It is not clear, however, how the distortions introduced by dispersion and frequency-dependent attenuation of the nonsinusoidal carrier signal would affect the performance of the proposed receiver implementation.

Application of nonsinusoidal or carrier-free signals to low-angle radar tracking is the subject of another of Harmuth's articles [34]. As discussed in Section 2.2, the principle limitation in these radar systems are the effects of multipath reflections from the earth's surface as the tracking angle gets closer to the horizon. The material in Ref. 34 concentrates primarily on addressing this limitation. In that article, Harmuth demonstrates that the reflection coefficient of both bare ground and sea water at near grazing incidence is very nearly -1 from 100 MHz to 10 GHz. Similar arguments are applied to the metallic surface of targets. With these results, Harmuth argues that the direct reflection will be reversed in polarity with respect to the transmitted waveform, while the multipath signal will not. He then claims that the use of a nonsinusoidal waveform (a video pulse of about 1 nsec duration) would allow this polarity-reversal to be used to discriminate between the two returns more easily than a conventional narrowband waveform. However, the basis for his recommendation of nonsinusoidal waveforms is qualitative and tenuous at best. Using simplistic forms for the return from a complex target such as an aircraft (see Fig. 8, [34]), Harmuth asserts that the sum of the direct and indirect return results in a more "detectable" signal in the presence of multipath. It is evident from the experimental data of Van

Blaricum, Fig. 4-3, that such a model for the return is not valid. While Harmuth's other arguments regarding lower atmospheric losses and reduced noise may favor nonsinusoidal waveforms, it is not possible to accept its use for low-angle tracking until a performance analysis of the tracking error, similar to that presented in Section 2.2.4 for narrowband signals, is carried out.

Analytical deficiencies such as that pointed out above are unfortunately typical of many of Harmuth's applications oriented articles. Often a great deal of effort is spent addressing a single, sometimes secondary, element of the total analysis, while the remainder is left to heuristic qualitative arguments. A second example of this occurs in a paper advocating the use of large relative bandwidth signals for over-the-horizon (OTH) radar [35]. Harmuth properly recognizes the fact that OTH systems are limited to signals with carrier frequencies occupying the 10 to 30 MHz range, thus ensuring reflection off one of several ionospheric layers. It is also true that in order to achieve even modest range resolution, the required signal bandwidths are sufficiently large (>5 MHz) such that the relative bandwidths, Eq. (4-2), are not characteristic of narrowband waveforms ($\eta < 0.05$). It is well known that signals of such bandwidths will suffer significant dispersion upon reflection by the ionosphere, along with frequency-dependent absorption [53]. These effects will severely distort the transmitted waveform and make reception of the return signal using methods based on a priori knowledge of the incident field nearly impossible. Rather than address this important issue, Harmuth devotes nearly the entire article to a discussion of modulation and demodulation technique for signals of the prescribed relative bandwidth which are founded on such a priori information. The question of the utility of large relative bandwidth signals for OTH radar applications remains therefore largely unanswered.

Harmuth suggests the use of nonsinusoidal signals for synthetic aperture radar (SAR) applications in a series of ten papers [36-45], each addressing a particular aspect of the SAR concept. Unfortunately, his treatment of these topics suffers from two serious shortcomings: a misunderstanding of the nature of conventional SAR theory and processing, and an emphasis on processing techniques for nonsinusoidal SAR which are insufficiently robust to noise and/or signal distortion for use in practical system implementations. It is regrettable that these limitations obscure what may be a valid application for large relative bandwidth signals (although not necessarily the signals suggested by Harmuth). Indeed, the improved performance of target detection in clutter suggested by the results in Section 3 for low frequency carrier (and hence large relative bandwidth) signals would certainly pertain to SAR applications.

Harmuth's most serious misconception regarding the principles of SAR is his statement that a SAR system relies upon the existence of a Doppler shift due to relative motion between the sensor and the scene in order to synthesize a large aperture from which improved resolution is achieved. He (correctly) suggests that a nonsinusoidal SAR radiating a narrow pulse can achieve similar improvements without the need for exploiting any Doppler effects [36,37]. From this he concludes that the standard SAR configuration of a single transmitter/receiver which synthesizes an aperture by radiating pulses periodically as it moves along the flight path can be replaced by a stationary array of transmitter/receivers located at the points where the pulses are radiated. It is further stated that with such an array, Doppler shifts could be used to detect target motion, since they are not being used to form the synthetic aperture. All these conclusions are indeed true. But, as stated above, they are also true for a SAR system radiating a conventional "chirped" signal. While the use of Doppler concepts are convenient in conveying the principles of synthetic aperture radar [70],

it is well known that the Doppler effects which occur during the reception of a single pulse must be neglected in order to properly formulate the SAR theory [71, Eq. (4)]. Thus, a system which could achieve a measurement of the scattered pulses from several points along a synthetic aperture while remaining stationary would actually perform better than one in motion. This could obviously be achieved using Harmuth's stationary array. Such an implementation has in fact been suggested by Farhat [72] using a conventional chirped waveform.

It is also worth noting that Harmuth's claim that such an array would require an element spacing of half a wavelength, while the spacing of a nonsinusoidal array would be much greater, (implying less elements and hence less complexity [36]), is also false. Both arrays would have spacings dictated by the rate of change of target distance from one element to another, so as to unambiguously sample the entire scene as defined by the beamwidth of the individual array elements. In both cases, this distance is many times the wavelength of the carrier and is given by the limits on the conventional SAR pulse repetition frequency [73]. It can thus be concluded that aperture synthesis can be obtained from any system capable of measuring distance to a target as a function of aspect direction. Certainly a radar using either a chirped signal or a nonsinusoidal pulse satisfies this requirement. Therefore, the arguments relating to the use (or non-use) of Doppler shifts made by Harmuth cannot justify a preference for nonsinusoidal waves in SAR applications.

A second claim which Harmuth expounds in several papers [36-45] in the "Nonsinusoidal SAR" series is that the use of nonsinusoidal waves leads to angular resolution which depends both on the signal bandwidth and the radiated power; a property, he claims, which is not true of narrowband SAR systems. There are, however, several fallacies in his arguments.

To show this, consider a classical SAR operating at a wavelength λ_0 with a bandwidth per pulse of Δf . It is important to distinguish the difference between range and cross-range resolution, given by [70]

$$\rho_r = \frac{k_r c}{2\Delta f} \quad (4-3)$$

$$\rho_a = \frac{k_a \lambda_0 R}{2L} = \frac{k_a cR}{2f_0 L} \quad (4-4)$$

respectively, where $k_{r,a} \geq 1$, R is the range, and L is the synthetic aperture length. Note that ρ_r exhibits the well known inverse dependence on bandwidth, while ρ_a is achieved by coherently tracking the phase of the carrier, hence the dependence on λ_0 .

For Harmuth's system, a nonsinusoidal pulse of duration ΔT is assumed to be radiated. Using a very idealistic model for the receiver transfer function, the received signal is assumed to be a triangular pulse of duration $2\Delta T$. The classical range resolution from such a pulse is simply

$$\rho_r = \frac{k_r c \Delta T}{2} = \frac{k_r c}{4\Delta f} \quad (4-5)$$

where Δf is the effective one-sided bandwidth of the receiver lowpass transfer function. Note that Eqs. (4-3) and (4-5) are in complete agreement provided that the two-sided lowpass bandwidth is used in Eq. (4-5). Since no carrier is available for tracking, the achievable cross-range resolution is a result of triangulation of the return for various points along the synthetic aperture length as a function of range. This can be shown to lead to a cross-range resolution of the form

$$\rho_a = \frac{k_a cR}{2\Delta fL} \quad (4-6)$$

which again is completely analogous to Eq. (4-4). This is also consistent with Brown's interpretation of SAR in the Fourier domain [74]. Eqs. (4-4) and (4-6) express the well known result that the azimuth resolution of a SAR improves with increasing carrier frequency; for a lowpass (no carrier) system, it is limited by the maximum frequency of the signal.* Thus, while the use of nonsinusoidal waves provides comparable range resolution to a classical narrowband SAR provided the same absolute bandwidth is transmitted, it will in general produce degraded cross-range resolution, since typically $\Delta f < f_0$.

In order to overcome this limitation associated with conventional processing of unconventional (i.e., nonsinusoidal) waveforms, Harmuth advocates the use of "slope processing" of the returned signals. Under the assumption that the scattered signal is the sum of many triangular pulses with different amplitudes and delays, he shows that measurement of the slopes of these pulses leads to improvement over the resolution given Eq. (4-6). Specifically, he asserts that

$$\rho_a = \frac{2k_a cR}{\Delta fL \sqrt{P/P_n}} \quad (4-7)$$

where $\sqrt{P/P_n}$ is the voltage signal-to-noise ratio (SNR) at the receiver [36,44]. While such a scheme may be valid theoretically under rather idealistic assumptions, it is not robust enough to be considered for practical implementation. This is because the unknown distortion of the pulse introduced by antenna and atmospheric dispersion as well as the complex scattering by the target (c.f. Fig. 4-3) makes any processing

*This result is also observed in computed tomography [75].

which depends on a specific pulse shape invalid. Furthermore, it is likely that for imaging applications $\sqrt{P/P_n} < 1$, making the use of Eq. (4-7) a moot point. Even under the circumstances for which slope processing is valid (i.e., high SNR and ideal pulse-shape preservation), the improvements suggested by Eq. (4-7) are not restricted to nonsinusoidal waveforms. Similar tradeoffs exist between bandwidth and SNR in the classical SAR for a variety of superresolution techniques. All lack the robustness required for operation under real world conditions, particularly for distributed targets, which is the typical mode of operation for a SAR when producing a radar image.

In fairness, it is worth mentioning a point made by Harmuth early in his treatment of SAR [36], wherein he states that the theoretical resolution limit of a SAR can be achieved for all points at arbitrary ranges provided one uses the differences of squares of time (or distance) instead of the differences of time alone. This is an important observation, and is equivalent to reconstruction by back-projection along spherical surfaces [76] instead of straight lines [77]. Such a method is, however, extremely computationally intensive and is hence less preferred than Fourier domain methods for range-curvature correction [78]. It is also true that such processing can be applied to conventional as well as nonsinusoidal signals, and hence does not provide justification for use of the latter.

The final application of nonsinusoidal waves expounded by Harmuth is their use in "anti-stealth radar," i.e., for detection of targets treated with absorbing materials for reduction of their radar cross-section. In the subject paper [46], Harmuth correctly observes that most radar absorbing material (RAM) coatings are restricted to relatively high frequencies due to thickness limitations (for ohmic RAM) or to small relative bandwidths (for tuned or resonant RAM). Furthermore, the application of RAM coatings is generally localized to

portions of a target associated with prominent "scattering centers" such as edges, corners, etc. This concept is by nature valid only at wavelengths much shorter than the target dimensions (i.e., it is a high frequency model). As a result, the localized RAM offers little potential for RCS reduction when the wavelength is increased to match the size of the target; in this case, the target resonates as a whole. In fact, these resonances are the basis of the SEM concepts discussed in Section 4.1.

It is, therefore, entirely appropriate for Harmuth to conclude that radar signals with large relative bandwidth are strong candidates for use in detecting RAM-treated targets. While the conclusions are valid, however, the reasons presented for justifying them are at best overly simplistic. Specifically, Harmuth discusses the situation of an infinite metallic half space coated with a lossy dielectric/magnetic material and illuminated at normal incidence by a baseband video pulse of finite duration. His arguments proceed as follows. By properly choosing the thickness and material properties of the coating, the reflected waveforms from the front and back surfaces can be made to cancel exactly for a sinusoidal signal at a given frequency. For a nonsinusoidal signal, on the other hand, the front and back surfaces would produce independent reflections which would not overlap provided the pulse was of sufficiently short duration. While all this is true, it is also irrelevant in practical applications. Even if the pulse shape could be preserved after propagation through the atmosphere, it is not possible to ignore the fact that a complex target would not preserve the shape, and more importantly, the duration, of the incident pulse (once again, see the waveforms of Fig. 4-3). This is because the incident wave is being scattered continuously from points along the range dimension of the target, and hence would consist of the superposition of a continuously delayed replicas of the incoming signal. This interpretation, which accounts from the early-time return (see

Section 4.1), is further complicated by the late-time resonances which follow. Thus, even if one could describe the scattered waveform as the sum of returns from the inner and outer layers of the coating (this itself is questionable), a system which relies on their "disjointness" in time would fail. What is amazing, as mentioned above, is that despite the shortcomings in Harmuth's reasoning, his conclusions regarding the utility of large relative bandwidth signals for detecting low observable targets is still essentially valid.

4.2.2 CARRIER-FREE RADAR: COMPONENTS STUDIES

In a more recent series of articles (save one), Harmuth addresses the realization of various critical components required for operating of nonsinusoidal radar systems, namely transmitting and receiving antenna elements and arrays [47-49], selective receivers [32], waveguides [50], and resonant cavities [51]. Each of these topics is discussed below.

The need for efficient, directive and distortionless, transmitting and receiving antennas is perhaps the most important requirement in implementing practical nonsinusoidal radar systems. While a great deal of research has been performed over the years on frequency independent antennas (see Chapter 6, [79], for example), the definition and analysis of radiating systems specifically for large relative bandwidth video signals is essentially new [80,81]. Harmuth's work in this area has emphasized the use of a radiating element which he calls a "large current radiator (LCR)," shown in Figure 4-4 [47]. The radiator is designed to operate much like a short electric dipole, and as such, radiates at a single frequency with the familiar figure-eight elevation pattern and isotropic azimuth pattern characteristic of dipole current elements. Directive radiation patterns are then achieved by combining several LCRs into an array [49]. The differences between the LCR and conventional short electric dipole are an attempt to overcome the

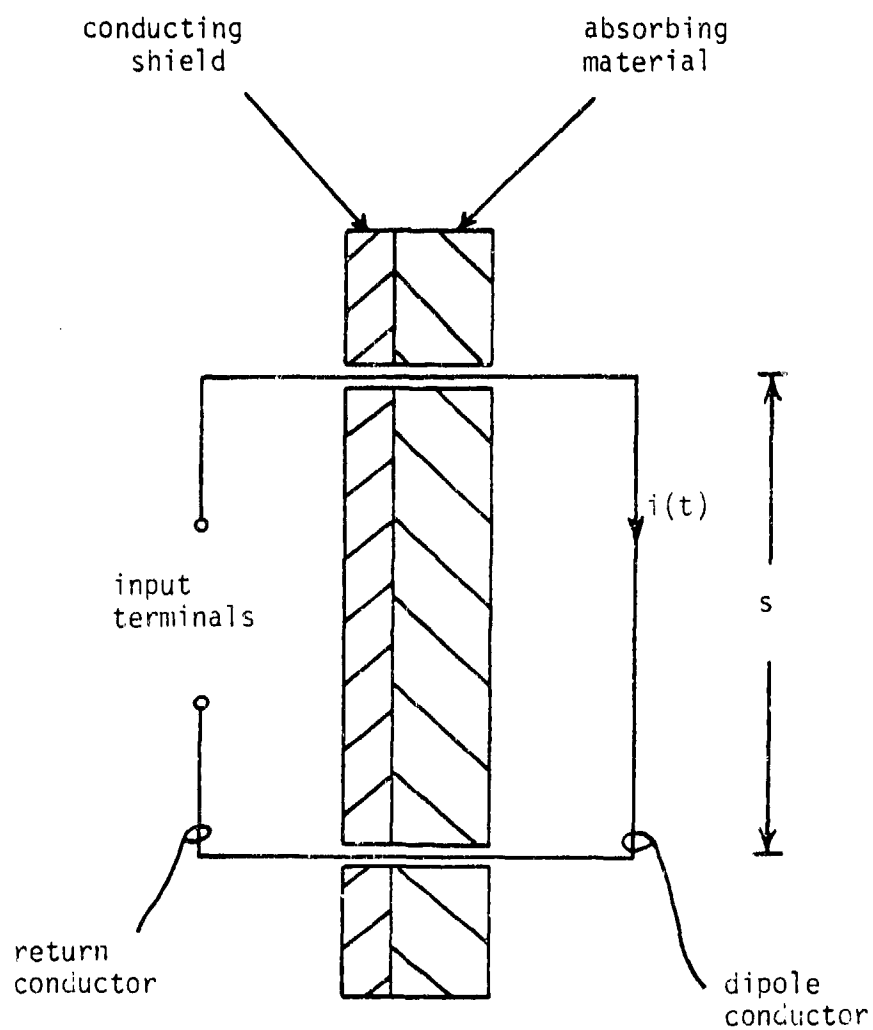


Figure 4-4. Schematic Diagram of the Large Current Radiator (after [47]).

limitations of the latter for radiation of low frequency signals. Because the electric dipole is by nature a capacitive structure, it cannot support large currents at low frequencies, even with top loading, since the current literally has "nowhere to go" [47-49]. In order to increase the current flowing along the dipole at low frequencies, the LCR feeds the dipole at its endpoints, and thus "closes the loop," giving the current a place to flow. Should the return path of the loop be symmetric with the dipole element, however, the total structure will radiate in the less efficient quadrupole mode. In order to emphasize the dipole mode of operation, the loop is intentionally made asymmetric by first isolating the return path from the dipole via a conducting shield, and then coating the shield with absorbing material to eliminate the "image" of the dipole formed by the conductor (see Figure 4-4). Further asymmetry can be introduced by using different conductor geometries for the dipole and the return path. Arrays of LCRs of this type have been successfully used to radiate and receive nonsinusoidal signals for into-the-ground radar probing applications [52].

Harmuth's analysis of the LCR attempts to address its performance as a transmitter and receiver [47,48], both alone and in arrays [49], in terms of standard measures for sinusoidal time dependence such as radiation resistance, input impedance, gain, directivity, efficiency, and so on. Each of these quantities, under the conventional definition, is frequency dependent, and hence for time-varying signals of nonvanishing bandwidth, each becomes a time-varying quantity. As a result, it is usually appropriate to define them in an average sense (with respect to time), so as to remove any dependence on the instantaneous variation of the waveform [80].

It is well known from Maxwell's equations that any antenna immersed in a linear stationary medium can be modeled as a linear, time-invariant system. Thus, the output of an antenna, for a given input, is

determined strictly from a knowledge of the transfer function (in the frequency domain) or the impulse response (in the time domain) of the system. Reciprocity guarantees that this fact holds regardless of whether the antenna is used for transmission or reception. (For details, see Appendix C.) Once the transfer function or impulse response is known, all of the above-mentioned performance parameters (gain, etc.) can be determined. For wire-like antennas, such as the LCR, the transfer function is most straightforwardly defined in terms of the current distribution along the wire. While it is not possible in general to determine analytically the exact current distribution in closed form, there exist well established "exact" numerical methods (such as the method of moments) for evaluating the current in either the frequency [82] or the time [83] domains. It then follows that the antenna performance parameters can likewise be numerically calculated.

Rather than apply this standard method of analysis, Harmuth uses a rather unconventional approach in his examination of the LCR. In an attempt to provide an analytical characterization of the performance of the LCR, Harmuth resorts to a series of approximations which are justified at best heuristically, thus leaving many of his results open to question. He begins by assuming the current is spatially uniform along the length of the LCR [47]. This is probably a reasonable assumption for short wire lengths and symmetric excitation. Harmuth's second approximation is critical to his results, and at the same time, subject to debate. First, a specified antenna current $i(t)$ is assumed to flow along the LCR. The instantaneous power delivered to the far zone is shown to be

$$P_1(t) = Z_0 \frac{s^2}{6\pi c^2} \left(\frac{di}{dt} \right)^2 \quad (4-8)$$

The essence of the approximation is to equate P_1 with the instantaneous power at the antenna terminals, i.e.,

$$P_1(t) = u(t)i(t), \quad (4-9)$$

where $u(t)$ is the terminal voltage. Given $i(t)$, P_1 can be obtained from Eq. (4-8) and $u(t)$ from Eq. (4-9). By modeling $u(t)$ as being generated by a Norton equivalent current source with driving current i_D and internal resistance R_i , it follows that the required time-varying source current $i_D(t)$ can be found.

Unfortunately, this procedure comes under scrutiny as to the validity of Eq. (4-9), which neglects the contributions to the terminal voltage from ohmic losses in the wire and reactive fields in the near zone of the antenna. Harmuth presents heuristic arguments for neglecting the latter when the current $i(t)$ has a sufficiently rapid rise time, but this begs the question since the required rise time may be limited by the neglected portions of the driving voltage, i.e., by the terminal inductance of the LCR wire loop. The ohmic losses are completely ignored by Harmuth, and yet it is known they represent a significant portion of the input resistance of a conventional dipole [79]. Whether the same is true for the LCR has yet to be determined.

The use of the LCR as the fundamental building block in an antenna array for directive radiation of nonsinusoidal waveforms is the topic of Ref. 49. Harmuth defines the directivity in terms of peak amplitude, peak power (amplitude squared), and energy (integrated power) patterns, the latter being the most robust concept and one which has found acceptance elsewhere [80]. Furthermore, from a target detection point of view, the energy pattern is the most relevant as shown in the analysis presented in Section 3 of this report. It is important to point out a specific definition of directivity is valid only to the extent that it is required by a more fundamental performance specification such as detection, resolution, or estimation. It is in this

context that a fourth directivity measure, the slope pattern, introduced by Harmuth as a means of improving the directivity, must be questioned. The ability to measure slope, as mentioned in Section 4.2.1, is extremely sensitive to noise and waveform distortion, and hence is not likely to provide a robust detection, resolution, and/or estimation capability.

Despite these shortcomings, the experimentally proven utility of the LCR for short distance, into-the-ground probing justifies its consideration as a candidate transmitting and receiving antenna for nonsinusoidal radar applications, provided further analysis supports the preliminary results demonstrated to date [47-49,52].

Another set of radar system components investigated by Harmuth for operation with large relative bandwidths is the lossless waveguide and waveguide cavity resonator [50,51]. These are important elements for the transmission and selective reception, respectively, of sinusoidal waveforms in conventional radar systems. In what is perhaps the most significant result of his research in nonsinusoidal waves, Harmuth has shown that certain signals with large relative bandwidth can propagate and resonate distortion-free in rectangular waveguides [50] and cavity resonators [51]. This finding goes against the intuitive view of waveguides and resonators as dispersive components, and opens up the possibility of extremely simple structures for the transmission and selective discrimination of periodic, nonsinusoidal waves, an issue which has been raised in arguments against the adoption of such waveforms [53]. Harmuth's result is based on the fact that there exist a denumerably infinite number of conventional waveguide modes and harmonically related frequencies for which the waveguide impedance and phase velocity are independent of frequency. Any superposition of these mode-frequency combinations constitute a valid distortion-free propagating signal. Because the frequencies are harmonically related, it

follows that the resulting signal is periodic with period

$$T = \frac{2\pi}{\omega}. \quad (4-10)$$

While the significance of this discovery cannot be downplayed, there remains additional work to be done before the utility of these components in nonsinusoidal radar applications is fully established. Most importantly is a need to establish the information "bandwidth" that can be propagated with each of the nonsinusoidal modes in the waveguide at some level of acceptable distortion, in the same way the conventional modulation is used to convey information on each of the sinusoidal modes. That is, if the nonsinusoidal modes are perturbed slightly through some modulation scheme (see [39], for example), does the resulting waveform still propagate without unacceptable dispersion down the guide? Excitation and detection of nonsinusoidal signals in the waveguides and cavity resonators must also be addressed.

Having reviewed two principal areas of research in wideband radar concepts (the SEM, Section 4.1, and carrier-free or nonsinusoidal radar, Section 4.2), the next section evaluates these concepts as to their technical merit and potential for improvement over conventional, narrowband radar systems. Practical limitations in implementing the preferred approaches are discussed.

4.3 COMPARISON TO NARROWBAND RADAR SYSTEMS

It is evident from the discussions in the previous sections that the use of wideband radar signals offers potential for improvement in many aspects of radar system performance. It is also true that there exist certain practical, and perhaps even fundamental, limitations on the implementation of radar systems using such signals with present day technology.

The discussions in Section 2 of this report suggest that improvements in the performance of conventional narrowband radar systems could be obtained over a wide range of applications through advances in the following generic areas:

1. Increased system signal-to-noise ratio (SNR).
2. Finer range and angular resolution at all ranges.
3. Clutter suppression.
4. Aspect and illumination independent target classification.

The potential of wideband, i.e., large relative bandwidth, signals for achieving advances in nearly all of the above areas has been identified in various places throughout this report. The signal scattered by a target, particularly one treated with RAM, can be greatly enhanced by operation in the resonance region of the target scattering domain, particularly with signals spanning several octaves. This fact has been recognized in both the SEM (see Section 3) and nonsinusoidal radar [46] research. Harmuth has also pointed out that the external noise in the 0.5 - 10 GHz region is considerably lower than at higher frequencies [52], making operation in this region desirable, all other considerations being equal. These two facts suggest improved SNR as a significant consequence of radar systems operating at frequencies below 10 GHz. Section 3 showed that enhanced clutter suppression is also possible with operation at lower frequencies.

Inasmuch as range resolution is fundamentally determined by the signal bandwidth, it becomes clear that fine range resolution and low frequency operation imply the use of large relative bandwidth signals. As discussed in Section 4.2.1, angular resolution, on the other hand, is governed primarily by the absolute frequency (not bandwidth) of the signal, whether real or synthetic aperture areas are used (neglecting non-robust superresolution methods). This suggests a tradeoff between

relative bandwidth and the need for both fine angular resolution and high SNR and/or low clutter. It should be pointed out that low angle tracking, while often considered to be limited by angular resolution, can also be improved through better range resolution because of the delay in the multipath signal.

Finally, regarding point (4) above, perhaps the single-most emphasized advantage of the SEM approach is the ability to completely characterize the scattering from a target with a finite number of parameters (the SEM poles) regardless of aspect or type of illumination. Of course, the excitation of many poles with significant energy requires a broadband waveform center about the resonant frequency range of the target, again suggesting the use of large relative bandwidth signals.

Given, then, the obvious potential of wideband radar signals for improved performance, it is necessary to quantitatively assess the extent to which this potential can be realized in a particular radar application. This can only be achieved with an end-to-end systems analysis so that the tradeoffs between advantages and disadvantages can be fully ascertained. Such an analysis for the problem of target detection in clutter plus noise was performed in Section 3. The results of that analysis clearly show the variability in the optimum waveform for differing system constraints. They also allow the effects of improvements in wideband components such as antennas, receivers, etc., to be incorporated in the performance prediction. These components, as discussed later in this section, are a major practical limitation in developing wideband radar systems. Perhaps the most important observation to be made from Section 3 is that one cannot simply argue for wideband versus narrowband signals; instead, each application must be addressed individually.

Regarding the use of the SEM for target classification, Van Blaricum and others readily admit the need for further studies before its promising potential can be realized [65]. In addition to improvements in the classification algorithm regarding pole extraction and recognition and the inclusion of early-time response data, Van Blaricum clearly states that an end-to-end system analysis is required to address practical issues such as the operating scenario, component design, etc.

Harmuth, on the other hand, is less willing to acknowledge the need for further extensions of his cursory studies of nonsinusoidal radar applications [32-46]. His simplifying and often piecemeal approach, coupled with his tendency to consider only particular types of waveforms, makes it difficult to assess the performance gain which might be obtained in each of the applications he considers should a more rigorous analysis be used. It is important to emphasize, however, that despite the shortcomings of his analyses, the applications suggested by Harmuth and discussed in Section 4.2.1 may still be enhanced through the use of wideband waveforms.

A major issue in implementing radar systems with large relative bandwidth is the existence of components capable of operating over wide ranges of frequencies. Harmuth's treatment of the principle limiting factors, namely transmission, radiation, sensing, and selective reception of nonsinusoidal waves [47-51], is much more satisfying than his work in WBR applications. This is an important distinction, since a component concept developed by Harmuth could prove useful in applications expounded elsewhere, such as using the SEM for target classification. While his work in NSR components also requires additional refinement, Harmuth's original contributions in the areas of antennas, waveguides, and cavity resonators represent a significant first step.

It is quite common in discussions regarding the potential of wideband radar systems to call out "fundamental limitations" inherent in the use of signals having large relative bandwidths [53,54]. One must carefully distinguish, however, those limitations which are "fundamental" from those which are "practical", i.e., those limited by current state-of-the-art technology. Perhaps the most significant fundamental limitation in the use of wideband radar signals is the distortion introduced by (unknown) dispersion and frequency-dependent attenuation due to the atmosphere, ionosphere, and to a lesser extent, terrain. Any WBR system concept must be sufficiently robust to tolerate this distortion, either by minimizing it a priori or correcting for it a posteriori. A second, potentially "fundamental" limitation concerns the efficient radiation and reception of baseband (or nearly baseband) signals. While it is true that radiation efficiency depends fundamentally on the acceleration rate (and hence frequency) of charges, it is not necessarily true that a reasonably efficient radiator at low frequencies could not replace a more efficient high radiator should the difference be made up in reduced noise or increased scattering from the target. What is currently needed is a quantification of just how "reasonably efficient" a radiator for large relative bandwidths can be. To this end, it is important to investigate not just conventional antenna designs, intended for signals with small instantaneous bandwidths, but to consider unconventional antennas whose design is motivated specifically by the desire to radiate wideband waveforms (such as Harmuth's LCR).

The above discussion is not meant to suggest that "practical" limitations are of lesser significance. Nonetheless, it is true that in today's technological environment, a concept which may not be practically implemented in the near term should not necessarily be disregarded for long term application, particularly when the potential payoff is high. What is important is to employ sound research methods

to both quantify this payoff and identify those critical technologies where improvements are required. Only then can the cost versus risk versus payoff be confidently established. Unfortunately, such an approach has not always been pursued; instead, emotional and defensive reactions have often colored what were to be otherwise scientific conclusions.

In summary, the theoretical potential of wideband radar systems for improved performance over conventional narrowband radar systems has been demonstrated repeatedly in the literature (see references). This potential is tempered by both fundamental and practical limitations in implementing such systems. Two major and distinct areas of research in wideband radar were reviewed in Sections 4.1 and 4.2. The advantages and disadvantages of each were discussed. It was concluded that in general, the system concepts based on the SEM were more robust to unknown perturbations in the radiated waveform, target shape and aspect, and resolution, than the techniques using baseband video pulses or "nonsinusoidal" waves suggested by Harmuth. On the other hand, the former have often not addressed the limitations imposed by present day technology; in this regard, the latter has introduced novel concepts for overcoming these limitations. Future research should aim at integrating both of these areas via an end-to-end system formulation and analysis to identify the tradeoffs in payoff and risk to better focus development of the critical technology areas. An example of such an analysis was presented in Section 3 for the problem of target detection in clutter and noise. The tradeoff between a system constraint (total radiated energy) and the optimum signal spectrum was clearly illustrated.

5.0 CONCLUSIONS AND RECOMMENDATIONS

A preliminary investigation into the potential advantages and perceived limitations of wideband radar (WBR) system concepts has been performed. A wideband radar is defined qualitatively as utilizing signals whose relative bandwidth is significantly larger than those used in the corresponding conventional narrowband radar system. The capabilities of wideband radar systems for providing improved performance over current narrowband radars was examined. At the same time, the limitations of each approach, both fundamental and practical, were defined. The most promising concepts for wideband radar applications and hardware components were identified. The results of the research effort are summarized below. Recommendations for further research conclude the section.

5.1 SUMMARY

A generic set of radar applications were identified in Section 2. These include search, target detection, tracking (particularly at low angles), high resolution imaging (SAR), and target classification/identification. The capabilities and limitations of current narrowband radar systems for several of these applications were discussed in detail. In general, improvements in performance could be realized in all areas, as might be expected, through advancement in one or more of the following categories:

1. Increased system signal-to-noise ratio (SNR)
2. Finer range and angular resolution at all ranges
3. Improved clutter suppression
4. Robust, aspect and illumination independent target classification

While this conclusion may appear obvious, it is important in that it provides a quantitative list of performance parameters by which a candidate WBR system can be judged.

Throughout the years, the utility of wideband or nonsinusoidal signals in radar applications has been the subject of (often intense) debate, particularly as regards the work of H. Harmuth and his colleagues [32-52]. The research program described herein was in part motivated by a need to objectively resolve the issues behind this controversy. It became apparent rather early in the program that the longevity of the controversy was promoted primarily for two reasons: (1) a tendency of some advocates to expound the virtue of the proposed WBR concepts beyond what is supported by their (often oversimplified) analyses, and (2) the emphasis by both proponents and opponents on a single element of a particular WBR system or application (e.g. antenna, atmospherics, etc.) in order to justify either acceptance or rejection of the entire concept. It was therefore concluded that in order to provide an objective evaluation of a specific nonsinusoidal radar concept, an end-to-end formulation and analysis of the system performance is required.

An example of such an analysis was presented in Section 3 for one of the above-mentioned generic radar applications, namely target detection in clutter. The analysis was supported by a formulation of the transfer function for a general radar system utilizing signals of arbitrary spectral content. The details of the formulation are contained in Appendix C. It was shown that for optimum detection, the shape of the power spectrum of the transmitted signal was highly dependent upon the spectral transfer function of the transmitting and receiving antennas, target, clutter, and noise. Furthermore, even when

these are fixed, the shape of the signal spectrum was highly dependent upon the total energy of the pulse, which was included in the analysis as a system constraint. These results demonstrate the importance of an end-to-end system analysis, wherein the limitations of system components (e.g. the antenna) can be traded off against the advantages of enhanced target scattered and/or reduced atmospheric attenuation. It should also be pointed out that the results of Section 3 show that only the power spectrum of the transmitted signal enters into the definition of the optimum receiver; the form of the temporal signal which conveys the prescribed spectrum is arbitrary, thus avoiding the need to necessarily radiate ultra-short video pulses to achieve large relative signal bandwidths (at least for the problem of target detection). This requirement has been one of the major focal points of the nonsinusoidal radar controversy [53, 54]. While the results of Section 3 are not completely general,* they do set the stage for future analyses of other potential WBR applications.

With this analytical groundwork in place, the research effort turned to a review of the recent work in unconventional, wideband radar concepts. The review, presented in Section 4, focused on research which met one or more of the following criteria:

1. A novel approach which cannot be realized using conventional, narrowband systems.
2. A controversial method for which an objective, end-to-end analysis is required for evaluation.

*The target transfer function was assumed fixed and known, implying a known target and aspect direction. Suggestions on how to mitigate these requirements are discussed in Section 3.

3. A technique which was specifically identified for consideration as part of the research program reported herein.

In order to limit the review to the scope of the program, a pair of research areas were selected which meet the above requirements: techniques based on the singularity expansion method (SEM), and the so-called "nonsinusoidal radar" studies based on the use of extremely narrow baseband, or video, pulse waveforms. The former has been used by a large number of researchers in a variety of applications; those specifically dealing in radar include the work at General Research Corporation (GRC) [55-57, 65] in "resonance-region radar" (R^3), studies at Michigan State University [58-60, 66, 67] on "radar waveform synthesis," and the investigations at Ohio State University [61-64] into ramp response waveforms and the "kill-pulse" concept. The latter has been carried out almost exclusively at Catholic University [32-52] by H. Harmuth and his colleagues.

The research activities in question could be divided into studies of wideband radar applications or wideband radar components. Virtually all the SEM work concentrates on the former, and depends in some manner upon the differences between the characteristic natural resonances of dissimilar targets to achieve target classification. Of significant importance is the fact that the natural resonances are intrinsic to each target and independent of both the aspect direction and spatial variations of the illuminated wave. This suggests that SEM-based classification schemes may provide robust performance in a variety of geometries using a small parameter set for target characterization (i.e., a few SEM poles). While all three of the above-mentioned groups have employed sound electromagnetic theoretical formulations to describe their concepts, each employs a somewhat different approach to achieving target discrimination. Specifically, each has different criteria for

determining the required transmitted waveform and each uses different algorithms for processing the receiver signal scattered by the target. As is to be expected in preliminary analyses of this type, simplifying approximations have been made to varying degrees regarding the effects of the antenna and intervening medium on the waveforms. Nonetheless, each demonstrates the potential for significant improvements in the classification of unresolved targets. Assessment of the relative performance (correct versus incorrect classification) of each technique, however, requires an appropriate end-to-end systems analysis similar to that presented in Section 3; such an analysis has yet to be performed for any of the candidate methods. In fact, GRC has also identified systems analyses as the next step in their study [57].

Harmuth's work in nonsinusoidal radar has addressed both radar applications [33-46] and radar system components [32, 47-51]. As discussed in Section 4.2.1, his approach to the former is often oversimplified and at times misdirected. Specifically, there is a tendency to overemphasize a single, sometimes secondary, aspect of the problem, thus leaving the major issues unresolved. The analysis is almost always driven to consideration of a specific radar waveform, a baseband video pulse, so that the results are highly dependent upon maintaining the specific form of the waveform after propagation through the medium and scattering by the target. This assumption leads to detection and/or processing schemes which are not sufficiently robust for practical operating conditions. This is unfortunate, since Harmuth's conclusions that wideband radar offers significant potential for improvement in the performance of conventional narrowband systems is essentially correct. The deficiencies in his analysis, however, have led to substantial criticism of the WBR concept.

In contrast to his treatment of radar applications, Harmuth's work in nonsinusoidal radar components, particularly antennas [47-49] and waveguide devices [50, 51] is thorough and rigorous. Although more research must be done to assess their full utility in WBR applications, Harmuth's novel concept of the large-current radiation (LCR) as an element for nonsinusoidal radar has already been used successfully for into-the-ground probing [52], and his demonstration that nonsinusoidal waves can propagate distortion-free in waveguides and resonant cavities represent important, new developments.

A summary assessment of the SEM-based and nonsinusoidal radar research reviewed herein is contained in Section 4.3. The reader is referred to that section for further details.

5.2 RECOMMENDATIONS

The long-term potential of using large relative bandwidth signals and wideband radar systems in military applications cannot be ignored. Significant improvement could be realized in detection of low observable targets, low-loss atmospheric propagation, robust target classification, and high resolution over-the-horizon applications, among others. It is also true that significant research is necessary to bring this potential to fruition, particularly in two areas:

1. More detailed systems and performance analyses of theoretical WBR concepts (e.g., resonance-region radar [57], radar waveform synthesis [58], kill-pulse and ramp waveforms [63, 64], etc.) to determine the optimum implementation of an SEM-based radar system for each candidate application, particularly regarding the waveform design and signal processing architecture.

2. Further development of devices and components for the above-mentioned wideband radar designs, with specific emphasis on transmitting and receiving antennas and antenna arrays, low noise

wideband receivers, and optimum signal processors.

The research efforts in these categories must obviously be coordinated, so that critical technology requirements identified in (1) can be properly addressed in (2). Considering the extent of the research performed to date (see the References) and the fact that the Department of Defense has funded longer-term, higher-risk sensor concepts such as those envisioned for the Strategic Defense Initiative, it is recommended that continued support be provided to the most promising WBR concepts, such as those based on the SEM, and components, such as the LCR and the time domain sensors being developed at the National Bureau of Standards [81], with the goal of an eventual demonstration of a prototype WBR system in a realistic radar application scenario. In order to achieve this goal, it is recommended first and foremost that the detailed performance analyses in (1) above be conducted on a comparative basis to define the approaches most worthy of consideration.

APPENDIX A
REMARKS ON LINEAR MAPPINGS AND FREQUENCY DOMAIN ANALYSIS

Part of the controversy over Nonsinusoidal radar (NSR) centers on the engineering community's use of sinusoids and Fourier analysis to describe linear systems. The purpose of this Appendix is to review the properties of such analysis techniques and thus to demonstrate that the techniques are not limiting the class of radar systems that can be considered. In addition, it is shown that the "complex envelope" notation, commonly used in radar systems analysis, is not limited to describing waveforms with narrow relative bandwidth.

A.1. LINEAR, TIME-INVARIANT MAPPINGS

Let L be a linear mapping of a space of functions into itself or another space of functions. (We proceed informally.)

DEFINITION: A linear mapping L is said to be "time-invariant" if, given that

$$y(t) = L\{x(t)\}$$

then

$$L\{x(t - \tau)\} = y(t - \tau).$$

We introduce the notation:

$$e(t; \omega) = L\{e^{i\omega t}\}.$$

THEOREM: If L is a linear, time-invariant (LTI) map, then

$$e(t; \omega) = e(0; \omega) \{e^{i\omega t}\}$$

Proof - As L is LTI, the following string of equalities holds:

$$e(t; \omega) = L\{e^{i\omega t}\} = e^{i\omega \tau} L\{e^{i\omega(t-\tau)}\} = e^{i\omega \tau} e(t - \tau; \omega).$$

Setting $t = 0$ and then making the change of variable $(-\tau) \rightarrow t$,

$$e(t; \omega) = e(0; \omega) e^{i\omega t}. \quad \text{Q.E.D.}$$

That is, the complex exponentials are the natural invariants of LTI maps, or LTI systems.

DEFINITION: $\tilde{x}(\omega) = e(0; \omega)$ is the "transfer function" associated with the LTI map L .

Since, speaking nonrigorously, any function $x(t)$ has a Fourier integral representation,

$$x(t) = \frac{1}{2\pi} \int_{-\infty}^{+\infty} e^{i\omega t} \tilde{x}(\omega) d\omega$$

where $\tilde{x}(\omega)$ is the spectrum (Fourier transform) of $x(t)$, one has a powerful "operational calculus" for LTI maps. For

$$\begin{aligned} y(t) &= L\{x(t)\} = \frac{1}{2\pi} \int_{-\infty}^{+\infty} L\{e^{i\omega t}\} \tilde{x}(\omega) d\omega \\ &= \frac{1}{2\pi} \int_{-\infty}^{+\infty} e^{i\omega t} \tilde{x}(\omega) \tilde{x}(\omega) d\omega \end{aligned}$$

(The assertion of the Theorem, recalling the introduced notation and definition, is

$$\tilde{\lambda}(\omega) e(t; \omega) = L\{e(t; \omega)\}$$

that is, $e(t; \omega) = \exp(i\omega t)$ is a "generalized eigenfunction" of L and $\tilde{\lambda}(\omega)$ is the corresponding "generalized eigenvalue." The ω -support of $\tilde{\lambda}(\omega)$, the spectrum of L , is generally the continuum.

A "linear antenna" is a more general idea. A receiving antenna is modeled by a mapping from a function of four variables, space and time, to a function of one variation, time. The converse is true for a transmitting antenna. In the latter case, we may imagine a function of time $v(t)$ impressed on a pair of terminals, the result being, say a scalar, electromagnetic field appearing at some suitable arbitrarily chosen reference plane PP' , as illustrated in Figure A-1.

DEFINITION: (1) A linear antenna structure has a linear mapping L , that is, for scalars α, β ,

$$L\{\alpha v_1(t) + \beta v_2(t)\} = \alpha L\{v_1(t)\} + \beta L\{v_2(t)\}$$

(2) A linear antenna structure is time-invariant if its associated mapping L is such that, if

$$L\{v(t)\} = E_{tr}(\bar{r}, t),$$

then

$$L\{v(t - \tau)\} = E_{tr}(\bar{r}, t - \tau).$$

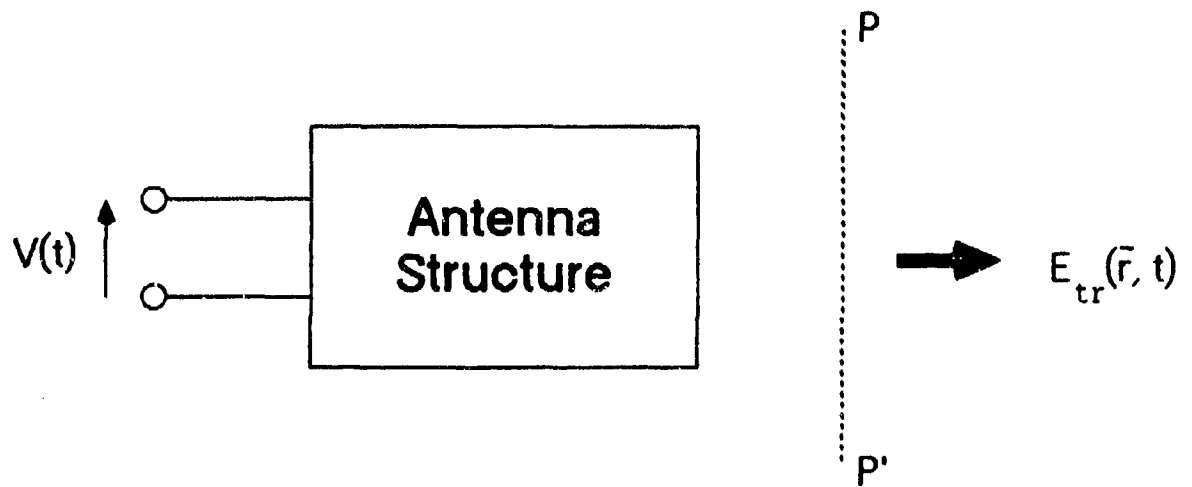


Figure A-1. Defining Structure for Antenna (Radiating) Element

We now introduce the notation

$$e(\bar{r}, t; \omega) = L \{e^{i\omega t}\}.$$

We have

$$e(\bar{r}, t; \omega) = L\{e^{i\omega t}\} = e^{i\omega\tau} L\{e^{i\omega(t-\tau)}\} = e(\bar{r}, t-\tau; \omega)$$

so that, in the same way as above,

$$e(\bar{r}, t; \omega) = e(\bar{r}, 0; \omega) e^{i\omega t}.$$

DEFINITION: $\tilde{x}_{tr}(\bar{r}, \omega) = e(\bar{r}, 0; \omega)$ is the "transfer function" of the associated LTI transmitting antenna. (Notice that, in this case, the transfer function depends upon the selected spatial location \bar{r} .)

In a similar manner, a transfer function may be defined for a receiving antenna structure.

A.2. LINEAR, TIME-VARIANT MAPS

More generally, linear mappings, of both bounded and unbounded nature, can have "generalized eigenvectors and eigenvalues", that is, spectral representations. Generally speaking, each time-variant, linear mapping has its own natural spectral representation. While this can be a complicated subject in functional analysis, even in the classical discussion of Sturm-Liouville differential equations, this is a well known phenomenon. For example, the Bessel functions, the Walsh functions, etc., are the natural orthonormal sets associated with certain differential equations with time-varying coefficients.

Given a spectral representation, generally speaking, there will exist an "operational calculus" that provides a spectral representation of a polynomial in the original mapping. However, unlike the case of linear, time-invariant mappings, polynomial combinations of a linear, time-variant maps are generally not of practical interest, and certainly not as widely applicable.

A.3. COMPLEX ENVELOPE NOTATION

As the preceding discussion has made clear, when an overall system is linear and time-invariant, the Fourier integral representation of an arbitrary waveform as a weighted sum of complex exponentials or sinusoids, is natural and greatly facilitating.

A separate matter that commonly arises in conjunction with this representation is variously labeled "the complex envelope representation" or "in-phase and quadrature representation", or "envelope and phase representation", or such. These are very convenient for both analysis and intuition and, are typically used for waveforms whose spectral support is small relative to their mean frequency, so called "narrowband" waveforms. However, more generally, the following may be established.

The complex representation from which the other representations may be derived, is a mapping or relation between a class of real bandpass functions and a class of complex functions. In order to be useful, the mapping must be one-to-one. The necessary condition for this is easy to state after a few definitions. First, the class of real "bandpass" functions have their spectral support in the frequency set

$$\Omega(\omega_0) = \{\omega: -\omega_0 - \Omega < \omega < -\omega_0 + \Omega\} \cup \{\omega; \omega_0 - \Omega < \omega < \omega_0 + \Omega\}$$

the collection of such function is denoted $R(\omega_0, \Omega)$. Second, the class of complex "low pass" functions have their spectral support in

$$\Omega_0 = \{\omega; |\omega| < \Omega\}$$

the collection of such functions is denoted $C(\Omega)$. The mapping from $C(\Omega)$ to $R(\omega_0, \Omega)$ is a mapping K such that $\forall F \in C(\Omega)$,

$$KF = \text{Re} \left\{ F e^{i\omega_0 t} \right\}.$$

It is easy to show that the range of K is $R(\omega_0, \Omega)$ and that:

THEOREM: K is one-to-one onto $R(\omega_0, \Omega)$ if and only if $\omega_0 > \Omega$.

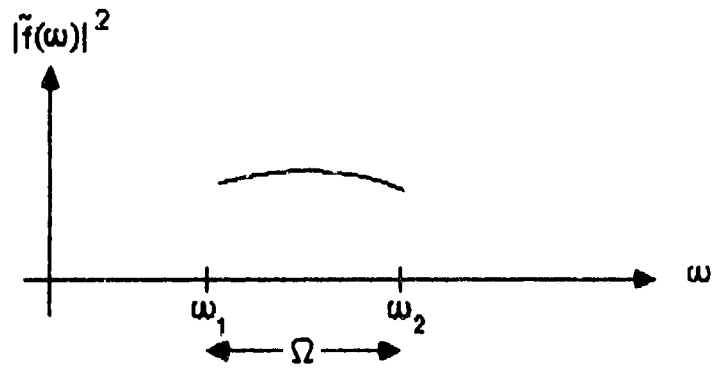
That is, as long as a "center frequency" ω_0 is chosen so that $\omega_0 > \Omega$, the complex representation is unique. Otherwise, ω_0 is arbitrary. And, in particular, note that the ratio $\omega_0/\Omega > 1$ may be arbitrarily close to 1, that is, ω_0 may be arbitrarily close to Ω . Hence, in this sense, the real bandpass signal does not have to be "narrowband", i.e., $\Omega/\omega_0 \ll 1$. Thus the often made conclusion that "if complex notation is used, the waveforms must have small relative bandwidth" is formally not correct.

APPENDIX B
THE GENERATION OF SPECIFIED SPECTRUM MODULUS
WITH A SPECIFIED SIGNAL TIME ENVELOPE

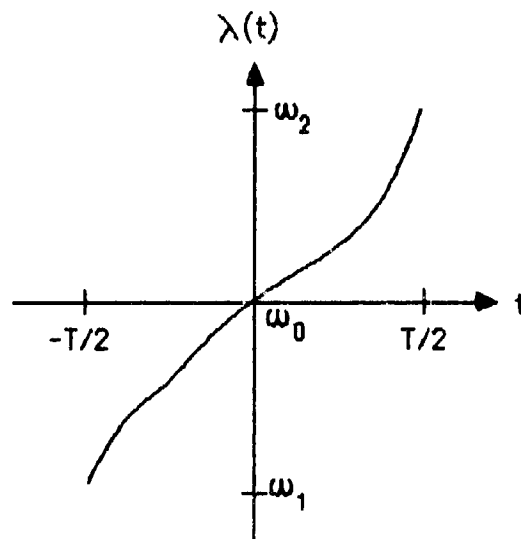
The solution to the system design problem posed in Chapter 3 resulted in the specification of the optimum signal modulation's spectral modulus, given an energy constraint. No other aspect of the signal modulation was, at least directly, specified. As a practical matter, the signal modulation's time envelope is usually a "rectangular pulse", of a duration T chosen, under a practical peak power constraint, of duration sufficient to meet the energy constraint.

One then arrives at a version of a classical problem: How, if possible at all, to specify the signal modulation's phase modulation to realize the specified pair (time envelope, spectral modulus). One such procedure, which applies where the "time-bandwidth product, TBP", that is, for example, the product of T times the extent of the support of the spectral modulus, is large [19, 20] will be described herein. Depending on the energy restraint and the peak power limit, this can be true here and, if so, presents a design problem.

The intuitive idea is this. Suppose the specified time envelope is rectangular, of duration T . Suppose also that the signal's spectrum modulus is, as sketched in Figure B-1a, the solution of the above-discussed optimization problem. When the TBP is large, it is possible to relate the spectral modulus to the signal's instantaneous frequency modulation, $\lambda(t)$, (the time-derivative of the signal's phase modulation). One imagines the "spectral modulus" as a "density" distributed in proportion to the relative time the instantaneous frequency spends near a given frequency. With this idea, one may construct the $\lambda(t)$ that will generate the above spectral modulus, to a good approximation when $T\Omega \gg 1$. (See the sketch in Figure B-1b).



a) Signal Modulus Constraint



b) Instantaneous Frequency Modulation

Figure B-1. Constrained Signal Modulus with Allowable Instantaneous Phase Modulation

To establish this approximation scheme, express the signal modulation in its Fourier integral (spectral) representation,

$$f(t) = |f(t)| e^{i \int^t \lambda(\tau) d\tau} = |f(t)| e^{i\phi(t)} = \frac{1}{2\pi} \int_{-\infty}^{+\infty} e^{i\omega t} |\tilde{f}(\omega)| e^{i\theta(\omega)} d\omega$$

and then evaluate the integral by the method of stationary phase. In the simplest, and usually appropriate case, there is one stationary point and the evaluation leads to a differential equation involving $|f(t)|$, $|f[\lambda(t)]|$, and $\phi[\lambda(t)]$. Involving the stationary condition on $\phi''[\lambda(t)]$, the solution is seen to be

$$\lambda(t) = \hat{G}^{-1}[2\pi G(t)],$$

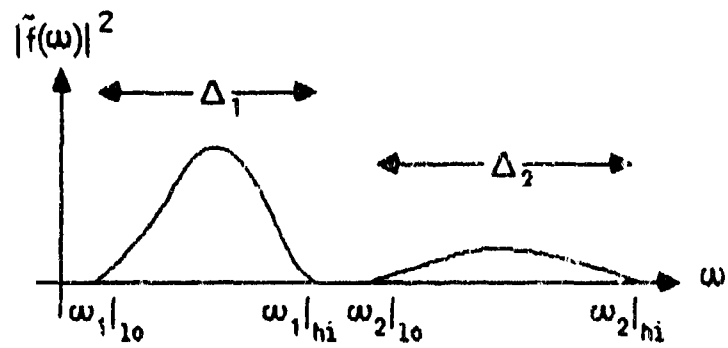
where

$$G(t) = \int^t |f(\tau)|^2 d\tau,$$

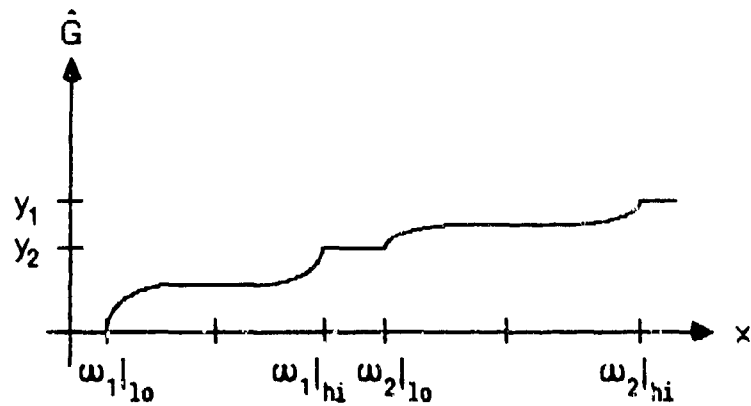
and \hat{G}^{-1} is the inverse, presumed to be definable, of

$$\hat{G}(x) = \int^x |\tilde{f}(\omega)|^2 d\omega.$$

In the present application the support of the optimal signal modulation was seen, in the specific examples, to have two disjunct supports (located near the specifically chosen object's "resonances"), for a certain interval of energy constraints. For example, a spectrum similar to that sketched was observed. In this case $G(x)$ will appear as sketched in Figure B-2b. Clearly \hat{G}^{-1} does not strictly exist. However, the situation is readily handled by dividing the range of \hat{G} into two sets, $Y_1 = \{y: 0 \leq y \leq y_1\}$ and $Y_2 = \{y: y_1 \leq y \leq y_2\}$; over each of these sets, \hat{G}^{-1} exists.



a) Typical Signal Modulus



b) Cumulative Distribution of Signal Modulus

Figure B-2. Typical Signal Modulus and Cumulative Distribution

Thus, a sketch of a likely sufficiently general algorithm to find such a frequency modulation and verify it is as follows:

1. Find $|\tilde{f}_0(\omega)|^2$ with the numerical procedure described in Section 3.4. $|\tilde{f}_0(\omega)|^2$ is stored as an array.

2. (a) Find the (finite number of) compact sets that make up the support of $|\tilde{f}_0(\omega)|^2$. Denote them $\Delta_1, \Delta_2, \dots, \Delta_N$. These may be stored as a $2 \times N$ array

(b) Calculate the indefinite integrals

$$\hat{G}_n(x) = \int_{\omega_n|_{10}}^x |\tilde{f}(\omega)|^2 d\omega, \quad x \in \Delta_n, \quad n = 1, \dots, N,$$

for a set of $\{x_{m,i}, i = 1, \dots, I\}$ and store as an $n \times I$ -dimensional array.

(c) Calculate the set of N images $y_n = \hat{G}(\omega_{n|hi})$, $n = 1, \dots, N$, and the set of images $\{y_{m,i} = \hat{G}(x_{m,i})\}$.

3. (a) For each $t_j \in T$, the $\{t_i\}$ a selected, suitable set of sampling points (stored as an array), calculate

$$y_j = G(t_j) = \frac{1}{T} (t_j + T/2).$$

(b) Determine which image Y_m contains y_j . Then evaluate

$$\lambda(t_j) = \hat{G}_m^{-1}(y_j) + x_m|_{10} ;$$

an interpolation scheme will be required, e.g., find the $\{y_{m,i}\}$ of the array 2(c) closest to y_j .

4. (a) Having the $\{\lambda(t_j), t_j \in T, i = 1, \dots, J\}$, integrate to find the phase modulation $\phi(t)$ at the $\{t_j\}$.

(b) As a verification, form $f_?(t) = |f(t)|_{\text{spec}} e^{i\phi(t)}$ and compute its (discrete) Fourier transform, e.g., by an FFT, and compare $|\tilde{f}_?(\omega)|^2$ to $|\tilde{f}_0(\omega)|^2$.

Appendix C

GENERAL TRANSFER FUNCTION AND IMPULSE RESPONSE OF A WIDEBAND (NONSINUSOIDAL) MONOSTATIC RADAR

An end-to-end formulation for the input-output relationship of a radar system operating with arbitrary wideband signals is developed in this Appendix. This type of formulation is required in order to fully understand the tradeoffs between the various elements of such a system. These tradeoffs will then allow an objective assessment of the advantages and limitations of using wideband signals in particular radar applications.

Section C.1 presents an antenna current-based representation of the total system transfer function founded on rigorous electromagnetic field theory. All potential frequency dependent quantities are identified. Section C.2 discusses how this representation is related to the antenna aperture-based formulation, which was used in Section 3 to demonstrate how the end-to-end system model can be applied to a particular radar scenario, namely target detection. Specifically, the antenna transfer functions on transmit and receive are identified using reciprocity, and the equivalence of the reflectivity and scattering matrix descriptions of a target is shown.

C.1. SYSTEM FORMULATION

A block diagram of a general (monostatic) radar system is shown in Figure C-1. The pertinent inputs and outputs of each major component are identified symbolically and will be defined in detail below. It is desired for analytic tractability that the overall system be linear; for this reason the quantities of interest will be voltages, currents, and fields, as opposed to powers, cross-sections, etc., which are proportional to the square of the former. Without a significant loss of generality, the system input is assumed to be a voltage waveform produced by an appropriate signal generator, while the output is also a

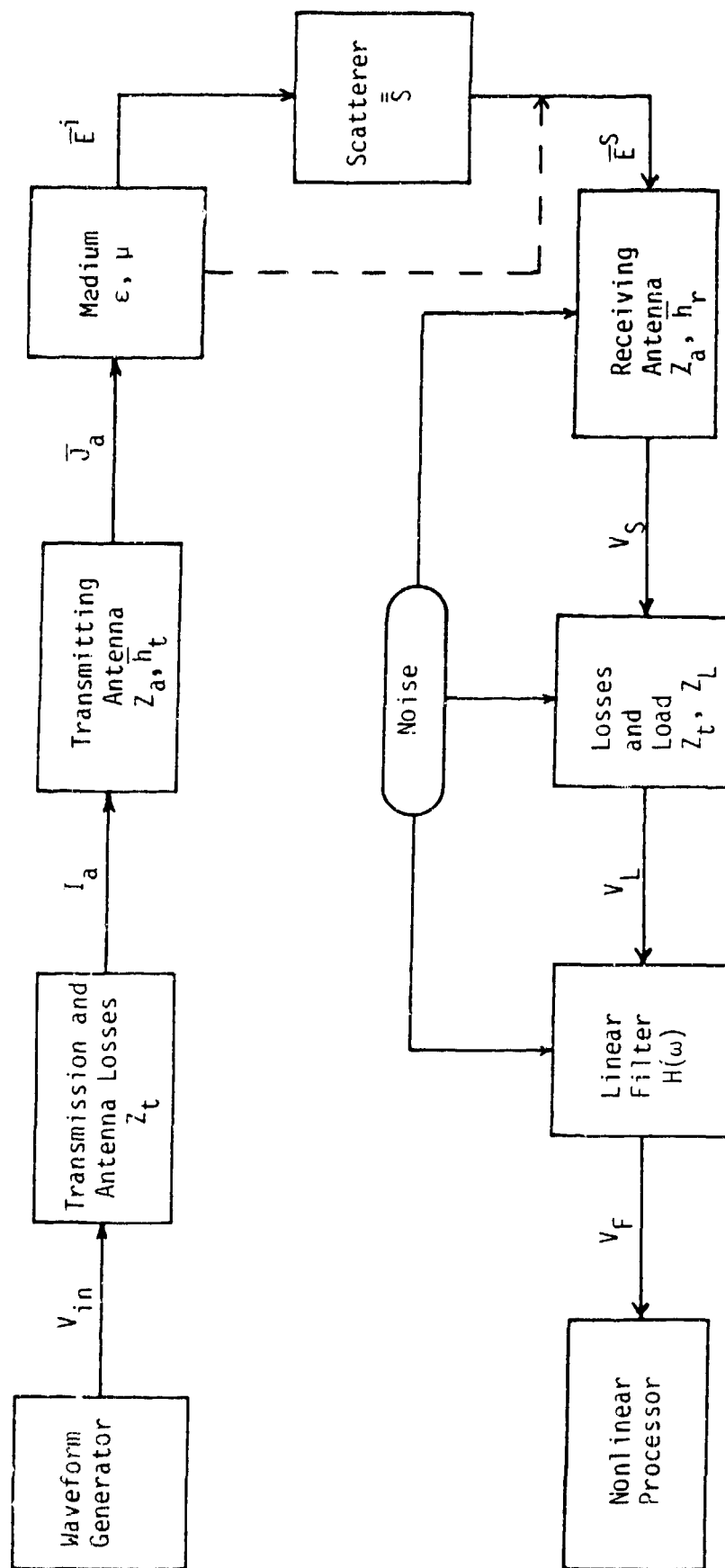


Figure C-1. Block Diagram of General Radar System

voltage corresponding to that which effectively appears at the terminals of the load resistance of the receiving antenna.* Contrary to claims made elsewhere [39], the analysis is most straightforwardly conducted in the frequency (ω) domain, where ω is an angular frequency variable associated with the temporal Fourier transform. This transform is defined as

$$F(\omega) = \int_{-\infty}^{\infty} f(t) e^{i\omega t} dt, \quad (C-1)$$

and its inverse

$$f(t) = \frac{1}{2\pi} \int_{-\infty}^{\infty} F(\omega) e^{-i\omega t} d\omega. \quad (C-2)$$

Some comments are appropriate. First, $f(t)$ and $F(\omega)$ can in general be distributions, so that the existence of Eqs. (C-1) and (C-2) is not an issue. Second, the temporal functions must satisfy causality, i.e.

$$f(t) = 0, \quad t < 0,$$

thus allowing the lower limit in Eq. (C-1) to be replaced by $t = 0$. Although a LaPlace transform is often used in this situation, it is not necessary to do so, and Fourier transform will be used here instead.

The radar transmitter, defined by an input voltage waveform $V_{in}(\omega)$, produces an output current $I_a(\omega)$ which is applied to the terminals of the transmitting antenna. It is convenient to write

*Some amount of amplification of other linear processing is allowable between the load resistance and the system output terminals.

$$V_{in}(\omega) = [Z_t(\omega) + Z_a(\omega)]I_a(\omega), \quad (C-3)$$

where $Z_t(\omega) = R_t(\omega) - iX_t(\omega)$ = transimpedance of transmitter,

$Z_a(\omega) = R_a(\omega) - iX_a(\omega)$ = input impedance of the antenna.

For convenience, R_a and X_a are the radiation resistance and reactance of the antenna, respectively. All other contributions to the antenna impedance (in particular, internal losses) have been assumed lumped with Z_t . By definition, then,

$$Z_t(\omega) = \left. \frac{V_{in}(\omega)}{I_a(\omega)} \right|_{Z_a=0}. \quad (C-4)$$

Let the current I_a be distributed among N infinitesimal radiators which constitute the antenna array.* This distribution is to occur in such a manner that the frequency dependence of each current radiator is the same as $I_a(\omega)$. Specifically, the vector current distribution of the antenna array has the form

$$\vec{J}_a(\vec{r}, \omega) = I_a(\omega) \sum_{n=1}^N a_n \delta(\vec{r} - \vec{r}_n) \hat{p}(\vec{r}_n), \quad (C-5)$$

where \hat{p} is a unit vector describing the orientation of each radiating element. For consistency, the units on $\delta(\vec{r} - \vec{r}_n)$ are inverse distance cubed (a density), while those of a_n are distance. In this manner, $a_n \hat{p}(\vec{r}_n)$ is the dipole moment of the n^{th} element. In general, the a_n are complex, to allow for a phase shift between elements. Furthermore, this

*More general current distributions will be considered later in this memo.

phase can be at most linearly dependent on frequency, thereby allowing a time delay to be specified between elements in the time domain. According to the discussion above, it is required that

$$\sum_{n=1}^N |a_n| = 1. \quad (C-6)$$

The distribution \bar{J}_a can be made continuous by letting $N \rightarrow \infty$ in an appropriate limit; however, for NSR systems, the expected antenna designs employ discrete radiating elements [47-49].

The far-zone electric field $\bar{E}^i(\bar{r}, \omega)$ generated by \bar{J}_a radiating into a linear, homogeneous, isotropic, dispersive medium whose permittivity, permeability, and conductivity are given by $\epsilon_0(\omega)$, $\mu(\omega)$, and $\sigma(\omega)$ is

$$\bar{E}^i(\bar{r}, \omega) = \frac{k^2(\omega)}{4\pi i \omega \epsilon(\omega)} \frac{e^{ik(\omega)r}}{r} \hat{r} \times \hat{r} \times \int_V \bar{J}_a(\bar{r}', \omega) e^{-ik(\omega)\hat{r} \cdot \bar{r}'} d^3 r' \quad (C-7)$$

$$= \frac{\omega \mu(\omega)}{4\pi i} \frac{e^{ik(\omega)r}}{r} I_a(\omega) \sum_{n=1}^N a_n \hat{r} \times \hat{r} \times \hat{p}(\bar{r}_n) e^{-ik(\omega)\hat{r} \cdot \bar{r}_n},$$

where

$\bar{r} = r\hat{r}$ = far-zone position vector

$$k(\omega) = \omega^2 \epsilon(\omega) \mu(\omega) \quad (C-8)$$

$$\epsilon(\omega) = \epsilon_0(\omega) + i \frac{\sigma(\omega)}{\omega}, \quad (C-9)$$

and V is a volume enclosing the antenna. Equation (C-7) is valid when \bar{r} , \bar{r}' satisfy the far-zone criterion

$$|\vec{r} - \vec{r}'| \approx r - \hat{r} \cdot \vec{r}'. \quad (C-10)$$

Equation (C-10) is generally valid when the origin of coordinates is taken to lie near the center of the antenna array. Under these circumstances, \hat{r} can be considered to specify an angular direction relative to the antenna in the far-field, as shown in Figure C-2.

Let the field \vec{E}^i be incident upon a scattering target whose center is given by the position \vec{r} . The target is bounded by a surface A, and for the moment is characterized by arbitrary constitutive parameters ϵ_t , μ_t , σ_t which may be functions of both position and frequency. It is also assumed that the target is sufficiently small that the antenna resides in the far-zone of the target, thereby satisfying a relationship analogous to Eq. (C-10).

For all practical situations, the field \vec{E}^s backscattered by the target can be described by a scattering matrix such that

$$\vec{E}^s(\vec{r}', \omega) = \frac{e^{ik(\omega)r}}{4\pi r} \bar{\bar{S}} \cdot \vec{E}^i(\vec{r}, \omega) e^{-ik(\omega)\hat{r} \cdot \vec{r}'}, \quad (C-11)$$

where $\bar{\bar{S}}$ is a 2 x 2 matrix in dyadic form. Note that $\bar{\bar{S}}$ is defined relative to the target center, that is, with respect to the position vector \vec{r} . In this manner, the propagation phase of the scattered field at the antenna phase center ($\vec{r}' = 0$), from Eqs. (C-9) and (C-11), is $2k(\omega)r$, as expected.

The elements of $\bar{\bar{S}}$ depend strongly on the incidence direction \hat{r} , the target orientation (aspect), and the frequency ω . The latter dependence is particularly significant here, and when necessary will be shown explicitly.

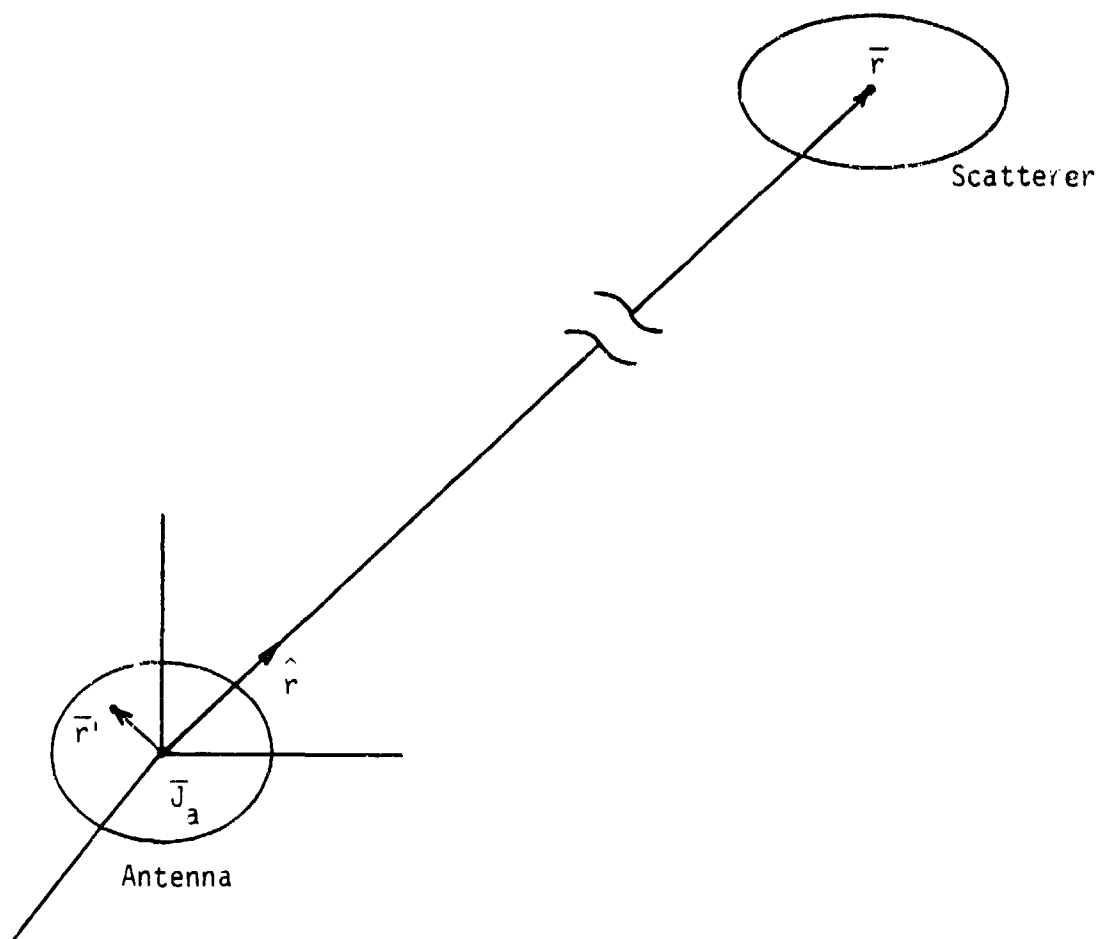


Figure C-2. Scattering Geometry. The scatterer phase reference is the position vector \bar{r} . The antenna terminals are the point $\bar{r}' = 0$.

The voltage $V_L(\omega)$ appearing across the terminals of the receiver when connected to a load impedance $Z_L(\omega)$ is best explained with the aid of Figure C-3. In Figure C-3(a), the antenna is operated as a transmitter, producing an input antenna current $I_a(\omega)$ in response to an input voltage $V_{in}(\omega)$. Equation (C-3) characterizes this relationship. In Figure C-3b, the antenna is operating as a receiver, with the load impedance Z_L replacing the input voltage generator. In addition, a new voltage source $V_s(\omega)$, generated by the scattered field \bar{E}^s , serves to drive the circuit. From the theory of receiving antennas [79], the voltage across the load is

$$\begin{aligned} V_L(\omega) &= Z_L(\omega) I_L(\omega) \\ &= \frac{Z_L(\omega) V_s(\omega)}{Z_L(\omega) + Z_t(\omega) + Z_a(\omega)}, \end{aligned} \quad (C-12)$$

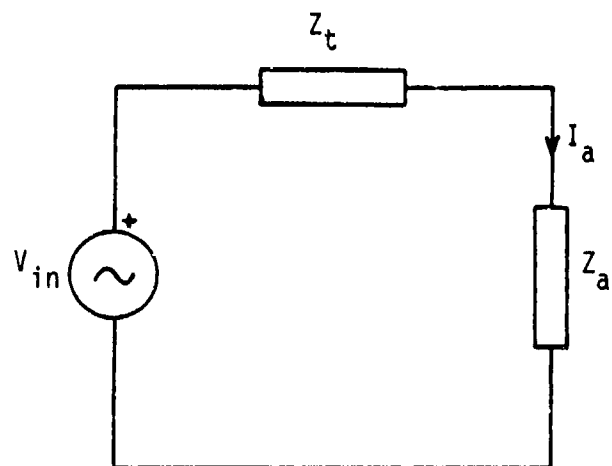
where

$$V_s(\omega) = \bar{h}(\hat{r}, \omega) \cdot \bar{E}^s(\vec{r}^1 = 0, \omega). \quad (C-13)$$

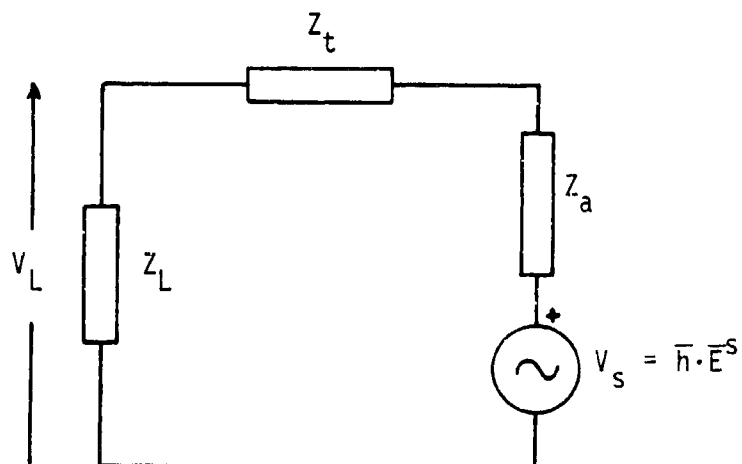
The parameter \bar{h} is the vector effective height of the antenna, and is given explicitly by

$$\begin{aligned} \bar{h}(\hat{r}, \omega) &= \frac{1}{I_a(\omega)} \int \bar{J}_a(\vec{r}, \omega) e^{-ik(\omega)\hat{r} \cdot \vec{r}^1} d^3r^1 \\ &= \sum_{N=1}^N \hat{a}_N \hat{p}(\vec{r}_N) e^{-ik(\omega)\hat{r} \cdot \vec{r}_N} \end{aligned} \quad (C-14)$$

The units of \bar{h} are length, which is why it is referred to as an effective height.



(a)



(b)

Figure C-3. Antenna Equivalent Circuits. (a) Transmitting antenna. (b) Receiving antenna.

The final step in the end-to-end analysis is the inclusion of a linear filter operating on the voltage V_L to produce a voltage V_F . Denoting the transfer function of the filter by $H(\omega)$, it follows that

$$V_F(\omega) = H(\omega)V_L(\omega). \quad (C-15)$$

In this respect, Z_L can be considered the input impedance of the filter.

By combining Eqs. (C-7) and (C-14), one can write

$$\bar{E}^i(\bar{r}, \omega) = \frac{\omega\mu(\omega)}{4\pi r} e^{ik(\omega)r} I_a(\omega) \hat{r} \times \hat{r} \times \bar{h}(\bar{r}, \omega). \quad (C-16)$$

The scattering matrix \bar{S} is transverse to the direction of propagation \hat{r} , i.e.

$$\hat{r} \cdot \bar{S} = \bar{S} \cdot \hat{r} = 0, \quad (C-17)$$

and since

$$\hat{r} \times \hat{r} \times \bar{h} = \hat{r}(\hat{r} \cdot \bar{h}) - \bar{h}, \quad (C-18)$$

it follows from Eqs. (C-16) through (C-18) that

$$\bar{S} \cdot \bar{E}^i = \frac{i\omega\mu(\omega)}{4\pi r} e^{ik(\omega)r} I_a(\omega) \bar{S} \cdot \bar{h}(\hat{r}, \omega). \quad (C-19)$$

The total input-output relationship for the system can be found from Eqs. (C-3), (C-11) through (C-13), and (C-19), namely

$$V_F(\omega) = H(\omega) \frac{Z_L(\omega)}{Z_L(\omega) + Z_t(\omega) + Z_a(\omega)} (Z_t(\omega) + Z_a(\omega))^{-1} \cdot \frac{i\omega\mu(\omega)}{(4\pi r)^2} e^{i2k(\omega)r} \bar{h}(\hat{r}, \omega) \cdot \bar{S} \cdot \bar{h}(\hat{r}, \omega) V_{in}(\omega). \quad (C-20)$$

The time-domain relationship is simply

$$\begin{aligned}
 v_F(\omega) &= \frac{1}{2\pi} \int_{-\infty}^{\infty} v_F(\omega) e^{-i\omega t} d\omega \\
 &= \int_0^t v_{in}(t') g(t-t') dt',
 \end{aligned}
 \tag{C-21}$$

where $v_{in}(t)$, $g(t)$ are the inverse Fourier transforms of $V_{in}(\omega)$ and

$$G(\omega) \equiv \frac{V_F(\omega)}{V_{in}(\omega)},
 \tag{C-22}$$

respectively. $G(\omega)$ and $g(t)$ are the transfer function and impulse response of the radar system. Causality and the assumption that $v_{in} = 0$ for $t < 0$ have been used to determine the limits of integration in Eq. (C-21).

The model for the system characterized by Eqs. (C-20) and (C-21) is sufficiently general to conform to most noiseless, backscatter, co-polarized radar systems over their linear operating region. The inclusion of a random, time-varying noise component can be inserted either before or after the filter $H(\omega)$ by addition to V_L or V_F , respectively (see Figure C-1). The generalization to a monostatic and/or bistatic geometry with arbitrarily polarized receiver is straightforward through identification of separate transmitter and receiver vector effective heights.

C.2 TRANSFER FUNCTION RELATIONSHIPS FOR ANTENNAS AND SCATTERERS

In this section, the relationships for the transfer functions of a transmitting/receiving antenna are provided. The role of reciprocity in transmission and reception is defined. The nature of these transfer relationships is that they avoid the need for explicit knowledge of the current or aperture field distribution of an antenna* in order to relate the excitation/received voltages to the far-zone radiated/scattered fields. Instead these distributions are implicitly contained in the definition of the "pattern factor"/vector effective height of the antenna, as will be shown below. These quantities are, in general, more "measurable" than the above-mentioned distributions. Thus, they are more useful in systems analysis for a specified antenna; they are less useful, however, for analyzing or designing an antenna for a particular application or to a given specification because of their "implicit" nature.

Attention is also be given to target scattering transfer relationships, in an attempt to cast the reflectivity (Section 3) and scattering matrix (Section C.1) models into a common framework. The utility of each model will be discussed.

C.2.1. THE ANTENNA TRANSFER FUNCTIONS

The far-zone electric field radiated by an antenna occupying a volume V is [84]

$$\vec{E}^i(\vec{r}, \omega) = -ik \frac{e^{ikr}}{4\pi r} Z_0 (\hat{r} \times \hat{r} \times \vec{N} - \hat{r} \times \vec{M}) \quad (C-23)$$

$$\vec{r} = r\hat{r}$$

*These explicit distributions were used in the formulations presented in Section C.1 and Section 3, respectively.

where \bar{N} , \bar{M} are the electric and magnetic current moments defined by

$$\bar{N} = \int_V \bar{J}_e(\bar{r}', \omega) e^{-ik\hat{r} \cdot \bar{r}'} d^3r' \quad (C-24)$$

$$\bar{M} = \frac{1}{Z_0} \int_V \bar{J}_m(\bar{r}', \omega) e^{-ik\hat{r} \cdot \bar{r}'} d^3r', \quad (C-25)$$

and

$$Z_0 = \sqrt{\frac{\mu}{\epsilon}} = \text{intrinsic impedance of the medium.}$$

The inclusion of the magnetic current density \bar{J}_m is a generalization of the results of Section C.1 to allow the definition of equivalent current distributions for apertures, etc. As before, the intrinsic impedance Z_0 and the wave number of the medium k are assumed to be functions of the angular frequency ω .

It is convenient to define a pair of quantities \bar{F} and \bar{h} , the field pattern factor and the antenna vector effective height, such that

$$\bar{E}^i(\bar{r}, \omega) = -iZ_0 I_a(\omega) \frac{e^{ikr}}{4\pi r} \bar{F}(\hat{r}, \omega) \quad (C-26a)$$

$$= -ikZ_0 I_a(\omega) \frac{e^{ikr}}{4\pi r} \bar{h}(\hat{r}, \omega). \quad (C-26b)$$

The pattern factor is a dimensionless quantity which describes the angular variations of the far-zone field at the frequency ω , while the vector effective height is a parameter with dimensions of length which represents the effective receiving length of the antenna as a function of angle and frequency. Both quantities also contain the full polarization properties of the antenna and its radiated field. As before, I_a is the input current at the antenna terminals.

From Eq. (C-26) it is clear that

$$\bar{F}(\hat{r}, \omega) = k\bar{h}(\hat{r}, \omega), \quad (C-27)$$

which is simply a statement of the Rayleigh-Carson reciprocity theorem for a linear antenna* in a linear, isotropic medium.

If the antenna excitation, referred to the antenna terminals, is characterized by a Thevenin equivalent circuit with an input voltage

$V_{in}(\omega)$ and a source impedance $Z_{in}(\omega)$,* it follows that

$$\bar{E}^i(\vec{r}, \omega) = V_{in}(\omega) \frac{-iZ_o(\omega)}{Z_a(\omega) + Z_{in}(\omega)} \frac{e^{ikr}}{4\pi r} \bar{F}(\hat{r}, \omega), \quad (C-28)$$

where Z_a is the antenna input impedance. A transmitting transfer function is now defined as [84]

$$\bar{H}_T(\hat{r}, \omega) = \frac{r\bar{E}^i(\vec{r}, \omega)}{V_{in}(\omega)} e^{-ikr} = -\frac{i}{4\pi} \left(\frac{Z_o}{Z_a + Z_{in}} \right) \bar{F}(\hat{r}, \omega), \quad (C-29)$$

*The term linear antenna is used in the sense of a linear (as opposed to nonlinear) system. It does not mean the antenna is necessarily wirelike.

which can be viewed as the range-normalized far-zone field response to a unit input voltage.

In a similar manner, a receiving transfer function \bar{H}_R can also be defined. Recall that the output voltage across a load impedance Z_L connected to the antenna terminals can be written as

$$V_L(\omega) = \frac{Z_L(\omega)}{Z_a(\omega) + Z_L(\omega)} \bar{h}(\hat{r}, \omega) \cdot \bar{E}^S(\omega). \quad (C-30)$$

where $\bar{E}^S(\omega) = \bar{E}^S(\bar{r} = 0, \omega)$ is the scattered field at the antenna terminals. Without loss of generality, the antenna terminals are assumed to be located at the origin of coordinates ($\bar{r} = 0$). The receiving transfer function is defined such that

$$V_L(\omega) = \bar{H}_R(\hat{r}, \omega) \cdot \bar{E}^S(\omega). \quad (C-31)$$

Thus, \bar{H}_R is the response to a unit amplitude scattered field polarized in the same sense as the receiving antenna. Explicitly,

$$\bar{H}_R = H_R \hat{h} = \left(\frac{Z_L}{Z_a + Z_L} \right) \bar{h}(\hat{r}, \omega), \quad (C-32)$$

and \hat{h} is the antenna polarization unit vector.

A fundamental result can be derived for the special case when $Z_L = Z_{in}$ is real, namely

$$\frac{H_T^j}{H_R^j} = - \frac{i\omega}{4\pi Z_L} \omega, \quad (C-33)$$

*Both Z_{in} and Z_L , Eq. (C-30), include the transmitter transimpedance Z_t defined in Section C.1.

where μ is the permeability of the medium and the superscript denotes the j^{th} scalar component. Since in practice μ is nondispersive (independent of ω), Eq. (C-33) is a statement of the well-known fact that the transmitting impulse response of an antenna is the time-derivative of the receiving impulse response. The fact is also evident from Eq. (C-27).

A final comment regarding the transfer function model of Eqs. (C-29) and (C-31). In the analysis of Section 3, an assumption regarding the spatial and frequency dependence of the equivalent current distributions \bar{J}_e and \bar{J}_m of the form

$$\bar{J}_{e,m}(\bar{r}, \omega) = \bar{J}_{e,m}(\bar{r})a(\omega) \quad (\text{C-34})$$

was made. It was argued that this assumption is valid for horn-like or reflector-like antennas. While this may be true over narrow or even moderate bandwidths, it is in general not applicable for wideband systems of large relative bandwidth such as those being considered in this research program. It can remain valid for array antennas, however, when the individual elements are "point-like" radiators and interactions between elements are negligible. This was exactly the antenna type considered in Section C.1. However, satisfaction of Eq. (C-34) may not be necessary for the results of Section 3 to remain valid.

C.2.2. SCATTERING TRANSFER RELATIONS

To complete the model of a wideband radar system, it remains to define the connection between the incident and scattered fields \bar{E}^i and \bar{E}^s , respectively. A rigorous, explicit relationship requires the solution of a boundary value problem, generally in the form of an

integral equation, over the surface of the scatterer. This is a difficult problem except in few situations, particularly if the effects of a clutter background are included. An implicit relationship that is often used, as it was in Section C.1, is to define a (dyadic) scattering matrix $\bar{\bar{S}}$, whereby

$$\bar{E}^S(\omega) = \frac{e^{ikr}}{4\pi r} \bar{\bar{S}}(\omega) \cdot \bar{E}^i(\bar{r}, \omega). \quad (C-35)$$

As with the antenna-based functions \bar{H}_T and \bar{H}_r , $\bar{\bar{S}}$ is a transfer function which relates the output \bar{E}^S of a linear system (the scatterer) to the system input \bar{E}^i .

Now the scattered field \bar{E}^S satisfies a relationship similar to Eq. (C-23), i.e.

$$\bar{E}^S(\omega) = -ikZ_0 \frac{e^{ikr}}{4\pi r} (\hat{r} \times \hat{r} \times \bar{N}_t + \hat{r} \times \bar{M}_t), \quad (C-36)$$

where \bar{N}_t , \bar{M}_t are the electric and magnetic current moments induced on the target by the incident field. If \bar{J}_{te} and \bar{J}_{tm} are the equivalent electric and magnetic currents defined on the target surface S , then, analogous to Eqs. (C-24) and (C-25),

$$\bar{N}_t = \int_S \bar{J}_{te}(\bar{r}_0, \omega) e^{ik\hat{r} \cdot \bar{r}_0} d^2r_0 \quad (C-37)$$

$$\bar{M}_t = \frac{1}{Z_0} \int_S \bar{J}_{tm}(\bar{r}_0, \omega) e^{ik\hat{r} \cdot \bar{r}_0} d^2r_0, \quad (C-38)$$

where \bar{r}_0 is a local position vector relative to the target "center." Equations (C-36) through (C-38) have been evaluated in the backscatter direction, which is equivalent to replacing \hat{r} by $-\hat{r}$ in Eqs. (C-24) and (C-25). It is evident from Eqs. (C-35) through (C-38) that the explicit form of \bar{S} is tied to the relationship between the current densities \bar{J}_{te} , \bar{J}_{tm} and the direction of incidence \hat{r} , and can be determined only by the solving the above-mentioned integral equations (which is in general not possible analytically).

Consider the possibility of reconciling the scattering model of Eq. (C-35) with the "reflectivity" model used in Section 3. First, it is important to note that Eq. (C-35) assumes the incident field to be locally plane in the vicinity of the scatterer (which is consistent with the far-zone approximation).

The model used in Section 3 for the received signal from the target is of the form (in the present notation)

$$v_H(t) = \frac{1}{2\pi} \int_{-\infty}^{\infty} V_H(\omega) e^{-i\omega t} d\omega, \quad (C-39)$$

where V_H is the spectrum of received voltage (analogous to V_L in the present model). Explicitly,

$$V_H(\omega) = a(\omega) V_{in}(\omega) \left(\frac{-ik}{4\pi r} \right)^2 e^{i2kr} \tilde{E}_0^2(\hat{r}, \omega) \int_S g_t(\bar{r}_0, \omega) e^{i2k\hat{r} \cdot \bar{r}_0} d^2r_0. \quad (C-40)$$

Here, $a(\omega) = a_T(\omega)a_R(\omega)$ is an antenna-related spectral transfer function and \tilde{E}_0 is a far-zone, field-like distribution. Of course, g_t is the target reflectivity density. In order to express these quantities in terms of the parameters used in this appendix, it is first noted that from the far-zone assumption, and the requirement of a localized target, Eq. (C-22) implies

$$\bar{E}^i(\bar{r} + \bar{r}_0, \omega) = \bar{E}^i(\bar{r}, \omega) e^{ik\hat{r} \cdot \bar{r}_0}, \quad (C-41)$$

that is, the incident field is locally plane, as assumed. Thus, from Eqs. (C-27) and (C-28)

$$\begin{aligned} \bar{E}^i(\bar{r} + \bar{r}_0, \omega) &= -ikV_{in}(\omega) a_T(\omega) \frac{e^{ikr}}{4\pi r} \hat{h}(\hat{r}, \omega) e^{ik\hat{r} \cdot \bar{r}_0} \\ &= E_0(\bar{r}, \omega) \hat{h} e^{ik\hat{r} \cdot \bar{r}_0}, \end{aligned} \quad (C-42)$$

where the unit vector \hat{h} is defined in Eq. (C-32).

Since the scattering process is (assumed) linear, it follows that \bar{J}_{te} and \bar{J}_{tm} are proportional to the amplitude of the incident \bar{E}^i . By introducing the normalized induced current densities $\bar{J}_{te,m}$ via

$$\bar{J}_{te,m} = E_0(\bar{r}, \omega) e^{ik\hat{r} \cdot \bar{r}_0} \bar{J}_{te,m}(\bar{r}_0, \omega), \quad (C-43)$$

and the corresponding co-polarized "reflectivity density,"

$$g_t(\bar{r}_0, \omega) = \hat{h} \cdot \hat{r} \times \left(\hat{r} \times \bar{j}_{te} + \frac{1}{Z_0} \bar{j}_{tm} \right), \quad (C-44)$$

Eq. (C-30) for the output voltage, combined with Eqs. (C-36) through (C-38) and (C-41) through (C-45), becomes

$$V_L(\omega) = a_T(\omega) a_R(\omega) V_{in}(\omega) \left(\frac{-ik}{4\pi r} \right)^2 e^{i2kr} |\bar{h}(\bar{r}, \omega)|^2 \cdot \int_S g_t(\bar{r}_0, \omega) e^{-i2k\hat{r} \cdot \bar{r}_0} d^2r_0, \quad (C-45)$$

where

$$a_R(\omega) = \frac{Z_L(\omega)}{Z_a(\omega) + Z_L(\omega)}. \quad (C-46)$$

The similarity to the result of Section 3, Eq. (C-40), is evident. However, it must be emphasized that g_t is also a function of the aspect direction \hat{r} , and of the form of the incident field (here assumed to be planar).

Whether or not it is necessary to introduce the concept of reflectivity into the analysis of Section 3 is not immediately evident. In fact, a quantity

$$u_t(\hat{r}, \omega) = \left(\frac{-ik}{4\pi r} \right)^2 \bar{E}_0^2(\hat{r}, \omega) \int_S g_t(\bar{r}_0, \omega) e^{i2k\hat{r} \cdot \bar{r}_0} d^2r_0, \quad (C-47)$$

is defined therein such that

$$V_L(\omega) = a(\omega) V_{in}(\omega) e^{i2kr} u_t(\hat{r}, \omega). \quad (C-48)$$

From Eqs. (C-27) though (C-30) and (C-35), one can easily deduce

$$u_t(\hat{r}, \omega) = \left(\frac{-ik}{4\pi r} \right)^2 |\bar{h}(\bar{r}, \omega)|^2 \left(\frac{i}{k} \hat{h} \cdot \bar{\bar{S}} \cdot \hat{h} \right), \quad (C-49)$$

from which a relationship between the reflectivity and scattering matrix can be obtained, viz.

$$\frac{i}{k} \hat{h} \cdot \bar{\bar{S}} \cdot \hat{h} = \int_S g_t(\bar{r}_0, \omega) e^{i2k\hat{r} \cdot \bar{r}_0} d^2 r_0. \quad (C-50)$$

It appears that u_t is the only important parameter for the approach used in Section 3, it is therefore possible that Eq. (C-49) can be used in place of Eq. (C-47).

REFERENCES

1. N. M. Blackman, "Sinusoids versus Walsh Functions," Proc. IEEE, Vol. 62, pp. 346-354, March 1974.
2. H. F. Harmuth, et al., "Comments on Sinusoids versus Walsh Functions," IEEE Trans. on Electromagn. Compat., Vol. EMC-17, pp. 194-195, August 1975. A reply by N. M. Blackman was also published.
3. H. M. Finn, "Adaptive Detection with Regulated Error Probabilities," RCA Review, Vol. 28, No. 4, pp. 653-678, December 1967.
4. H. M. Finn and R. S. Johnson, "Adaptive Detection Mode with Threshold Control As a Function of Spatially Sampled Clutter Level Estimates," RCA Review, Vol. 29, No. 3, pp. 414-454, September 1968.
5. G. B. Goldstein, "False Alarm Regulation in Log-Normal and Weibull Clutter," IEEE Trans. on Aerospace and Elect. System, Vol. AES-9, No. 1, pp. 84-92, January 1973.
6. L. M. Novak, and F. W. Vote, "Millimeter Airborne Radar Target Detection and Selection Techniques," NAECON Proceedings, May 1979.
7. V. G. Hansen, "Constant False Alarm Rate Processing in Search Radars," Proc. Int. Conf. on Radar - Present and Future, IEEE Conference Publication No. 105, pp. 325-332, October 23-25, 1973.
8. F. M. Staudaher, "Airborne MTI," Chapter 18 in the Radar Handbook, M. E. Skolnik, editor, McGraw-Hill, New York, 1970.
9. J. S. Shuster, "Multiple Arrested Synthetic Aperture Radar," Ph.D. Dissertation, Air Force Institute of Technology, Wright-Patterson AFB, OH, 45433, May 1981.
10. S. A. Meltzer, S. Thaler, "Detection Range Predictions for Pulse Doppler Radar," Proceedings of the IRE, Vol. 49, No. 8, pp. 1299-1307, August 1961.
11. G. E. Pollon, G. W. Lank, "Angular Tracking of Two Closely Spaced Radar Targets," IEEE Trans. on Aerospace and Elect. Syst., Vol. AES-4, pp. 514-520, July 1968.
12. S. Sherman, "The Use of 'Complex Indicated Angles' in Monopulse Radar to Locate Unresolved Targets," Pros. Natl. Electronics Conf., Vol. 22, p. 243, 1966.

13. P. Z. Pebbles, "Futher Results on Multipath Error Reduction Using Multiple Target Methods," IEEE Trans. on Aerospace and Elect. Syst., Vol. AES-9, pp. 654-659, September 1973.
14. R. O. Harger, Synthetic Aperture Radar Systems: Theory and Design, Academic Press, New York, 1970.
15. L. W. Pearson, et al., "A New Method of Radar Target Recognition Based on the Singularity Expression for the Target," 1975 IEEE International Radar Conference Record, pp. 452-457, April 1975.
16. M. L. VanBlaricum and R. Mittra, "A Technique for Extracting the Poles and Residues of a System Directly from Its Impulse Response," IEEE Trans. Ant. and Prop., Vol. AP-23, pp. 777-781, January 1975.
17. M. Kanda, "Time Domain Sensors for Radiated Impulsive Measurements," IEEE Trans. Ant. and Prop., Vol. AP-31, pp. 438-444, May 1983.
18. R. O. Harger, "On the Mapping Associated with the Complex Representation of Functions and Processes," IEEE Trans. Aero. Elec. Sys., Vol. AES-8, pp. 851-853, November 1972.
19. R. O. Harger, "A Note on the Realization of Ambiguity Functions," IEEE Trans. Sp. Electr. Telemetry, Vol. SET-9, pp. 127-130, December 1963.
20. R. O. Harger, "An Optimum Design of Ambiguity Function, Antenna Pattern and Signal for Side-Looking Radars," IEEE Trans. Mil. Electr., Vol. MIL-9, pp. 264-278, July-October 1965.
21. C. W. Helstrom, Statistical Theory of Signal Detection, 2nd Ed., Pergamon Press, New York, 1975.
22. H. L. Van Trees, Detection, Estimation and Modulation Theory: Part I, Wiley Interscience, New York, 1967.
23. S. Stein and S. Jones, Modern Communication Principles, McGraw-Hill, New York, 1967.
24. J. A. Stratton, Electromagnetic Theory, McGraw-Hill, New York, 1941.
25. D. E. Kerr, Propagation of Short Radio Waves, McGraw-Hill, New York, 1951.

26. R. K. Moore, "Ground Echo," Chapter 25 in Radar Handbook, Me. E. Skolnik, editor, McGraw-Hill, New York, 1970.

27. C. E. Baum, "On the Singularity Expansion Method for the Solution of Electromagnetic Interaction Problems," Air Force Weapons Laboratory Interaction Note 86, December 11, 1971.

28. C. E. Baum, "The Singularity Expansion Method," Chapter 3 in Transient Electromagnetic Fields, L. B. Felsen, editor, Volume 10 in Topics in Applied Physics, Springer-Verlag, Berlin, 1976.

29. M. L. VanBlaricum and R. Mittra, "A Technique for Extracting the Poles and Residues of a System Directly from Its Transient Response," IEEE Trans. Ant. Prop., Vol. AP-23, pp. 777-781, November 1975.

30. F. M. Tesche, "On the Analysis of Scattering and Antenna Problems Using the Singularity Expansion Technique," IEEE Trans. Ant. Prop., Vol. AP-21, pp. 53-62, January 1973.

31. L. Marin and R. W. Latham, "Representation of Transient Scattered Fields in Terms of Free Oscillations of Bodies," Proc. IEEE, Vol. 60, pp. 640-641, May 1972.

32. H. F. Harmuth, "Selective Reception of Periodic Electromagnetic Waves with General Time Variation," IEEE Trans. Electromagn. Compat., Vol. EMC-19, pp. 137-144, August 1977.

33. H. F. Harmuth, "Frequency Sharing and Spread Spectrum Transmission with Large Relative Bandwidth," IEEE Trans. Electromagn. Compat., Vol. EMC-20, pp. 232-239, February 1978.

34. H. F. Harmuth, "Low Angle Tracking by Carrier-Free Radar," IEEE Trans. Electromagn. Compat., Vol. EMC-20, pp. 419-425, August 1978.

35. H. F. Harmuth, "Radio Signals with Large Relative Bandwidth for Over-the-Horizon Radar and Spread Spectrum Communications," IEEE Trans. Electromagn. Compat., Vol. EMC-20, pp. 501-512, November 1978.

36. H. F. Harmuth, "Synthetic Aperture Radar Based on Nonsinusoidal Functions. I - Moving Radar and Stationary Arrays in One or Two Dimensions," IEEE Trans. Electromagn. Compat., Vol. EMC-20, pp. 426-435, August 1978.

37. H. F. Harmuth, "Synthetic Aperture Radar Based on Nonsinusoidal Functions. II - Pulse Compression, Contrast, Resolution and Doppler Shift," IEEE Trans. Electromagn. Compat., Vol. EMC-21, pp. 40-49, February 1979.

38. H. F. Harmuth, "Synthetic Aperture Radar Based on Nonsinusoidal Functions. III - Beamforming By Means of the Doppler Effect," IEEE Trans. Electromagn. Compat., Vol. EMC-21, pp. 122-131, May 1979.

39. H. F. Harmuth, "Synthetic Aperture Radar Based on Nonsinusoidal Functions. IV - Tracking Radar and Beam Rider," IEEE Trans. Electromagn. Compat., Vol. EMC-21, pp. 245-253, August 1979.

40. H. F. Harmuth, "Synthetic Aperture Radar Based on Nonsinusoidal Functions. V - Look-Down Radar," IEEE Trans. Electromagn. Compat., Vol. EMC-22, pp. 45-53, February 1980.

41. H. F. Harmuth, "Synthetic Aperture Radar Based on Nonsinusoidal Functions. VI - Pulse Position and Pulse Shape Coding," IEEE Trans. Electromagn. Compat., Vol. EMC-22, pp. 93-106, May 1980.

42. H. F. Harmuth, "Synthetic Aperture Radar Based on Nonsinusoidal Functions. VII - Thumbtack Ambiguity Function," IEEE Trans. Electromagn. Compat., Vol. EMC-22, pp. 181-190, August 1980.

43. H. F. Harmuth, "Synthetic Aperture Radar Based on Nonsinusoidal Functions. VIII - Velocity and Acceleration Processing," IEEE Trans. Electromagn. Compat., Vol. EC-22, pp. 308-319, November 1980.

44. H. F. Harmuth, "Synthetic Aperture Radar Based on Nonsinusoidal Functions. IX - Array Beam Forming," IEEE Trans. Electromagn. Compat., Vol. EMC-23, pp. 20-27, February 1981.

45. H. F. Harmuth, "Synthetic Aperture Radar Based on Nonsinusoidal Functions. X - Array Gain, Planar Arrays, Multiple Signals," IEEE Trans. Electromagn. Compat., Vol. EMC-23, pp. 72-79, May 1981.

46. H. F. Harmuth, "On the Effect of Absorbing Materials on Electromagnetic Waves with Large Relative Bandwidth," IEEE Trans. Electromagn. Compat., Vol. EMC-25, pp. 32-39, February 1983.

47. H. F. Harmuth and S. Ding-Rong, "Antennas for Nonsinusoidal Waves. I - Radiators," IEEE Trans. Electromagn. Compat., Vol. EMC-25, pp. 13-24, February 1983.

48. H. F. Harmuth and S. Ding-Rong, "Antennas for Nonsinusoidal Waves. II - Sensors," IEEE Trans. Electromagn. Compat., Vol. EMC-25, pp. 107-115, May 1983.

49. H. F. Harmuth, "Antennas for Nonsinusoidal Waves: Part: III - Arrays," IEEE Trans. Electromagn. Compat., Vol. EMC-25, pp. 346-357, August 1983.
50. H. F. Harmuth, "Nonsinusoidal Waves in Rectangular Waveguides," IEEE Trans. Electromagn. Compat., Vo. EMC-26, pp. 34-42, February 1984.
51. H. F. Harmuth, "Nonsinusoidal Waves in Cavity Resonators," IEEE Trans. Electromagn. Compat., Vol. EMC-26, pp. 84-89, May 1984.
52. H. F. Harmuth, Nonsinusoidal Waves for Radar and Radio Communication, Academic Press, New York, 1981.
53. J. R. Davis, et al., "Some Physical Constraints on the Use of 'Carrier-Free' Waveforms in Radio Transmission Systems," Proc. IEEE, Vol. 67, pp. 884-890, June 1979.
54. H. F. Harmuth, "Comments on 'Some Physical Constraints on the Use of 'Carrier-Free' Waveforms in Radio Wave Transmission'," Proc. IEEE, Vol. 67, pp. 890-891, June 1979.
55. M. A. Morgan, "Singularity Expansion Representations of Fields and Currents in Transient Scattering," IEEE Trans. Ant. Prop., Vol. AP-32, pp. 466-473, May 1984.
56. L. W. Pearson, "A Note on the Representation of Scattered Fields As a Singularity Expansion," IEEE Trans. Ant. Prop., Vol. AP-32, pp. 520-524, May 1984.
57. J. R. Auton, et al., "Radar Target Identification and Characterization Using Natural Resonance Extraction," General Research Corp. Final Report to CR-84-1309 to the Office of Naval Research, Contract N00014-82-C-0079, September 1984 (3 Volumes).
58. K.-M. Chen, "Radar Waveform Synthesis Method - A New Radar Detection Scheme," IEEE Trans. Ant. Prop., Vo. AP-29, pp. 553-566, July 1981.
59. K.-M. Chen and D. Westmoreland, "Radar Waveform Synthesis for Exciting Single-Mode Backscatters from a Sphere and Application for Target Discrimination," Rad. Sci., Vol. 17, pp. 574-588, May-June 1982.
60. K.-M. Chen, et al., "Radar Waveform Synthesis for Single-Mode Scattering By a Thin Cylinder and Application for Target Discrimination," IEEE Trans. Ant. Prop., Vol. AP-30, pp. 867-880, September 1982.

61. E. M. Kennaugh and D. L. Moffatt, "Transient and Impulse Response Approximations," Proc. IEEE, Vol. 53, pp. 893-901, August 1965.
62. D. L. Moffatt and R. K. Mains, "Detection and Discrimination of Radar Targets," IEEE Trans. Ant. Prop., Vol. AP-23, pp. 358-367, May 1975.
63. D. L. Moffatt, et al., "Transient Response Characteristics in Identification and Imaging," IEEE Trans. Ant. Prop., Vol. AP-29, pp. 192-205, March 1981.
64. E. M. Kennaugh, "The K-Pulse Concept," IEEE Trans. Ant. Prop., Vol. AP-29, pp. 327-331, March 1981.
65. M. L. VanBlaricum and R. Mittra, "Problems and Solutions Associated with Prony's Method for Processing Transient Data," IEEE Trans. Ant. Prop., Vol. AP-26, pp. 174-182, January 1982.
66. E. J. Rothwell, et.al., "Synthesis of Kill-Pulse to Excite Selected Target Modes," presented at 1984 IEEE Antennas and Propagation Society International Symposium, Boston, MA, June 25-29, 1984.
67. L. Webb and K.-M. Chen, "Target Discrimination Using K-Pulses, Single-Mode Excitation Signals, and Prony's Method," presented at 1984 IEEE Antennas and Propagation Society International Symposium, Boston, MA, June 25-29, 1984.
68. R. M. Lewis, "Physical Optics Inverse Diffraction," IEEE Trans. Ant. Prop., Vol. AP-17, pp. 308-314, May 1969.
69. W.-M. Boerner and C. M. Ho, "Analysis of Physical Optics Far Field Inverse Scattering for the Limited Data Case Using Radon Theory and Polarization Information," Wave Motion, Vol. 3, pp. 311-333, October 1981.
70. W. M. Brown and L. J. Porcello, "An Introduction to Synthetic-Aperture Radar," IEEE Spectrum, Vol. 6, pp. 52-62, September 1969.
71. E. N. Leith, "Quasi-Holographic Techniques in the Microwave Region," Proc. IEEE, Vol. 59, pp. 1305-1317, September 1971.
72. C. K. Chan and N. H. Farhat, "Frequency Swept Tomographic Imaging of Three-Dimensional Perfectly Conducting Objects," IEEE Trans. Ant. Prop., Vol. AP-29, pp. 312-319, March 1981.

73. K. Tomiyasu, "Tutorial Review of Synthetic-Aperture Radar (SAR) with Applications to Imaging of the Ocean Surface," Proc. IEEE, Vol. 66, pp. 563-583, May 1978.
74. W. M. Brown, "Walker Model for Radar Sensing of Rigid Target Fields," IEEE Trans. Aero. Elec. Sys., Vol. AES-16, pp. 104-107, January 1980.
75. H. J. Scudder, "An Introduction to Computer Aided Tomography," Proc. IEEE, Vol. 66, pp. 628-637, June 1978.
76. S. J. Norton and M. Linzer, "Ultrasonic Reflectivity Imaging in Three Dimensions Exact Inverse Scattering Solutions for Plane, Cylindrical, and Spherical Apertures," IEEE Trans. Biomed. Eng., Vol. BME-28, pp. 202-220, February 1981.
77. D. C. Munson, Jr., et al., "A Tomographic Formulation of Spotlight-Mode Synthetic Aperture Radar," Proc. IEEE, Vol. 71, pp. 917-925, August 1983.
78. I. G. Cumming and J. R. Bennett, "Digital Processing of SEASAT SAR Data," in Proc. Int. Conf. on Acoustics, Speech, and Signal Processing, Washington, D.C., pp. 710-718, 1979.
79. W. A. Stutzman and G. A. Thiele, Antenna Theory and Design, Wiley and Sons, New York, 1981.
80. L. Susman and D. Lamensdorf, "Picosecond Pulse Antenna Techniques," Sperry Rand Research Center Final Report RADC-TR-71-64 to Rome Air Development Center, Contract F30602-70-C-0088, May 1971.
81. M. Kanda, "Time Domain Sensors for Radiated Impulsive Measurements," IEEE Trans. Ant. Prop., Vol. AP-31, pp. 438-444, May 1983.
82. W. A. Imbriale, "Applications of the Method of Moments to Thin-Wire Elements and Arrays," Chapter 2 in Numerical and Asymptotic Techniques in Electromagnetics, R. Mittra, editor, Volume 3 in Topics in Applied Physics, Springer-Verlag, Berlin, 1975.
83. R. Mittra, "Integral Equation Methods for Transient Scattering," Chapter 2 in Transient Electromagnetic Scattering, L. B. Felsen, editor, Volume 10 in Topics in Applied Physics, Springer-Verlag, Berlin, 1976.

84. D. L. Sengupta and C.-T. Tai, "Radiation and Reception of Transients by Linear Antennas," in Transient Electromagnetic Scattering, L.B. Felsen, editor, Volume 10 in Topics in Applied Physics, Springer-Verlag, Berlin, 1976.